THE ROLE OF σ1 LENGTH AND FLEXIBILITY IN REOVIRUS REPLICATION

By

Magdalena Bokiej

Dissertation

Submitted to the Faculty of the

Graduate School of Vanderbilt University

in partial fulfillment of requirements

for the degree of

DOCTOR OF PHILOSOPHY

in

Microbiology and Immunology

December, 2012

Nashville, Tennessee

Approved:

Dr. Terence S. Dermody, M.D.

Dr. Jens Meiler, Ph.D.

Dr. H. Earl Ruley, Ph.D.

Dr. Benjamin Spiller, Ph.D.

Dr. John V. Williams, M.D.

To my teachers of life, medicine, and science:

may your lessons guide me in service of others

***

Moim nauczycielom życia, medycyny i nauki:

niech Wasze starania prowadzą mnie

w niesieniu pomocy innym

ACKNOWLEDGEMENTS

The very first person I would like to thank for arriving at this milestone is Dr. Terence Dermody for serving as my mentor for the past three years. His advice has been helpful, timely, and steady. Terry has provided an environment in which I could grow not only as a scientist but also as a physician. Aided by his encouragement, I developed the confidence, skills, and critical thinking required to ask questions of nature. Terry has also introduced me to the arts of public speaking and scientific writing. I will surely benefit from and build on this knowledge as I progress in my career. The Dermody laboratory has been a wonderful environment to learn. These motivated, kind, and knowledgeable individuals have supported me through difficulties and have always been great company. I could not have chosen a better group of people to train with. I would also like to acknowledge the contribution of a former student at the Dermody laboratory, Kristen M. Ogden, who has been the source of much good advice.

I would like to thank all of the members of my thesis committee for their contributions to my graduate education. I thank Dr. Earl Ruley, the committee chair, for lessons of critical thinking, the scientific method, and equanimity. I thank Dr. John Williams for his interest, kindness, and insightful questions. I thank Dr. Jens Meiler for his advice in structural biology. Since our first encounter at one of my Research in Progress presentations, Dr. Benjamin Spiller has taken a genuine interest in my graduate education. I thank him for his encouragement and guidance.

There are many other groups at Vanderbilt University who have made this work possible and enjoyable. I thank the administration of the Medical Scientist Training

Program for offering me the opportunity to embark on the challenging and rewarding endeavor of gaining knowledge in both biomedical science and medicine. I thank the clinical and basic science faculty at the Vanderbilt University School of Medicine who have developed and delivered courses I attended. I thank all my friends and colleagues in the Department of Pathology Program in Microbiology and Immunology for their attendance of my seminars, good questions, and helpful advice. I am also grateful for working with individuals who truly care about one another and unremittingly emphasize the importance of work-life balance. Their support has allowed me to maintain health of body and spirit during even the most challenging times. I would also like to thank the staff and faculty in the Division of Pediatric Infectious Diseases for providing a welcoming and supportive work environment as well as sharing reagents and advice. I thank Dr. Melanie Ohi and Melissa Chambers for making electron microscopy studies of reovirus a possibility.

Countless individuals have contributed immensely to my growth as a person and thus must be charged with considerable responsibility for my success in life and this doctoral training. I thank my parents for guiding me to realize that true achievement comes from conquering oneself rather than engaging in competition with fellow human beings. I am grateful to my brother whose presence in my life has made me who I am today: a strong, compassionate, and independent woman. I also owe much gratitude to the good friends I have had over the years. I thank Ewa Pieczyrak for bringing out a sense of adventure in me. I thank Anne Thierbach for teaching me how to connect with myself through reaching out to others. I thank Livia Vastag for showing me that impossibility is merely a figment of my imagination. I thank Manju Bala and Hannah Epelbaum for

grounding and centering me time after time. My wonderful partner, Lance Eckerle, has seen me through all the ups and downs of this doctoral training. His love, support, and understanding have been my fuel over the past two years. Thank you, Lance, for being my rock. I love you.

This work was financially supported by Public Health Service awards T32 GM07347 for the Medical Scientist Training Program and R01 AI76983, and the Elizabeth B. Lamb Center for Pediatric Research. Additional support was provided by Public Health Service awards P30 CA68485 for the Vanderbilt-Ingram Cancer Center and P60 DK20593 for the Vanderbilt Diabetes Research and Training Center.

TABLE OF CONTENTS

Page

LIST OF TABLES

Table Page

LIST OF FIGURES

LIST OF ABBREVIATIONS

AU	absorbance units
BBB	blood-brain barrier
BSA	bovine serum albumin
CAR	coxackievirus and adenovirus receptor
cryo-EM	cryo-electron microscopy
DAPI	4',6-diamidino-2-phenylindole
DMEM	Dulbecco's modified Eagle medium
ds	double-stranded
EM	electron microscopy
FLISA	fluorescence linked immunosorbent assay
HA	hemagglutination
HI-FBS	heat-inactivated fetal bovine serum
IC	intracranial
IDR	inter-domain region
Ig	immunoglobulin
IM	intramuscular
ISVP	infectious subvirion particle
IgSF	immunoglobulin superfamily
JAM-A	junctional adhesion molecule-A
LC-MS	liquid chromatography-mass spectrometry
M	microfold

mAb	monoclonal antibody
MEL	murine erythroleukemia cells
MFI	mean fluorescence intensity
MOI	multiplicity of infection
PBS	phosphate buffered saline
PO	peroral
PFU	plaque-forming units
RBD	receptor-binding domain
RdRp	RNA-dependent RNA polymerase
RT	room temperature
RT-PCR	reverse-transcription PCR
SA	sialic acid
SD	standard deviation
SDS-PAGE	sodium dodecyl sulfate- polyacrylamide gel electrophoresis
SEM	standard error of the mean
SMEM	spinner-modified minimum essential medium
T1	type 1
T1L	type 1 Lang
T2J	type 2 Jones
T3	type 3
T3D	type 3 Dearing
TJ	tight junction

CHAPTER I

BACKGROUND

Introduction

Attachment to cells is the first step in the viral life cycle and an important determinant of tissue tropism and pathogenesis. A precise understanding of mechanisms that govern receptor engagement is not available for most viruses. However, it is clear that this process can involve multistep adhesion accompanied by considerable conformational rearrangements of viral and host molecules (64, 66) as well as stimulation of intracellular signaling (101). Enveloped viruses engage receptors using glycoproteins that stud the outside of their lipid bilayers, e.g., the glycoprotein complex of HIV (77, 81), gp350 of Epstein-Barr virus (98), and the hemagglutinin of influenza virus (49, 70). Nonenveloped viruses engage receptors by capsid protrusions, e.g., VP4 of rotavirus (83) or indentations, e.g., VP1 of rhinovirus (35, 114). Adenovirus and reovirus are exceptions among nonenveloped animal viruses. These viruses feature elongated and flexible attachment spikes that span the equivalent of a capsid radius in length (53, 108). The distinguishing structural features of adenovirus fiber and reovirus σ1 raise the possibility that these molecules serve functions in viral replication that are distinct from cell attachment. In fact, adenovirus fiber length and flexibility determine adenovirus tropism (120) and internalization (139) efficiency, respectively. However, it is not understood how the conformation of the reovirus attachment molecule contributes to receptor

engagement and subsequent replicative steps. Development of this understanding is the goal of this doctoral thesis.

Mammalian orthoreoviruses (reoviruses) are nonenveloped viruses composed of two concentric protein shells (43) that enclose 10 segments of double-stranded (ds) RNA (60). Sequence analysis (100), electron microscopy (EM) studies (53), and high-resolution crystal structures (32, 73, 113) have revealed that the reovirus attachment molecule σ1 is a flexible filamentous trimer with segmented morphology. The virion-proximal tail of the protein is composed of a long α-helical coiled-coil followed by an unstructured flexible region and a stretch of seven triple β-spiral repeats interrupted by a short coiled-coil and another amorphous region of flexibility. The tail of σ1 ends in a globular head composed of two Greek-key motifs that fold into a compact β-barrel. The reovirus attachment protein serves its function by engaging cellular receptors using two distinct receptor-binding domains (RBDs) via adhesion strengthening (7, 8, 30, 73, 113). Sequences in the σ1 tail of type 3 (T3) reoviruses bind sialic acid (SA) (105), whereas sequences in the σ1 head engage serotype-independent receptor junctional adhesion molecule-A (JAM-A) (8).

Structural and functional parallels between adenovirus fiber and reovirus σ1 are quite obvious. Both proteins are flexible (32, 34, 53, 123), trimeric (34, 125) filaments that serve as attachment spikes (34, 79). Both fiber and σ1 engage receptors that are immunoglobulin superfamily (IgSF) members, coxackie virus and adenovirus receptor (CAR) (13, 128) and JAM-A (8), respectively. However, σ1 with its two amorphous regions of flexibility (32, 53) appears to have greater potential for intramolecular mobility. In fact, EM and cryoelectron microscopy (cryo-EM) evidence suggests that σ1

folds on the virion surface and assumes an extended conformation only upon proteolytic processing of the outer capsid to form infectious subvirion particles (ISVPs) during viral disassembly (43, 54). Another difference between the adenovirus fiber and σ1 is the mode of receptor engagement. Most adenoviruses engage CAR as their sole receptor (13, 128). In contrast, σ1 sequentially interacts with SA and JAM-A via adhesion strengthening (7, 8, 30, 105). These discrepancies suggest that functions of fiber and σ1 may be similar but not identical.

In my dissertation research, I attempted to define the role of σ1 length and flexibility in reovirus replication since these structural features distinguish σ1 among other nonenveloped virus attachment spikes. In Chapter II, I report the role of σ1 flexibility in stable σ1 encapsidation. In Chapter III, I present a systematic study of the role of σ1 length and flexibility in reovirus replication. Finally, in Chapter IV, I present preliminary EM studies of virion-associated σ1 molecules. This work enhances an understanding of events at the virus-cell interface that lead to productive infection. My research also paints a picture of σ1 as a participant in replicative steps other than cell attachment. This new knowledge may inform development of reovirus vectors for vaccine delivery and oncolytic purposes.

The reovirus virion and the reovirus attachment protein σ1

The reovirus genome is composed of three large (L), three medium (M) and four small (S) gene segments (59, 94, 119, 134) (Figure I-1A). The names of reovirus proteins are derived from letters designating the encoding gene segment: λ for L, μ for M, and σ for S. The inner core of reovirus is made up of 60 asymmetric λ1 dimers and 150 σ2

monomers (43). Minor inner core components μ2 (20 copies/particle) and λ3 (12 copies/particle) (36) are involved in RNA binding and RNA-dependent RNA polymerization (37, 68, 71). Pentameric turrets of λ2 span both protein shells of the capsid and enclose the N-terminus of the reovirus attachment molecule σ1 at the virion vertices (43). The outer capsid is composed of 200 heterohexamers of μ1 and σ3 (43). Sigma 3 functions as the cap for the membrane-penetrating protein μ1 (43) (Figure I-1A and B). The nonstructural protein σ1s plays an important role in hematogenous dissemination of reovirus, but it is dispensable for reovirus replication in cultured cells (15, 16). Other nonstructural reovirus proteins σNS, μNS, and μNSC have more elusive functions but appear to be involved in reovirus RNA packaging and assembly of new particles (4).

Structural analysis of the C-terminal two-thirds of type 3 Dearing (T3D) σ1 (residues 170–455) (113) reveals the presence of two main structural segments: an N-terminal β-spiral repeat region (residues 170-309) interrupted by a short α-helix (residues 236-250) and a head composed of eight anti-parallel β-sheets folded into two Greek key motifs at the C-terminus (residues 310-455) that folds into a compact β-barrel in the σ1 trimer (Figure I-2). Loops connecting the individual strands of the σ1 head are short with the exception of the loop connecting β strands D and E (D-E loop), which contains a 3_{10} helix. The tertiary structure of the σ1 tail is unusual in that in contains triple β-spiral repeats, a rare trimerization motif found to date only in reovirus σ1 (32, 113), the adenovirus fiber (111), and the PRD1 bacteriophage P5 spike protein (91). Sequence analysis (100) and recent crystallographic data (unpublished) suggest that the N-terminus

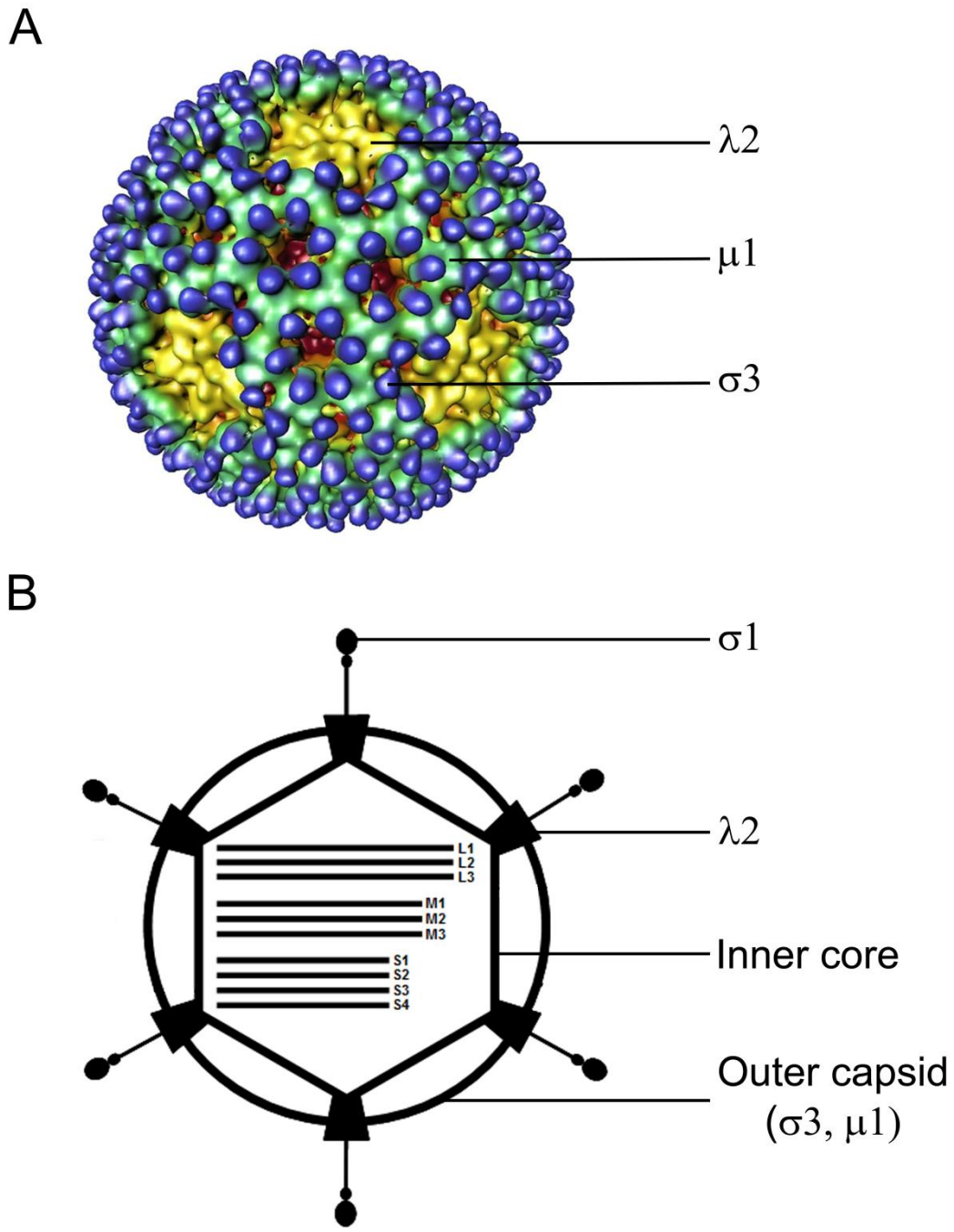

FIGURE I-1. Structure and composition of the reovirus virion. (A) Cryo-electron microscopic rendering of the reovirus virion. Major outer capsid proteins are pointed out. The trimeric σ1 molecule could not be reconstructed using this technique due to a symmetry mismatch with the icosahedral virion. Image adapted from Nason et al. (97). (B) Schematic representation of the reovirus virion. The bulk of the outer capsid is composed of σ3 and μ1. Reovirus σ1 is tethered to the virion by pentameric turrets of λ2 at capsid vertices. The inner core encloses the reovirus genome composed of ten segments of double-stranded RNA.

of σ1 is α-helical in nature. The unstructured flexible linkers of the reovirus attachment protein termed inter-domain regions 1 and 2 (IDR1 and 2) are located at the α-helix/β-spiral junction in the tail (residues 155-166) and at the C-terminal head (residues 291-294), respectively (32, 53) (Figure I-3).

Structural analysis of the C-terminus of σ1 (residues 246-455) shows a distinct bend between the three-fold axes of the head and tail domains of the molecule (32). While this bend was likely induced by crystal packing forces, its presence suggests a considerable potential for mobility at IDR2. Interestingly, EM images of full-length σ1 also show three distinct regions of flexibility in the reovirus attachment protein (53). Two of these regions dimensionally correspond to IDR1 and IDR2, and the third is located at the virion-enclosed N-terminus of σ1 (Figure I-2, Figure I-3). This flexibility within the reovirus attachment protein may allow movement of the spatially-separate RBDs with respect to one another and the rest of the virion during receptor engagement or viral assembly or disassembly.

Potential for structural rearrangement in σ1

Pentameric turrets of λ2 enclose the N-terminus of trimeric σ1 at virion vertices (43). While such symmetry mismatches have been observed elsewhere (e.g., adenovirus penton base and fiber (19), VP1/VP2 polyomavirus complex (33), AB_5 toxins (50), the F1 ATP synthase (1)), they are certainly not common and indicate interactions of limited specificity or strength. Proteins making such contacts with each other often undergo rearrangements. Therefore, the 3:5 relationship of σ1: λ2 indicates a strong potential for

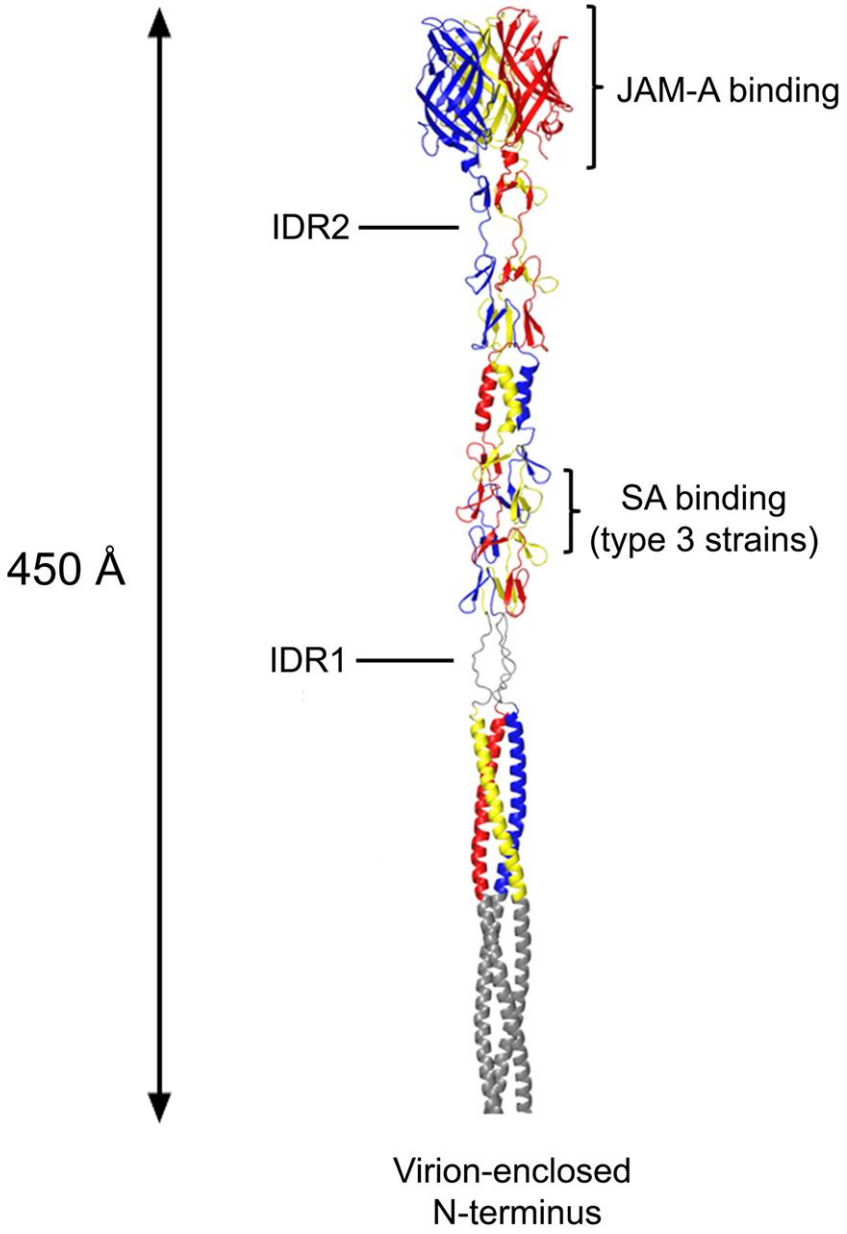

FIGURE I-2. Ribbon diagram of full-length reovirus σ1. This model is based on the available crystal structures of σ1 fragments (depicted in color) (32, 113) and predictions from sequence analysis (depicted in grey) (100). The virion-enclosed N-terminus gives rise to a long coiled-coil that is followed by a flexible linker IDR1 and a sequence of seven triple β-spiral repeats interrupted by a short coiled-coil and another flexible region (IDR2). The compact β-barrel head of σ1 binds junctional adhesion molecule-a (JAM-A) and β-spiral repeats 2 and 3 of the σ1 tail engage sialic acid (SA) in type 3 reoviruses.

structural reorganization at icosahedral vertices of the reovirus particle following receptor engagement or during disassembly.

Evidence suggests that the σ1 molecule undergoes major conformational changes during uncoating. These structural alterations may aid σ1 in receptor binding or destabilize σ1 at capsid vertices to facilitate efficient functional disassembly of the reovirus particle in the endosome. EM studies of reovirus virions and ISVPs suggest that σ1 is folded on the virion surface and assumes an extended conformation only upon proteolytic cleavage of σ3 in the ISVP (54). Cryo-EM renditions of type 1 Lang (T1L) reovirus virions lack visible σ1 at capsid vertices (Figure I-4) (43). However, similar reconstructions of T1L ISVPs reveal discontinuous densities that extend approximately 100 Å from the fivefold symmetry axes of the particles (Figure I-4) (43). Full-length virus-bound σ1 could not be reconstructed using cryo-EM because σ1 trimers do not obey icosahedral symmetry required for image reconstruction of reovirus particles by icosahedral averaging. Moreover, σ1 possesses structural flexibility, which also may preclude its visualization by this technique.

Another potential source of structural instability in σ1 is an unusual cluster of conserved aspartic acid residues located in the base of the σ1 head at the trimer interface (116). EM evidence suggests that the head of σ1 can assume a multilobed conformation (53). Hence, the aspartic acid cluster may allow pH-dependent conformational changes in σ1 following reovirus entry into the acidic environment of the endocytic compartment. Acid-dependent structural protein rearrangements of enveloped viruses, such as influenza (21) and tick-borne encephalitis virus (124), are well-documented. The significance of the structural instability at the base of the σ1 head is poorly understood.

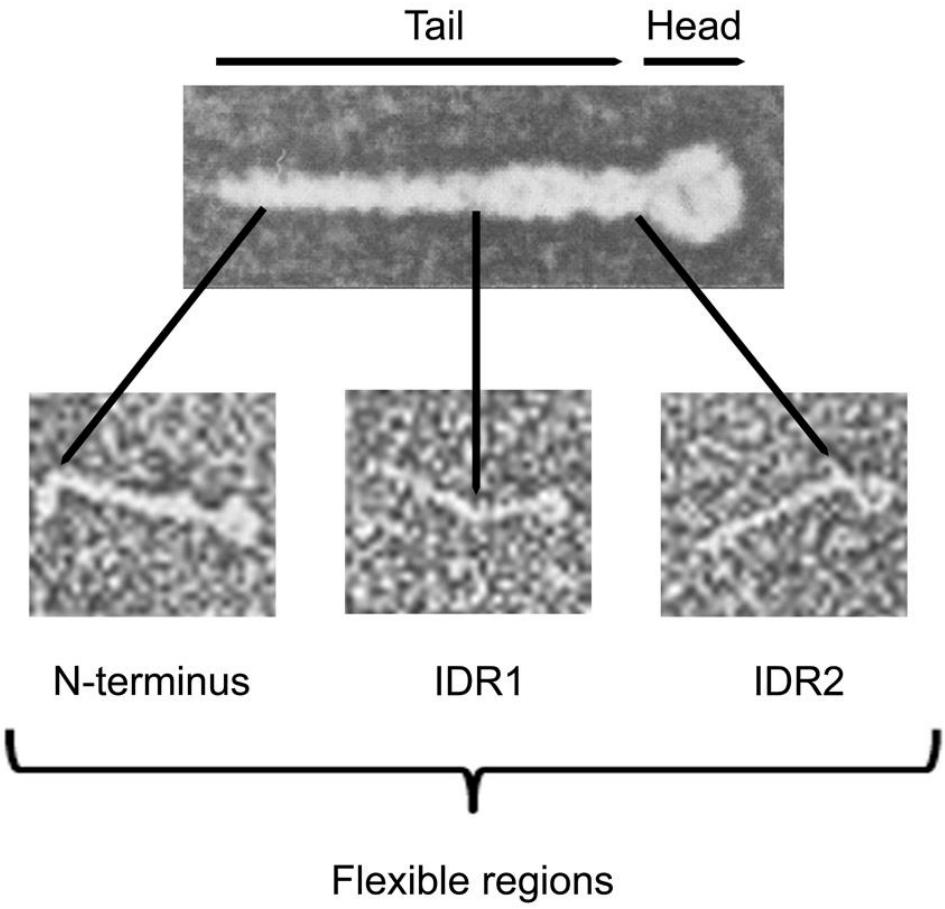

FIGURE I-3. Regions of flexibility within the σ1 protein. These computer-processed electron micrographs of negatively-stained σ1 show the reovirus attachment molecule in four different conformations. Regions of flexibility within the protein at the N-terminus, IDR1, and IDR2 are pointed out. Images adapted from Fraser et al. (53).

JAM-A and its interactions with σ1

JAM-A is a serotype-independent proteinaceous receptor for reovirus (8). This type I transmembrane protein is a widely-expressed IgSF member involved in tight junction (TJ) formation (82). JAM-A is composed of two concatenated extracellular immunoglobulin-like (Ig-like) domains (D1 and D2), a single transmembrane region, and a cytoplasmic tail that contains a PDZ-binding motif (82, 90, 103, 110). High-resolution crystal structures of the extracellular segments of JAM-A suggest that JAM-A forms

homodimers via cis-interactions of the membrane-distal D1 domains (110) (Figure I-5A). Homophilic trans-interactions between JAM-A monomers on adjacent cells may also be possible (76). The cytoplasmic PDZ-binding motif of JAM-A interacts with PDZ domains of scaffolding proteins (e.g., AF6 and ZO-1 (47))) and signal mediators

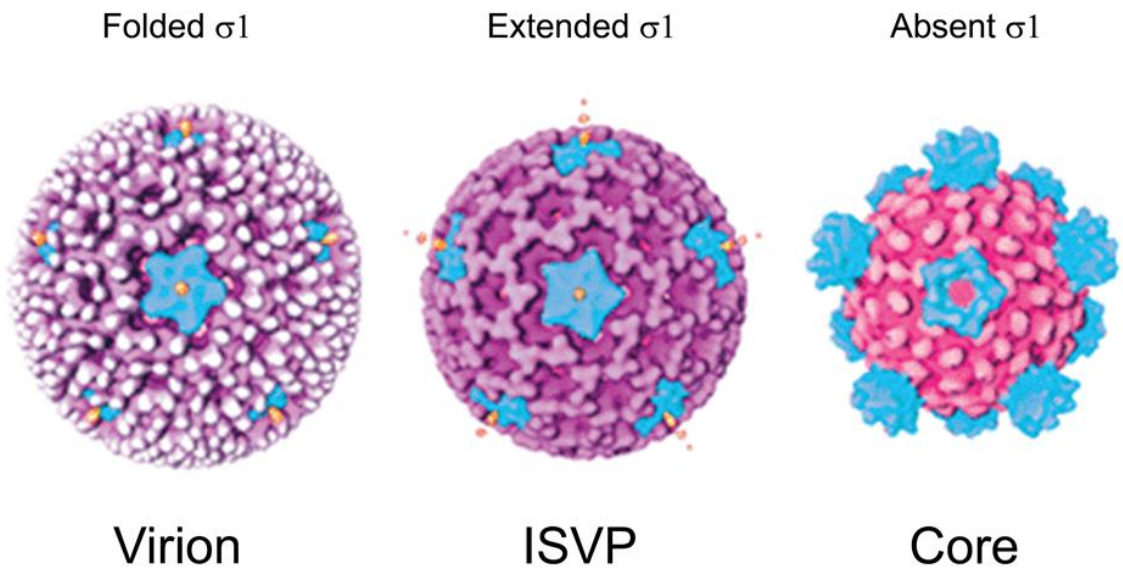

FIGURE I-4. Reovirus disassembly intermediates. Surface-shaded cryoelectron microscopy reconstructions of reovirus particles viewed along a fivefold symmetry axis. Progression of changes in the physical relationship between σ1 and the capsid is pointed out. Image adapted from Dryden et al. (43).

(e.g., Par3 (69)). Deletion of JAM-A dimerization or PDZ-binding domains results in defective epithelial cell migration (118). However, outside-in signaling mediated via JAM-A is poorly understood.

JAM-A monomers associate in an “arm-wrestling” grip via a large concave dimerization interface composed of four β-strands (C, C’, F, and G) located in the

membrane-distal D1 domain (110) (Figure I-5A). Four salt bridges found at the center of this binding interface are the principal means of interaction between JAM-A monomers. These bonds are formed by Arg59, Glu61, Lys 63, and Glu121. All of these residues are buried and inaccessible to solvent. Salt bridges are usually energetically favorable interactions, but their stability depends on the characteristics of the surrounding environment. The energy associated with salt bridge formation is increased under apolar conditions, and diminished by surroundings of high ionic strength or low pH. Concordantly, JAM-A can dissociate into monomers when exposed to high salt or acidic environments (11). This dynamic nature of the JAM-A dimerization interface may allow the association between JAM-A and the C-terminus of reovirus σ1 (Figure I-5B, Figure I-6).

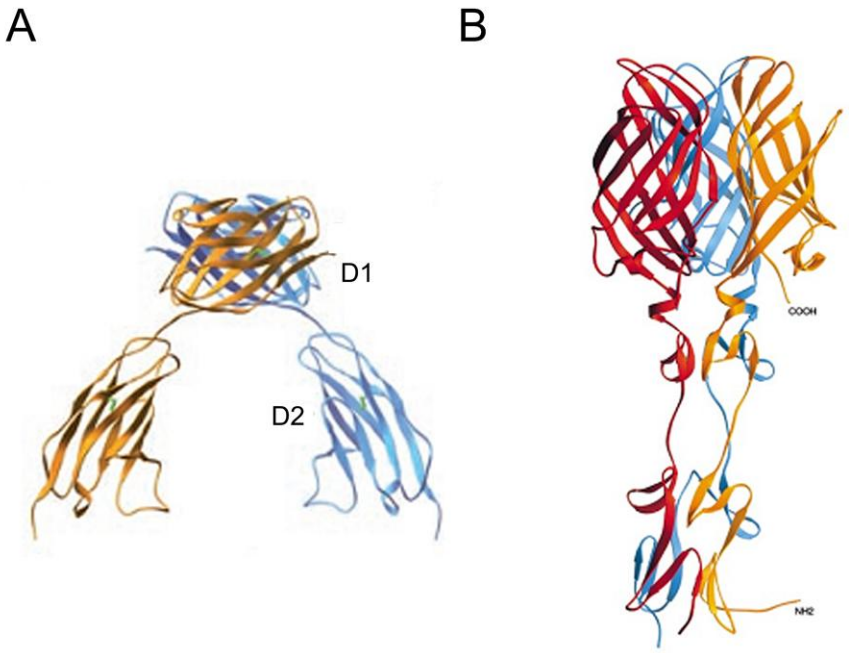

FIGURE I-5. Structures of JAM-A and σ1. (A) Crystal structure of JAM-A monomers (depicted in blue and yellow) interacting in an "arm-wrestling" grip via their D1 domains. Image adapted from Prota et al. (110) (B) Crystal structure of the JAM-A-engaging C-terminal region of σ1. Monomers of σ1 are shown in blue, yellow, and red. Image adapted from Chappell et al. (32).

JAM-A was identified as a receptor for reovirus by flow cytometry-based expression cloning using a human neuronal precursor cDNA library (8). Three lines of evidence support this discovery. First, transient expression of JAM-A in normally non-permissive cells results in reovirus binding and infection (8). Second, treatment of normally permissive cells with JAM-A specific antibodies prevents reovirus binding and

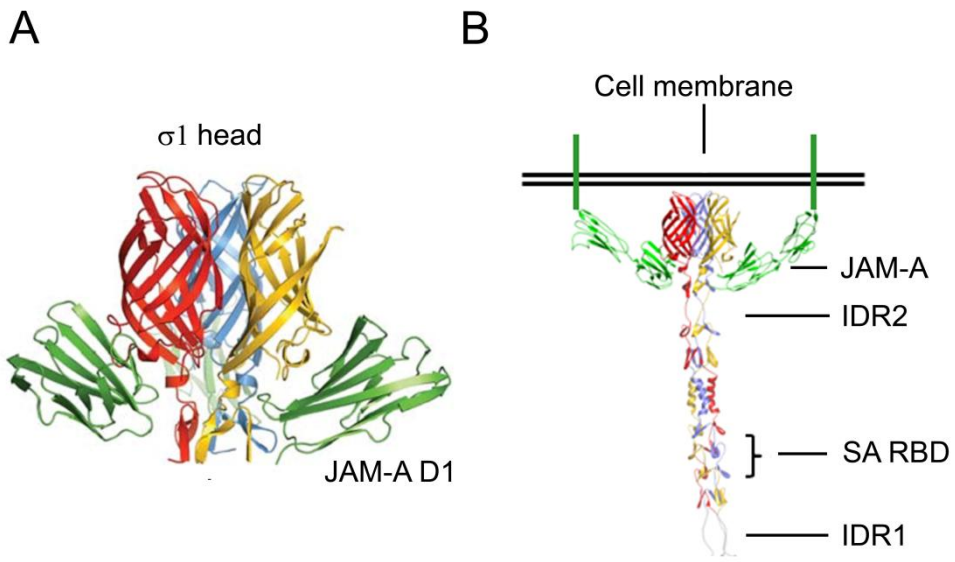

FIGURE I-6. Sigma 1 interactions with JAM-A. (A) Crystal structure of the complex between σ1 head trimers (depicted in blue, yellow, and red) and monomeric JAM-A D1 domains (depicted in green) viewed from the side. Image adapted from Kirchner et al. (73). (B) Model of σ1 trimer (depicted in blue, yellow, and red) interaction with JAM-A monomers (depicted in green) at the cell surface. Image adapted from Prota et al. (110), Kirchner et al. (73), and Reiter et al. (113).

infection (8). Third, the K_D of the interaction between σ1 and JAM-A is 6×10^{-8} M (8), which suggests that reovirus has a very high affinity for JAM-A.

Compelling evidence also suggests that the head of reovirus σ1 interacts with the D1 domain of JAM-A (Figure I-6A and B). Release of σ1 during reovirus core formation results in a 1,000,000-fold loss of infectivity (27). T3 reovirus infection can be

neutralized by monoclonal antibody 9BG5 which recognizes a conformationally-specific epitope in the σ1 head (22, 107). Concordantly, the capacity of 9BG5 to bind and neutralize reovirus is markedly diminished upon proteolytic processing of σ1 during ISVP formation (99). ISVPs also have diminished infectivity in comparison with virions (99), but they retain the capacity to engage SA (29). Taken together, these findings suggest that σ1 contains at least two separate RBDs and that the σ1 head facilitates receptor interactions that are distinct from SA binding mediated by the σ1 tail. In turn, domain-swapping experiments revealed that JAM-A engages the σ1 head via the D1 domain (52).

The formation of the JAM-A-σ1 complex (Figure I-6A and B) is preferred to JAM-A D1 dimerization. The K_D of the JAM-A D1-σ1 interaction is approximately 1000-fold lower than that of the association between two JAM-A D1 domains (61, 73). Additionally, chemical cross-linking of JAM-A prevents reovirus binding to JAM-A *in vitro* and negates the competitive effect of soluble JAM-A on reovirus attachment to cells (52). These findings are supported by a 3.4-Å crystal structure of the σ1 head in complex with the D1 domain of JAM-A (73), which shows that each σ1 monomer binds a single JAM-A molecule (Figure I-6A). Therefore, up to three JAM-A monomers may form a clamp around the σ1 head during reovirus attachment at the cell surface (Figure I-6B).

Reovirus engages the concave surface of the JAM-A dimerization interface primarily via the long D-E loop of the σ1 head (73). These contacts are largely polar in nature, featuring numerous salt bridges and hydrogen bonds. There are also important hydrophobic interactions between the very C-terminal β-spiral of the σ1 tail and the membrane-distal regions of the JAM-A D1 domain (73). The majority of residues

involved in JAM-A dimerization also engage σ1 (73, 110). The stability of the σ1-JAM-A interaction lies in the nearly perfect complementarity of the interacting surfaces. In contrast, JAM-A dimers contain a water-filled 6.9 Å-cavity at the dimerization interface (73, 110). Interactions of water molecules with amino acid residues involved in salt bridge and hydrogen bond formation may weaken the homophilic interaction of JAM-A monomers.

Interactions of sialic acid with σ1

The first step of reovirus attachment is the binding reovirus σ1 to cell-surface SA (Figure I-7). This low-affinity interaction brings the virus in close proximity to the plasma membrane and allows it to diffuse laterally and later engage its primary receptor JAM-A in an essentially irreversible fashion (7). Although JAM-A is a serotype-independent receptor for reovirus (8), the major reovirus serotypes appear to recognize different carbohydrates, which may explain serotype-specific differences in routes of spread and tropism for host tissues (130, 136, 137).

T1L, type 2 Jones (T2J), and T3D reoviruses all display the capacity to agglutinate erythrocytes of several mammalian species (80). In type 3 reoviruses, this property is mediated by σ1 interactions with terminal α-linked SA residues on several glycosylated proteins such as glycophorin A (55, 106). Treatment of L929 cells with neuraminidase to remove cell-surface SA diminishes reovirus binding (55). Type 3 reovirus attachment to L929 cells can be blocked by sialosides containing terminal α-2,3- and α-2,6-linked sialic acid moieties (105). T1L reovirus bearing SA-binding T3D σ1

proteins binds SA-containing glycophorin with an avidity of 5×10^{-9} M (7), a property mediated by the tail of the σ1 attachment protein (30).

Interactions of σ1 with SA at the cell surface is required for T3 reovirus infection of murine erythroleukemia (MEL) cells (115). Studies of T3 reovirus field isolates have revealed that Asn198, Arg202, and Pro204 located in the σ1 tail determine the capacity of reovirus to perform these functions (31, 39). Attachment to SA also changes the reovirus-host interaction *in* vivo. SA binding accelerates reovirus spread from the intestine to secondary sites of infection in newborn mice (9). Moreover, the capacity to engage sialic acid allows reovirus to infect bile duct epithelium, which results in obstructive liver disease (9).

The crystal structure of the σ1 head and β-spiral region in complex with α-2,3-siallyllactose has been determined at a 2.25-Å resolution (113) (Figure I-7). The oligosaccharide binds in a shallow groove adjacent to the loop connecting the second and third β-spiral repeats of the σ1 tail. The trimeric σ1 protein contains three identical SA RBDs that show indistinguishable contacts with α-2,3-sialyllactose in the crystal structure. Interestingly, σ1 can also form complexes with α-2,6-siallylactose and α-2,8-disiallylactose. Contacts between the terminal sialic acid moieties of these compounds and the σ1 protein resemble those of α-2,3-sialyllactose at the σ1 SA RBD. Point mutations at Asn198, Arg202, Leu203, Pro204, and Gly205 of σ1 result in diminished reovirus hemagglutination (HA) capacity and MEL cell infection, suggesting that these residues are required for efficient SA engagement by reovirus (113).

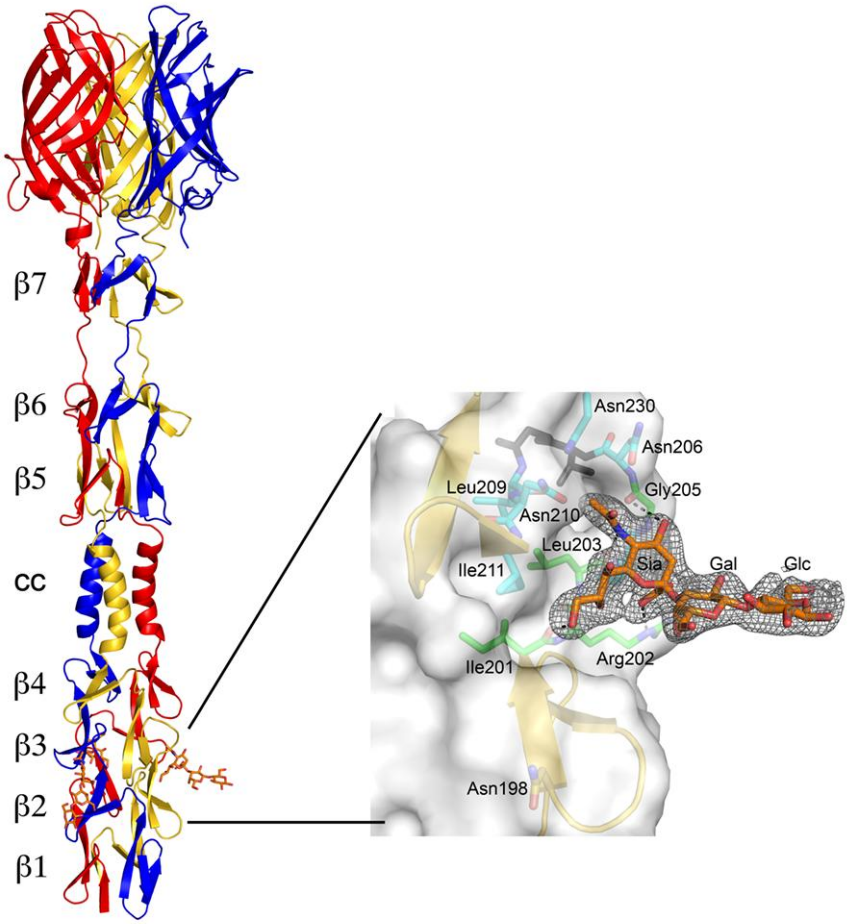

FIGURE I-7. Interactions of sialic acid with σ1. Ribbon diagram of the T3D σ1 tail and head domains in complex with α-2,3-sialyllactose. Monomers of σ1 are shown in red, blue, and yellow. The body domain consists of seven triple β-spiral repeats (β1-β7) and a helical coiled-coil domain (cc) that is inserted between β-spiral repeats β-4 and β-5. The bound α-2,3-sialyllactose is shown in stick representation and colored in orange. The density map inset shows the sialic acid binding domain of σ1 in more detail. The sugar moieties are labeled Sia (sialic acid), Gal (galactose), and Glc (glucose). Images adapted from Reiter et al. (113).

Type 1 reoviruses engage SA in some contexts. T1 reoviruses do not bind or infect MEL cells (115), and they do not show decreased infection upon neuraminidase treatment of L929 cells (99). However, T1L, but not T3D, binds the apical surface of microfold (M) cells in rabbit Payer's patches (65). This property segregates with the S1

gene and can be blocked by pre-incubating tissue with lectins that recognize α-2,3-linked SA. Taken together, these findings suggest that the functional glycans engaged by T1 and T3 reoviruses are different, even though these glycans appear to terminate in α-2,3-linked sialic acid. Concordantly, studies using expressed σ1 protein chimeras suggest that T1L σ1 engages carbohydrates using a domain that is distinct from the T3D σ1 SA RBD (30).

Reovirus attachment to cells via adhesion strengthening

The presence of two spatially-distinct RBDs in T3 reovirus attachment protein σ1 (73, 113) suggests that reovirus binding to the cell surface is a multi-step process. Monoreassortant reoviruses containing σ1 molecules of either SA-binding T3C44-MA or SA-non-binding T3C44 field isolates in a T1L genetic background (T3SA+ and T3SA-, respectively) were used to study the mechanism of reovirus attachment to cells (7). Sequences of T3SA+ and T3SA- σ1 molecules differ by a single amino acid residue at position 204 (proline for T3SA+ and leucine for T3SA-). Proline at position 204 of σ1 correlates with reovirus capacity to engage SA (39). In radioligand binding studies, the steady state avidity of T3SA+ for HeLa cells was determined to be approximately five-fold higher than that of T3SA- (7). This increased binding was attributable to an accelerated k_{on} of T3SA+. The steady state avidity and k_{on} of T3SA+ both decreased to levels observed for T3SA- following treatment of cells with neuraminidase, suggesting that the higher avidity and k_{on} of T3SA+ are both attributable to SA binding. T3SA+ but not T3SA- reovirus infection of HeLa cells is blocked by adding sialyllactose to the virus inoculum during the first 30 minutes of virus adsorption (7). In contrast, the capacity of neutralizing mAb 9BG5 specific for the σ1 head to inhibit infectious attachment of both

T3SA+ and T3SA- reoviruses to HeLa cells remained evident even at late times during virus adsorption (7). Taken together, these findings suggest that reovirus engages its receptors via the process of adhesion strengthening, in which the initial rapid but low-affinity binding to SA is followed by higher-affinity binding to JAM-A. In this model, engagement of SA serves to concentrate reovirus on the cell surface and enable lateral diffusion of virions until they encounter JAM-A. A similar receptor engagement strategy has been proposed for α-herpesviruses. Their primary interaction with cells occurs between viral glycoproteins and heparin sulfate, whereas virus penetration is mediated by a proteinaceous receptor (e.g., HVEM or nectins) (23).

Reovirus internalization, disassembly, and particle formation

Following adhesion strengthening, reovirus is internalized via receptor-mediated endocytosis (17, 85) (Figure I-8). A JAM-A truncation mutant lacking the cytoplasmic tail can support reovirus infection in normally non-permissive cells, suggesting that cellular factors other than JAM-A are responsible for assembling the internalization machinery required for reovirus entry (84). Concordantly, there is evidence to suggest that β1 integrins serve as reovirus internalization receptors. First, the surface-exposed loops of outer-capsid protein λ2 contain integrin-binding motifs KGE and RGD (20, 112, 117). Second, antibodies against β1 but not other integrins block reovirus infection (84). Reovirus ISVPs do not require endocytosis for entry and their infection is not inhibited using β1 integrin-specific antibodies (17, 84). Third, β1 integrin-deficient cells are substantially less susceptible to reovirus infection than β1 integrin-expressing cells. However, ISVPs infect both of these cell types equally (84).

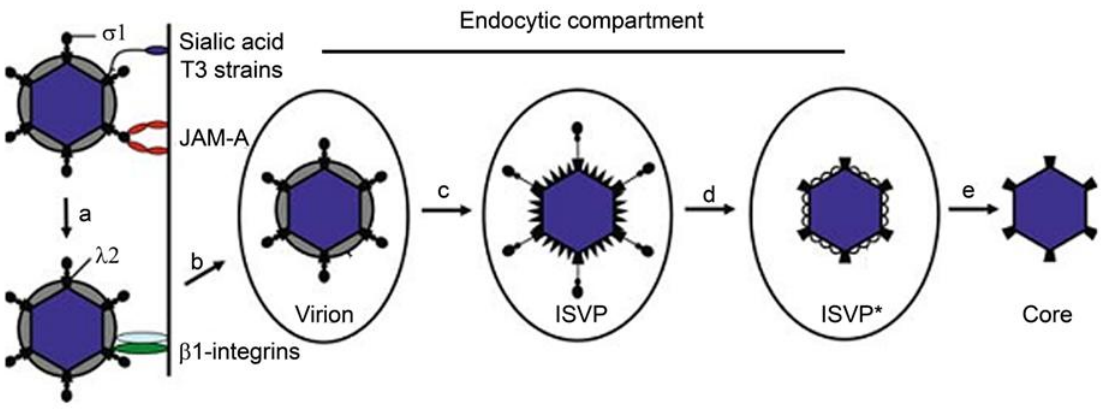

FIGURE I-8. Schematic of the reovirus cell entry pathway. Following attachment to cell-surface carbohydrate (sialic acid for T3 strains) and JAM-A (a), reovirus undergoes β1-integrin-dependent endocytosis (b). Upon internalization, virions undergo pH-dependent proteolytic processing in the endocytic compartment. The first disassembly intermediate is the ISVP (c) characterized by loss of σ3, cleavage of μ1, and conformational changes in σ1. Shedding σ1 and exposure of hydrophobic regions in μ1 transforms ISVPs into ISVP*s (d). ISVP* formation is associated with membrane penetration and release of reovirus cores into the cytoplasm (e). Cores are the end-product of reovirus disassembly. These particles lack all outer capsid proteins and are transcriptionally-active. Figure adapted from Danthi et al. (38).

This β1 integrin-dependent reovirus internalization can occur via the formation of clathrin-coated pits. Reovirus virions have been observed to colocalize with clathrin in living cells (48). Additionally, treatment of cells with a clathrin-specific inhibitor (chlorpromazine) diminishes reovirus internalization and infection (85). Beta1 integrins also contain a cytoplasmic NPXY motif. Many cellular receptors use this motif to recruit adaptor protein 2 or disabled protein 2 to initiate clathrin assembly at the plasma membrane (95, 102). Concordantly, when the β1 integrin NPXY is substituted with NPXF, reovirus internalization becomes inefficient (85). Interestingly, NPXF β1 integrins also traffic reovirus to the lysosome for degradation (85). Taken together, these

findings suggest that β1 integrins are required for clathrin-dependent reovirus endocytosis and appropriate intracellular trafficking of reovirus particles.

Once in the endocytic pathway, reovirus undergoes functional protease-mediated disassembly. The first intermediate in this process is the ISVP, which is characterized by the loss of σ3, cleavage of μ1 into the δ and φ fragments, and a conformational change in σ1 (5, 18, 28, 122, 126) (Figure I-4, Figure I-8). The acid-dependent endosomal cysteine proteases cathepsins B and L are responsible for reovirus uncoating in fibroblasts (5, 40, 126). These enzymes have also been identified as facilitators of Ebola virus (26), Hendra virus (104), and SARS coronavirus (67) infection. The acid-independent cathepsin S mediates disassembly of some reovirus strains in macrophages (57, 58). Reovirus virions can also be converted to ISVPs in the small intestine of newborn mice following peroral inoculation by the resident serine proteases trypsin and chymotrypsin (10, 14). The physical and functional properties of ISVPs generated by intestinal and endocytic enzymes appear to be identical (6, 46). A subsequent reovirus disassembly intermediate, the ISVP*, is characterized by changes in the conformation of the μ1 δ fragment, loss of σ1 from the pentameric λ2 turrets at capsid vertices, and an increase in the overall hydrophobicity of the particle (24, 25) (Figure I-8). In contrast to virions and ISVPs, ISVP*'s are transcriptionally active, and their formation correlates with reovirus membrane penetration and entry into the cytoplasm (24, 25).

Reovirus cores are the end-products of disassembly (Figure I-4, Figure I-8). These particles are characterized by a 1,000,000-fold decrease in infectivity compared with virions due to loss of all outer-capsid proteins (μ1, σ1, and σ3) (27). Cylindrical channels enclosed by λ2 turrets at the vertices of viral cores connect the interior of the reovirus

core with the outside environment (43). In virions and ISVPs, these cavities are obstructed by the N-terminus of σ1 (43). The inside surfaces of λ2 channels have guanylyltransferase and methyltransferase capacities and function as mRNA capping complexes (112).

The reovirus core owes its title of a "molecular machine" to its capacity to synthesize capped viral mRNA transcripts *in vitro* when incubated with the appropriate substrates (140). Concordantly, particles similar to cores are thought to initiate transcription of the reovirus genome when exposed to the cytoplasm. Core proteins λ3 and μ2 form the RNA-dependent RNA polymerase (RdRp) complex of reovirus (37, 68, 71). Nascent viral mRNAs are capped in λ2 channels (112) as they exit reovirus cores (56) and serve as templates for viral protein synthesis.

Reovirus particle assembly takes place in non-membranous intracytoplasmic inclusions composed of viral RNA and proteins (129). Studies of inclusions in infected cells and inclusion-like assemblies induced by ectopic protein expression suggest that multimers of μNS form the essential inclusion matrix and recruit σNS and structural proteins for particle assembly (129). The order of inner and outer capsid shell formation is not known. However, pre-formed multimers of σ3 and μ1 may be required for outer capsid assembly (129). The mechanism of σ1 encapsidation is not understood.

Reovirus pathogenesis

Reoviruses have a wide geographic distribution and infect virtually all mammals (129) but cause significant disease only in the very young (88, 127). Newborn mice have been used as the preferred experimental system for the study of reovirus pathogenesis

because they are especially susceptible to reovirus infection (133). Following oral or intramuscular inoculation of newborn mice, T1 and T3 reovirus strains use different routes of dissemination to the CNS and produce distinct patterns of disease. T1 reovirus disseminates via the blood stream, infects ependymal cells and causes non-lethal hydrocephalous (130, 136, 137). In contrast, T3 reovirus spreads via both neural and hematogenous routes and infects neurons, which leads to lethal encephalitis (15, 96, 127, 130, 136, 137). Studies with T1×T3 reassortant viruses have shown that these differences segregate with the S1 gene segment (41, 130, 137), which encodes attachment protein σ1 and a nonstructural protein σ1s (79, 135). Since receptor engagement often correlates with virus tropism, these studies implicate σ1 as the main disease determinant. However, σ1s is required for the hematogenous dissemination of reovirus (15, 16). Therefore, σ1 is not the only determinant of reovirus spread and tropism.

Significance of research

Reovirus provides a well-established and highly-tractable experimental system to study the mechanisms that underlie viral disease. In my work, I employed plasmid-based reverse genetics (74, 75) to investigate the role of discrete regions of σ1 in the reovirus replicative cycle. This approach represents an innovative strategy that overcomes long-standing obstacles in the field to engineering reovirus mutants with specific and considerable deletions of protein sequence. Research using reoviruses bearing σ1 proteins of varying length and flexibility allowed me to learn that the role of σ1 in reovirus replication is not limited to attachment. My findings suggest that σ1 flexibility allows reovirus to efficiently exit the endocytic compartment and permits stable σ1

encapsidation. Mechanisms underlying these new functions of σ1 remain to be elucidated. Therefore, research described in this doctoral thesis opens a field of scientific inquiry about reovirus σ1 that has not been explored previously.

Since it is non-pathogenic in humans (129), reovirus is currently being tested in clinical trials as a vector for vaccine delivery and oncolytic purposes. Reovirus preferentially infects transformed cells (44, 63) and kills them at least in part via induction of apoptosis (89). Altering reovirus tropism by structural modification of σ1 could broaden the range of tumors treatable using reovirus-based therapies. On the other hand, the immunogenic potential of reovirus σ1 could be employed to generate recombinant vaccine vectors for a variety of communicable diseases. In fact, reovirus-based vaccine vectors bearing σ1 molecules that contain short sequences of HIV glycoproteins are currently being tested in our laboratory. Development of reovirus-based oncolytics and vaccines requires an understanding of the functions of submolecular structures of σ1 in reovirus replication. Modification of inappropriate sites within σ1 could result in the generation of defective vectors. Therefore, research presented in this dissertation may contribute to improved design of reovirus-based therapeutics.

CHAPTER II

FLEXIBILITY AT INTER-DOMAIN REGION 1 OF REOVIRUS σ1 IS REQUIRED FOR STABLE σ1 ENCAPSIDATION

Introduction

The reovirus attachment molecule σ1 is a long and flexible filament (32, 43, 53, 79). These structural features distinguish σ1 among the attachment spikes of other nonenveloped animal viruses that engage their receptors via capsid protrusions (e.g., VP4 of rotavirus (83)) or indentations (e.g., VP1 of rhinovirus (35, 114)). Negative-stain EM images of reovirus particles suggest that σ1 is folded on the virion surface and assumes an extended conformation only in the ISVP (54). Concordantly, cryo-EM images reveal a σ1 density extending 100 Å away from capsid vertices in ISVPs but not virions (43). Moreover, ISVPs are more susceptible to loss of infectivity following exposure to heat, presumably in part due to release of σ1 from λ2 turrets (93). Therefore, the capacity of σ1 to assume a folded conformation at the fivefold symmetry axes of the virion may be required to maintain the filamentous σ1 within the outer capsid.

In this chapter, I investigated the role of σ1 length and flexibility in stable σ1 encapsidation. I used reverse genetics (74, 75) to generate a panel of reovirus mutants with σ1 molecules of varying length and flexibility (Figure II-1A) and evaluated the altered σ1 proteins in terms of folding, functionality, and relative capsid content. I reduced the length of the α-helical σ1 tail to engineer L1 and L2 reoviruses and deleted midpoint and head-proximal σ1 IDRs to generate ΔIDR1 and ΔIDR2, respectively

(Figure II-1A, Table II-1). I found that the deletions introduced in σ1 to generate this mutant panel did not result in functional or conformational alterations in σ1. However, the findings indicate that σ1 IDR1, but not σ1 IDR2 or length, is required for stable σ1 encapsidation. I acknowledge Kristen Guglielmi Ogden for assistance in generating the mutants.

Results

Generation of the σ1 length and flexibility reovirus mutant panel- To investigate the function of σ1 length and flexibility in the reovirus life cycle, I engineered a panel of recombinant reoviruses bearing σ1 molecules of varied length and flexibility using reverse genetics (74, 75) (Figure II-1A). Mutations altering the length and flexibility of σ1 were introduced into the S1 gene-containing plasmid pT7-T3DS1.T249I by site-directed mutagenesis. I used a parental plasmid encoding a T249I substitution in the T3D σ1 protein to prevent proteolytic degradation of σ1 (29). As the sialic acid-binding pocket in σ1 resides in the second and third β-spiral repeats of the σ1 body domain (113), I truncated sequences in the α-helical region of the σ1 tail (45, 100) to alter σ1 length. Amino acid residues 51-100 were removed from mutant L1, and residues 83-155 were removed from mutant L2 (Figure II-1A, Table II-1). IDR1 (residues 155-164) and IDR2 (residues 291-294) were deleted from σ1 to engineer ΔIDR1 and ΔIDR2 reoviruses, respectively (Figure II-1A, Table II-1). Despite three attempts, a reovirus mutant lacking both IDR1 and IDR2 (ΔIDR12) could not be recovered (Table II-1). L and IDR mutant reovirus S1 gene sequences were verified using cDNA obtained by RT-PCR from purified viral dsRNA. Electrophoresis of the dsRNA gene segments of mutant reoviruses

revealed the anticipated genotypes (Figure II-1B). Thus, reovirus mutants with alterations in σ1 length and truncations of each of the IDRs can be recovered by reverse genetics.

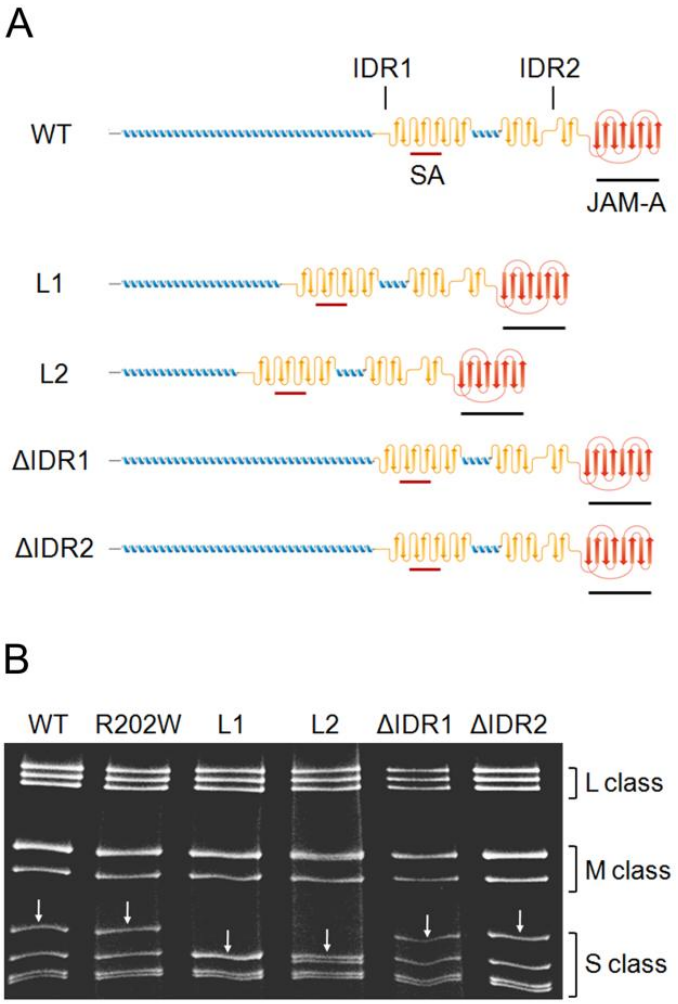

FIGURE II-1. Sigma 1 length (L) and interdomain region (IDR) reovirus mutants. (A) Schematic of wild-type (WT), L1, L2, ΔIDR1, and ΔIDR2 reovirus σ1 proteins. The α-helices, β-spiral repeats, and β-barrel are shown in blue, yellow, and red, respectively. Receptor-binding domains are indicated by underlines. SA, sialic acid; JAM-A, junctional adhesion molecule-A; IDR1, interdomain region 1; IDR2, interdomain region 2. (B) Segmented dsRNA genomes of L and IDR mutant viruses. Viral gene segments from virions of WT, R202W, L1, L2, ΔIDR1, and ΔIDR2 reovirus strains were resolved by SDS-PAGE, stained with ethidium bromide, and visualized by UV transillumination. Large (L), medium (M), and small (S) class gene segments are designated. S1 gene segments are indicated by white arrows.

Specific infectivities of the L and IDR reoviruses- As a first step to determine whether any properties attributable to σ1 are altered in the L and IDR mutants, I tested the infectivity of the L and IDR reoviruses by calculating particle:plaque-forming-unit (PFU) ratios for several independent purifications of each virus (Table II-1). The majority of virus stocks had particle:PFU ratios between 150 and 650, which is consistent with previously reported values for reovirus (42, 62). Despite some sample-to-sample variation, only ΔIDR1 had a significantly higher particle:PFU ratio compared with wild-type (WT) virus (Student's *t* test, $P < 0.01$). This result suggests that removal of IDR1 from the σ1 molecule diminishes the efficiency of reovirus replication.

TABLE II-1. Characterization of L and IDR mutant reoviruses.

Virus strain	Mutation in σ1	Particle:PFU ratio[a]
WT[b]	-	149.1 (8)
R202W[c]	R202W	162.1 (3)
L1	Δ 51Q-100S	245.3 (3)
L2	Δ 83R-155Q	213.4 (6)
ΔIDR1	Δ 155Q-164T	543.0 (5)[d]
ΔIDR2	Δ 291S-294P	285.3 (3)
ΔIDR1/2	Δ 55Q-164T/Δ291S-294P	NR[e]

[a] Virus particle concentration was determined by spectrophotometry using the equivalence of 1 AU at 260 nm = 2.1×10^{12} particles/ml. Titers (in PFU/ml) were determined by plaque assay. Number of pure virus preparations used to determine the particle:PFU ratios is mentioned in parentheses.

[b] rsT3D.σ1.T249I (WT)

[c] rsT3D.σ1.R202W/T249I (R202W)

[d] $P < 0.05$ in comparison with WT virus

[e] Not recoverable

Neutralization of L and IDR reovirus infection with mAb 9BG5- To assess whether the mutant σ1 proteins are folded properly, I determined whether pre-treatment of L and IDR mutant virions with monoclonal antibody (mAb) 9BG5, which binds to a conformational epitope in the σ1 head (107), inhibits infection (Figure II-2). Cells were adsorbed with either vehicle (PBS)- or antibody-treated virus stocks at an MOI of 2 PFU/cell at room temperature (RT), incubated in fresh medium at 37°C for 22 h, and stained with a polyclonal reovirus-specific serum. Following adsorption with a control $IgG_{2\alpha}$ antibody, each of the viruses tested retained full capacity to infect L929 cells. In contrast, the infectivity of WT, L, and IDR reoviruses was substantially diminished by incubation with mAb 9BG5. These results suggest that the L and IDR mutant reoviruses harbor σ1 molecules with head regions that are properly folded.

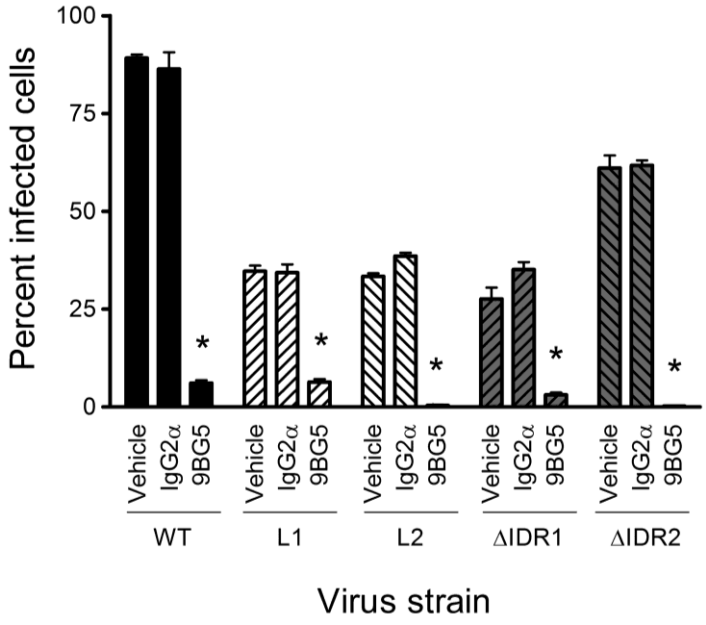

FIGURE II-2. Infection by L and IDR mutant reoviruses is dependent on σ1. WT, L, and IDR reoviruses were incubated in PBS, PBS containing mouse $IgG_{2\alpha}$, or PBS containing σ1-specific mAb 9BG5 at RT for 1 h prior to adsorption at an MOI of 2 PFU/cell onto L929 cells at RT for 1 h. Cells were washed and incubated in fresh medium at 37°C for 20 h. Infectivity was assessed by indirect immunofluorescence. Results are expressed as mean percent of infected cells in a 10X field of view for three independent experiments. Error bars represent SEM. *, $P < 0.01$ in comparison to the mock-treated condition (PBS).

Assessment of L and IDR reovirus hemagglutination capacity- To assess the capacity of σ1 to engage SA, I performed hemagglutination (HA) assays using bovine erythrocytes. The capacity of reovirus to produce HA is determined by binding to sialylated glycans on erythrocytes (55, 106). Serial dilutions of virus were incubated with red blood cells at 4°C, and HA titer was determined following a 3.5-h incubation (Figure II-3A and B). The HA capacity of L1, L2, and ΔIDR2 was comparable to that of WT virus. The T3D σ1-R202W mutant cannot bind sialic acid (113) and, consequently, produced no HA in this assay. In contrast, the HA titer of ΔIDR1 was approximately 80% less than that of WT. From these data, I concluded that the reduced capacity of ΔIDR1 to cross-link erythrocytes is attributable to either altered folding of the σ1 sialic-acid-binding region or decreased encapsidation of σ1 onto the ΔIDR1 virion.

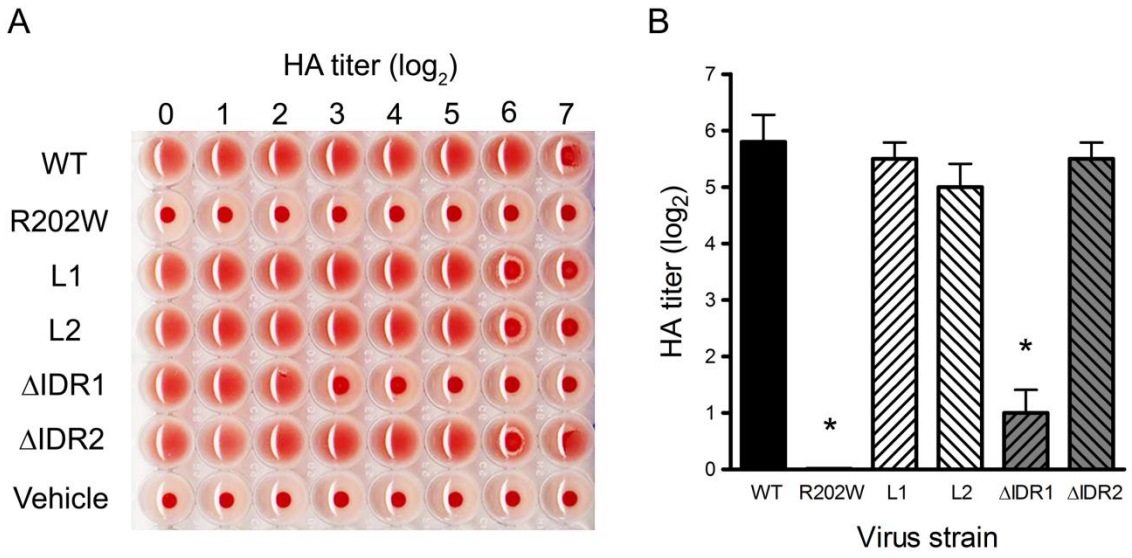

FIGURE II-3. Hemagglutination (HA) assay of L and IDR mutant reoviruses. (A) Purified virions were serially diluted in PBS and incubated with bovine erythrocytes (1% vol/vol in PBS) at 4°C for 3.5 h. Erythrocyte shields indicate HA, and erythrocyte buttons indicate absence of erythrocyte cross-linking. (B) Results are expressed as mean $\log_2$ (HA titer) for four independent experiments. HA titer is defined as 10^{11} particles divided by the number of particles/HA unit. One HA unit equals the particle number sufficient to produce HA. Error bars represent SEM. *, $P <$ 0.001 in comparison to WT virus.

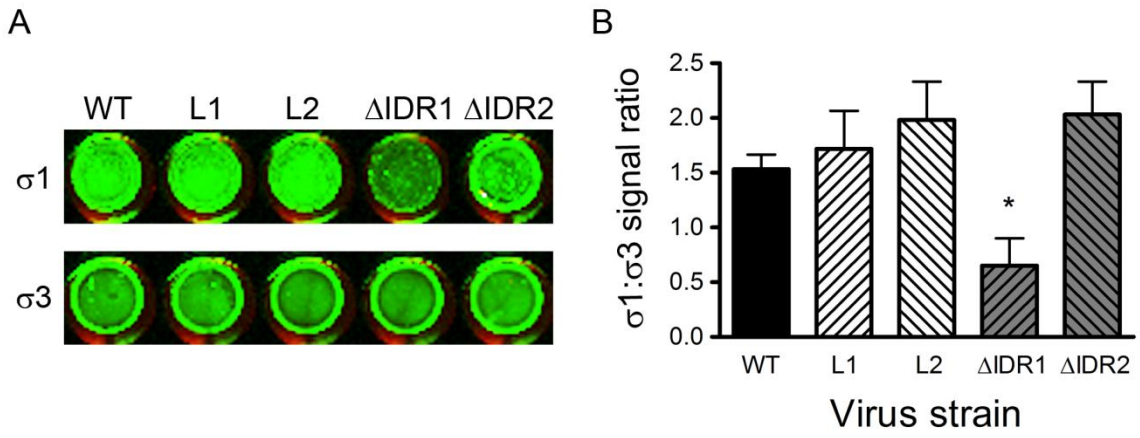

FIGURE II-4. Fluorescence linked immunosorbent assay (FLISA) of L and IDR mutant virus particles using σ1-specific mAb 9BG5 and σ3-specific mAb 4F2. (A) Purified virions (4×10^{10}) were adsorbed onto 96-well high-binding ELISA plates, incubated with primary antibodies, exposed to fluorescent secondary antibodies, and visualized using an infrared imaging system. This panel shows representative signals obtained for σ1 and σ3. (B) Quantification of the σ1:σ3 FLISA signal intensity ratio for L and IDR mutant reoviruses. Results are expressed as mean well fluorescence intensity ratio for two independent experiments. Error bars represent SEM. *, $P <$ 0.05 in comparison to WT virus.

Quantification of relative σ1 content in L and IDR reoviruses- To distinguish between these two possibilities, I quantified relative amounts of capsid-associated σ1 and σ3 in WT, L, and IDR virions using σ1-specific mAb 9BG5 (22) and σ3-specific mAb 4F2 (132) by fluorescence-linked immunosorbent assay (FLISA) (Figure II- 4A and B). After normalizing the σ1 signal intensity to the σ3 signal intensity to control for viral particle number, the σ1 signal for ΔIDR1, but not the other mutants, was decreased compared with WT virus. To confirm these results, I quantified relative amounts of σ1 on L and IDR capsids by immunoblotting virion proteins using a polyclonal serum specific for the σ1 head and σ3-specific mAb 4F2 (132) as a loading control (Figure II-5A-D). Concordant with the FLISA results, the relative amount of encapsidated σ1 was diminished exclusively for ΔIDR1. Taken together, these results suggest that the σ1 molecules of the L and IDR reoviruses are folded properly, but the amount of σ1

expressed on the ΔIDR1 capsid is diminished. It is possible that the lower amount of σ1 displayed by ΔIDR1 occurs as a consequence of either reduced stability of σ1 at capsid vertices or decreased encapsidation of σ1 during viral assembly.

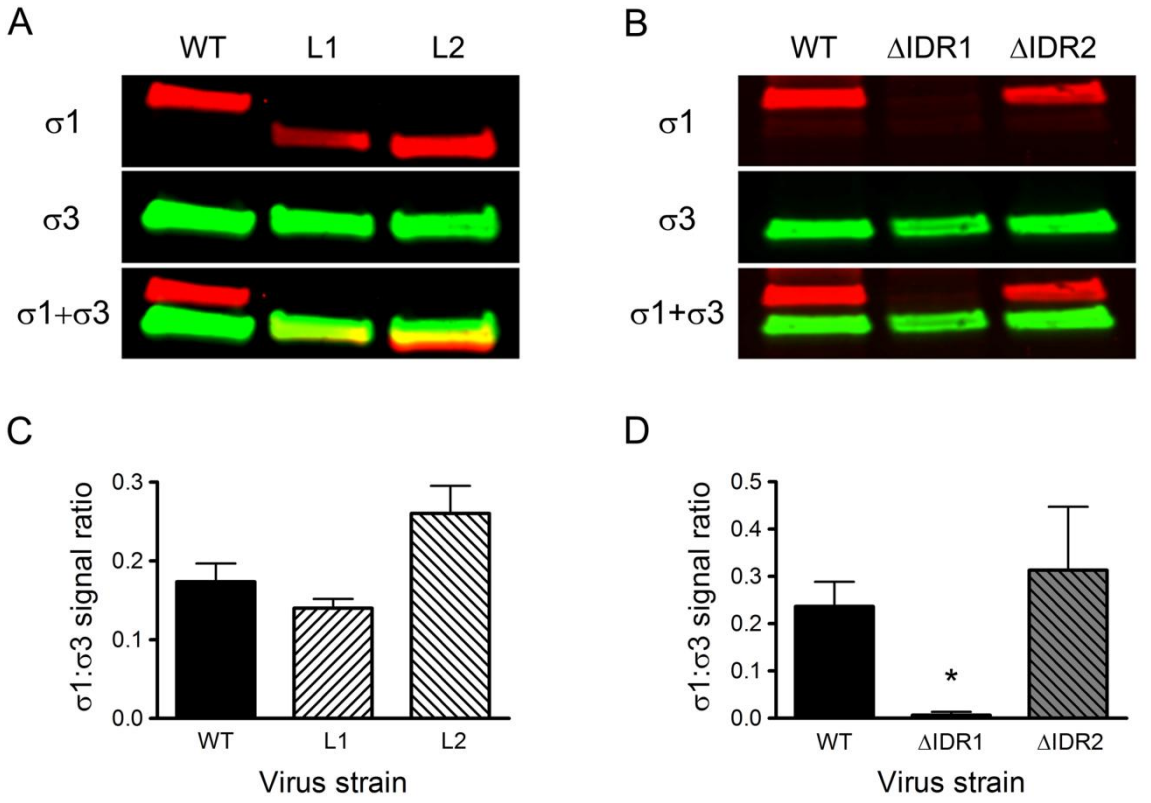

FIGURE II-5. Immunoblot analyses of (A) L and (B) IDR mutant reovirus σ1 and σ3 proteins. WT, L1, L2, ΔIDR1, and ΔIDR2 virion proteins were resolved by SDS-PAGE and transferred onto nitrocellulose membranes. Membranes were probed with a polyclonal σ1 head-specific serum and σ3-specific mAb 4F2. After incubation with fluorescent secondary antibodies, protein bands were visualized using an infrared imaging system. The σ3 band serves as an internal loading control. Quantification of the σ1:σ3 immunoblot band intensity ratio for L (C) and IDR (D) mutant reoviruses. Results are expressed as mean protein band fluorescence intensity ratio for three independent experiments. Error bars represent SEM. *, $P < 0.05$ in comparison to WT virus.

Content of σ1 in ΔIDR1 virions is decreased- Larson et al. (1994) (78) found that when pure reovirus virions were subjected to electrophoresis in agarose gels, thirteen well-separated bands were formed. These bands corresponded to thirteen distinct reovirus

populations that differed solely in their σ1 content: particles with 0, 1, 2, etc., up to 12 σ1 trimers. The most abundant virions contained 7-10 σ1 trimers. However, only three σ1 trimers were required for full infectivity (78). Virions with higher σ1 content exhibited a lower electrophoretic mobility than those with fewer σ1 trimers (78).

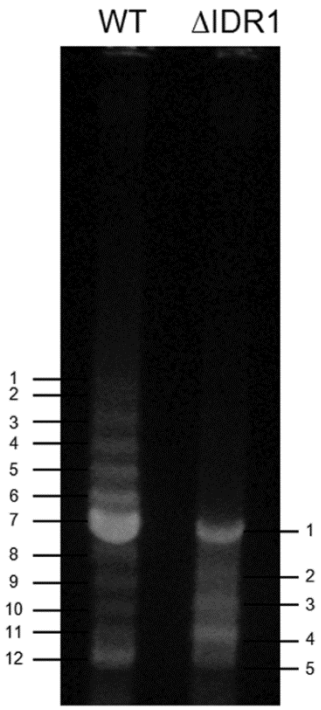

FIGURE II-6. Electrophoretic migration of WT and ΔIDR1 reovirus virions in a 0.7% agarose gel. Individual bands are enumerated. Ethidium bromide staining.

When I resolved purified preparations of whole WT and ΔIDR1 virions in a 0.7% agarose gel, I observed the formation of 12 and 5 bands for WT and ΔIDR1 reoviruses, respectively (Figure II-6). Absence of a 13th band for WT virus may be attributed to inadequate band resolution in our gel. The most intense bands detected for WT virus were located approximately halfway between bands with the highest and lowest electrophoretic mobility, suggesting that the most abundant WT virions bear 5-7 σ1

trimers. Interestingly, bands detected for ΔIDR1 appear to correspond to WT bands resembling virion populations with fewer than 5 σ1 trimers (Figure II-6).

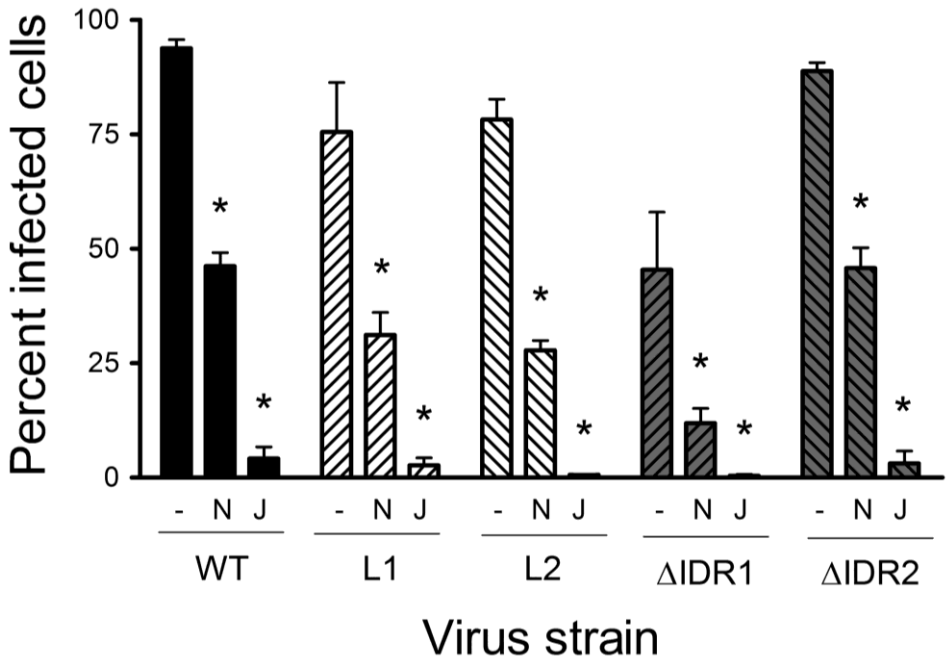

FIGURE II-7. Infectivity of L and IDR mutant reoviruses is dependent on SA and JAM-A. HeLa cells were treated with PBS (-), 40 mU/ml *A. ureafaciens* neuraminidase (N), or 10 μg/ml hJAM-specific mAb J10.4 (J) prior to adsorption with WT, L, and IDR mutant reoviruses at an MOI of 500 PFU/cell at RT for 1 h. Cells were washed and incubated in fresh medium at 37°C for 20 h. Infectivity was assessed by indirect immunofluorescence. Results are expressed as mean percent of infected cells in a 10X field of view for three independent experiments. Error bars represent SEM. *, $P < 0.01$ in comparison to the untreated condition (PBS).

L and IDR reovirus infection is dependent on SA and JAM-A- To test whether the L and IDR reovirus mutants engage the known reovirus receptors, I tested the infectivity of WT and mutant reoviruses using HeLa cells after treatment with vehicle, *Arthrobacter ureafaciens* neuraminidase, or JAM-A-specific mAb J10.4 (82). Pre-treated cells were adsorbed with reovirus strains at an MOI of 500 PFU/cell, incubated in fresh medium at

37°C for 22 h, and stained with a polyclonal reovirus-specific antiserum (Figure II-7). Following treatment with neuraminidase, the infectivity of the L and IDR viruses was decreased by 50-70% in comparison to the vehicle-treated condition. Similarly, incubation of cells with mAb J10.4 diminished infectivity of the L and IDR viruses by 90% in comparison to cells treated with vehicle (PBS). These data suggest that the L and IDR reoviruses engage sialic acid and JAM-A in a mechanism that leads to infection.

Discussion

Generation of the L and IDR reovirus mutants- I shortened the reovirus attachment protein by deleting parts of the α-helical tail domain (100) to avoid altering the SA RBD located in the β-spiral body domain of the molecule (30, 113). Seven and 10 α-helical turns were removed from σ1 to generate the L1 and L2 reoviruses, respectively (Figure II-1A and B, Table II-1). I also deleted the midpoint and head-proximal IDRs of σ1 to engineer ΔIDR1 and ΔIDR2, respectively (Figure II-1A and B, Table II-1). I was unable to recover a virus lacking both IDR1 and IDR2 (Table II-1). Since my results indicate that both of these sequences are required for efficient reovirus replication (Figure II-2), a double IDR deletion virus may not be viable.

IDR1 of σ1 is required for stable σ1 encapsidation- The mutations altering length and flexibility of σ1 described in this chapter do not appear to affect σ1 folding. L and IDR virus infection of L929 cells was neutralized by mAb 9BG5, which recognizes a conformational epitope in the σ1 head domain (22, 107) (Figure II-2). This finding suggests that there are no gross alterations in the σ1 head. Moreover, following adsorption of HeLa cells with JAM-A-specific mAb J10.4 (82), infection by the L and

IDR mutants was abolished (Figure II-7), suggesting that the JAM-A RBD of these reoviruses is not misfolded. Surprisingly, FLISAs using 9BG5 revealed that the relative amount of encapsidated σ1 is reduced in ΔIDR1 but not in L1, L2, or ΔIDR2 (Figure II-4A and B). Immunoblot analysis of L and IDR capsid proteins using a polyclonal antiserum specific for the σ1 head also showed that only ΔIDR1 of the mutants tested harbors less σ1 compared with WT virus (Figure II-5A-D). In addition, resolution of pure ΔIDR1 virions in an agarose gel revealed that a higher proportion of ΔIDR1 virions contained fewer than three σ1 trimers compared with pure preparations of WT virus (Figure II-6). Finally, the particle:PFU ratio for ΔIDR1 was increased (Table II-1), suggesting that a higher proportion of ΔIDR1 than WT virions is functionally impaired.

Since a mAb specific for the σ1 sialic acid RBD is not available, I tested the capacity of the L and IDR mutants to engage SA using HA assays (Figure II-3A and B). The HA capacities of L1, L2, and ΔIDR2 were comparable to WT virus, suggesting that the SA RBD of these viruses is properly folded. However, the HA titer of ΔIDR1 was decreased by approximately 80%. This reduction is not likely caused by misfolding of the ΔIDR1 SA RBD. Following treatment of HeLa cells with neuraminidase to remove cell-surface sialic acid, infection of WT, L, and IDR reoviruses was reduced to the same extent (Figure II-7), suggesting that all of the viruses tested rely in part on SA binding for infection and, therefore, that their σ1 SA RBD is properly folded. These results provide further evidence that the conformations of the L and IDR mutant σ1 molecules are not grossly altered and that the amount of σ1 on the ΔIDR1 capsid is reduced.

Hypothetical mechanism for σ1 IDR1 involvement in stable σ1 encapsidation- The hydrophobic N-terminus of σ1 directly interacts with pentameric turrets formed by λ2 at the capsid vertices and thus tethers the reovirus attachment molecule to the virion surface (43). Other outer-capsid proteins have not been reported to directly interact with σ1. However, the reovirus attachment molecule is likely collapsed in some way on the surface of virions and extends outward only upon proteolytic removal of σ3 during the formation of infectious subvirion particles (ISVPs) during viral disassembly (43, 54, 92). Interestingly, ISVPs display decreased infectivity following exposure to heat (93), which might be attributable to decreased stability of the extended conformer of σ1 at the capsid vertices. Therefore, IDR1 may stabilize σ1 by allowing it to adopt a folded conformation on the virion surface. Alternatively, IDR1 may permit σ1 to assume a conformation amenable to capsid assembly. The finding that IDR1 is required for stable σ1 encapsidation begins to paint a picture of the reovirus attachment protein as a participant in replicative steps other than engagement of receptors on the cell surface.

CHAPTER III

OPTIMUM LENGTH AND FLEXIBILITY OF REOVIRUS σ1 ARE REQUIRED FOR EFFICIENT REOVIRUS INFECTION

Introduction

Adenovirus and reovirus feature elongated attachment spikes that span the equivalent of a capsid radius in length (53, 108). Flexibility of the adenovirus fiber permits simultaneous engagement of multiple receptors (139). In turn, fiber length appears to influence adenovirus tropism (121). It is not understood how the conformation of the reovirus attachment protein contributes to receptor engagement and subsequent replicative steps.

Reovirus σ1 is a long fiber-like trimer comprised of three discernible structural regions that are partitioned by two flexible linkers IDRs 1 and 2 (32, 53, 113) (Figure I-2, Figure I-3). It is possible that optimal interactions between σ1 and its cellular receptors require that the reovirus attachment protein be long and flexible. Intramolecular mobility of σ1 at IDR1 and IDR2 (32, 53, 113) may allow movement of the spatially-independent RBDs with respect to one another as well as to the rest of the virion and permit efficient, sequential engagement of SA and JAM-A during adhesion strengthening. On the other hand, σ1 length may limit steric hindrance from the bulk of the virion and thus facilitate σ1-receptor interactions that result in productive infection. Considering that the utilization of molecular length and flexibility for receptor engagement is rare among nonenveloped animal viruses, the role of σ1 may extend beyond host cell binding. Some

evidence suggests that σ1 is folded on the surface of virions and extends only upon proteolytic cleavage of the virus particle during disassembly (43, 54, 92). Hence, length and flexibility of σ1 might allow the attachment molecule to assume a conformation during particle assembly that primes it for subsequent disassembly events. The fate of σ1 upon reovirus entry into the endocytic compartment is not known. However, it is clear that σ1 must be released from the λ2 pentamers to allow exit of nascent mRNAs from transcribing core particles (24). Length and flexibility of σ1 may be required to facilitate this process.

In this chapter, I report the results of experiments to evaluate the capacity of the L and IDR reovirus mutants (described in Chapter II) bearing σ1 proteins of varying lengths and flexibilities (Figure II-1) to bind the cell surface, internalize, uncoat, induce protein synthesis, assemble, and replicate. I found that σ1 length and flexibility are required for efficient reovirus infectivity and replication. L1, L2, and ΔIDR1 showed reduced capacity to attach to cells. In comparison with WT virus, none of the σ1 mutant viruses exhibited defects in internalization. Although not altered in attachment, ΔIDR2 was impeded at a post-disassembly replication step. None of these differences were attributable to changes in the folding of the mutant σ1 molecules. This research begins to paint a picture of σ1 as a participant in replicative steps other than cell attachment and reports structural features of σ1 than confer functionality.

Results

Sigma 1 length and flexibility are required for reovirus replication in cell culture- To directly test whether σ1 length and flexibility influence reovirus replication, I quantified

viral yields following infection of L929 cells over a 24-h time course. Cells were infected with WT, L, or IDR reoviruses at an MOI of 0.01 PFU/cell, and viral titers were determined by plaque assay at various intervals post-adsorption (Figure III-1A and B). The L and IDR mutants exhibited longer eclipse periods compared with WT virus. L2 and ΔIDR2 produced yields similar to WT following completion of the first replicative cycle (24 h) (12), but the replication kinetics of these viruses were significantly delayed (Student's *t* test, $P < 0.05$). On the other hand, L1 and ΔIDR1 replicated more slowly than WT virus throughout the course of the first replicative cycle (Student's *t* test, $P < 0.05$). These data suggest that length and flexibility of σ1 are required for reovirus replication in cultured cells.

Sigma 1 length and flexibility are required for reovirus infection in cell culture- Given the key role of σ1 in reovirus attachment (7, 8, 30, 73, 113), I next quantified L and IDR mutant infectivity in a viral protein production assay to evaluate the efficiency of the initial stages of infection. Monolayers of L929 cells were adsorbed with WT, L, and IDR reoviruses at an MOI of 2 PFU/cell, and viral infectivity was scored at various times post-adsorption by indirect immunofluorescence (Figure III-1C and D). The L and IDR reoviruses showed delayed kinetics of viral protein synthesis indicative of decreased infection compared with WT virus (Student's *t* test, $P < 0.05$). The percentage of cells infected by L1, L2, and ΔIDR1 was only 25% of that produced by WT virus at 24 h post-adsorption. In comparison with the other mutant viruses, ΔIDR2 appeared less disabled. The percentage of cells infected by this virus was 60% of that observed for WT virus at 24 h post-adsorption. These findings suggest that an impediment to L and IDR reovirus

mutant replication occurs at a step in the viral life cycle prior to or during translation of viral proteins.

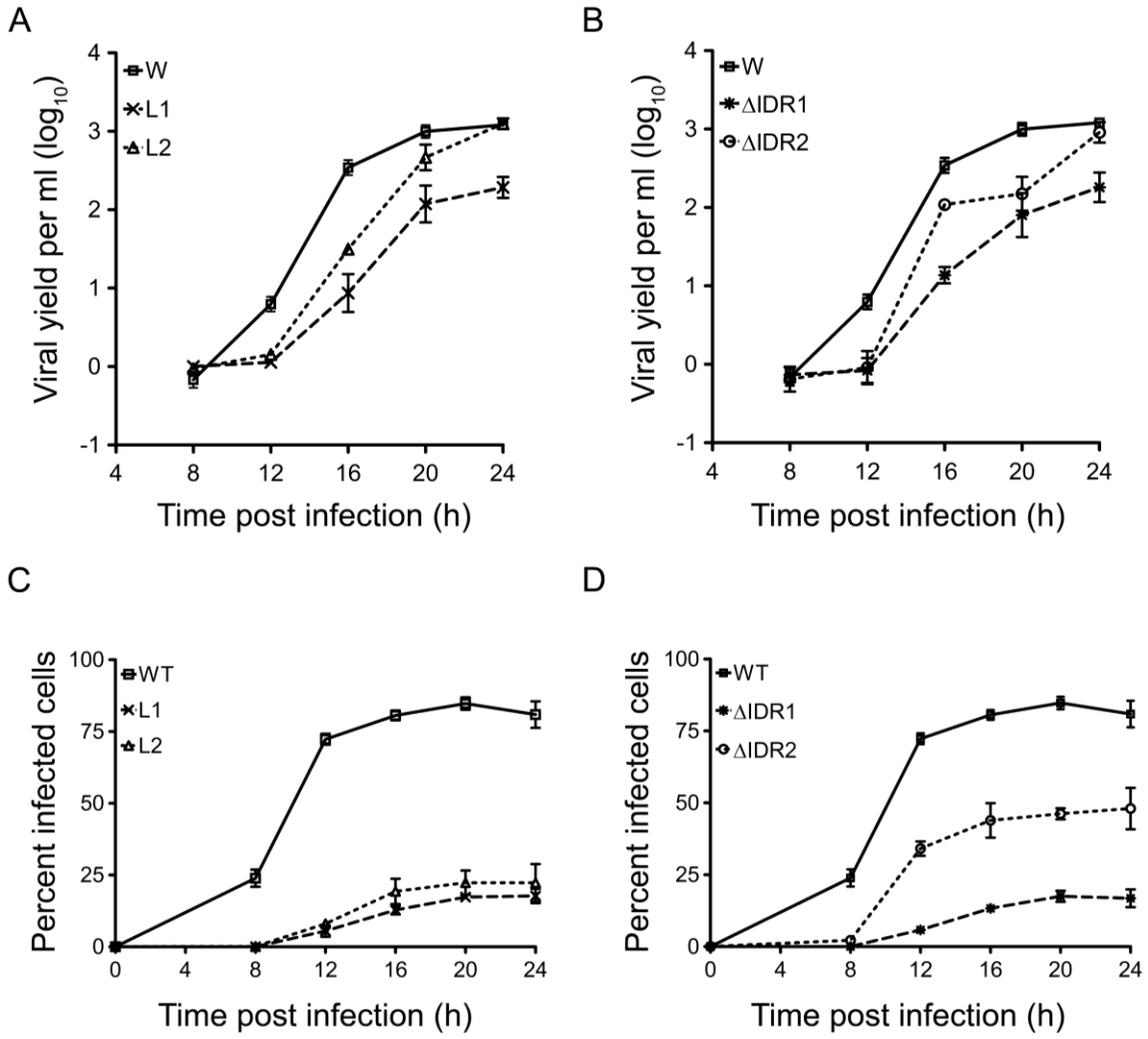

FIGURE III-1. Mutant reovirus replication and infectivity in L929 cells. (A, B) Cells were adsorbed with WT, L (A), and IDR (B) mutant reoviruses at an MOI of 0.01 PFU/cell. The inoculum was removed, fresh medium was added, and cells were incubated at 37°C for the times shown. Titers of virus in cell lysates were determined by plaque assay using L929 cells. Results are expressed as mean viral yield, which is defined as $\log_{10}(\text{titer})_{tx} - \log_{10}(\text{titer})_{t0}$ where *tx* is time post-adsorption, for three independent experiments. Error bars represent SEM. (C, D) Cells were adsorbed with WT, L (C), and IDR (D) mutant reoviruses at an MOI of 2 PFU/cell and processed for indirect immunofluorescence at the times shown post-adsorption. Results are expressed as mean percent of infected cells in a 10X field of view for three independent experiments. Error bars represent SEM.

The L and IDR replication defect occurs prior to endosomal escape- Following attachment to host cells, reovirus is internalized into the endocytic pathway where the viral particle undergoes acid-dependent proteolytic disassembly (5, 18, 28, 46, 122, 126), which allows the virus to gain access to the cytoplasm (2, 25). To determine whether σ1 length and flexibility are required for steps in the reovirus life cycle preceding endosomal escape, monolayers of L929 cells were adsorbed with reovirus strains at an MOI of 25 PFU/cell at 4°C to synchronize attachment, incubated at 37°C in fresh medium, and exposed to ammonium chloride to prevent endosomal acidification at defined intervals post-adsorption. After an overnight incubation, cells were scored for infection by indirect immunofluorescence (Figure III-2A and B). L1, L2, and ΔIDR1 mutant viruses bypassed the ammonium chloride blockade more slowly than WT reovirus (Student's *t* test, $P < 0.05$). These findings indicate that σ1 length and IDR1 are required for steps in reovirus replication that precede endosomal escape. The ΔIDR2 mutant bypassed the pH blockade with kinetics similar to those observed for WT virus (Student's *t* test, $P > 0.05$), suggesting that IDR2 is required for efficient completion of replication steps that temporally fall between endosomal escape and viral protein synthesis.

Internalization of L and IDR mutants is not altered- To directly assess the role of σ1 length and flexibility in reovirus internalization, I adsorbed L929 cells with Alexa Fluor 488-labeled L and IDR mutant reoviruses at 50,000 particles/cell and fixed cells at 0 and 60 min post-adsorption. Cells were then stained without prior permeabilization with phalloidin to visualize actin and polyclonal reovirus-specific serum (138) to

visualize extracellular reovirus particles. Internalization of reovirus virions was quantified by

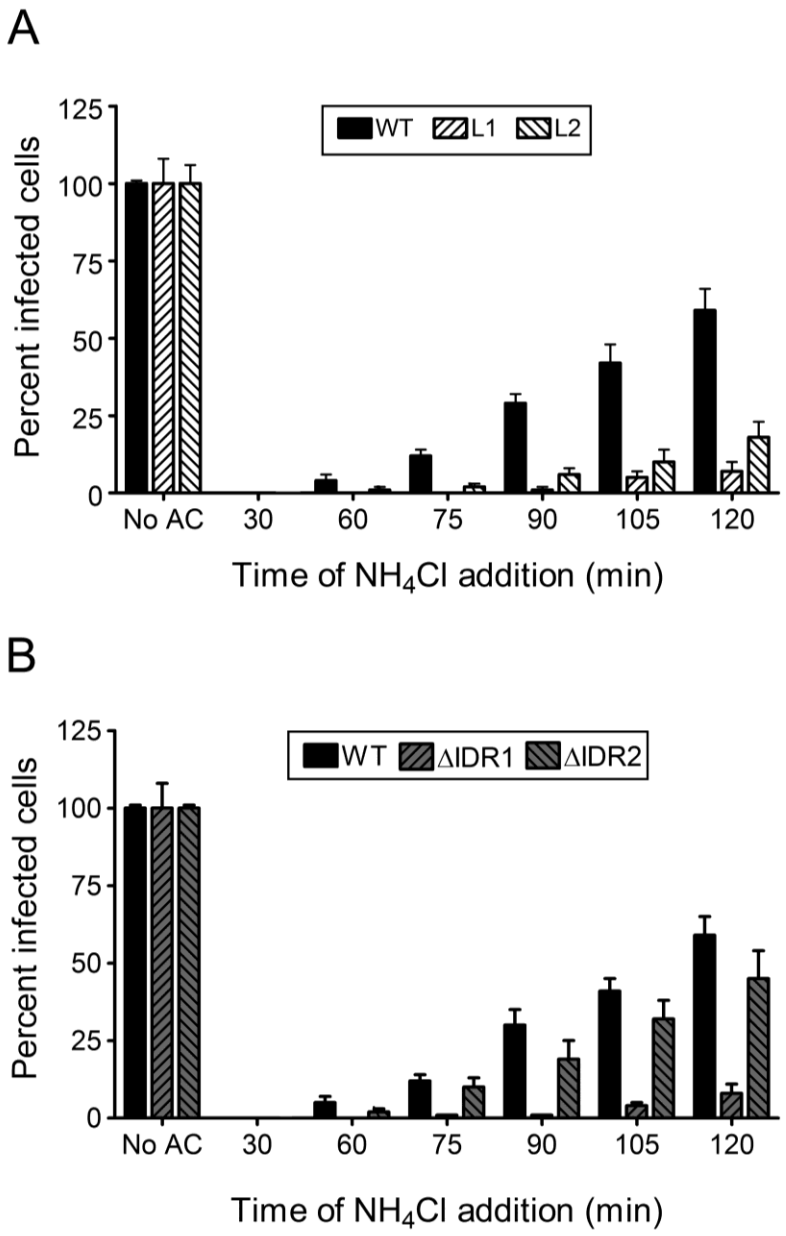

FIGURE III-2. Kinetics of ammonium chloride blockade bypass by (A) L and (B) IDR mutant reoviruses in L929 cells. Cells were adsorbed with the reovirus strains shown at an MOI of 25 PFU/cell at 4°C for 1 h. Following adsorption, cells were washed with cold PBS and incubated in fresh medium at 37°C for 20 h. Ammonium chloride was added to the medium at the indicated times post-adsorption to achieve a final concentration of 25 mM. Infectivity was assessed by indirect immunofluorescence. Results are expressed as mean percent of infected cells in a 10X field of view normalized to the untreated condition (No AC) for three independent experiments. Error bars represent SEM.

confocal microscopy. The inoculum dose used in this experiment allowed detection of signal for the most disabled L and IDR mutant viruses and has been used previously for evaluation of reovirus internalization (84-87). Representative confocal micrographs of reovirus-infected L929 cells are shown in Figure III-3A. Cell surface-associated and intracellular particles are depicted in aquamarine and green, respectively. The average number of total particles per cell (extracellular and intracellular) was significantly diminished for L1, L2, and ΔIDR1 at 0 (Figure III-3A, data not shown) and 60 min (Figure III-3A and B) post-adsorption, suggesting a defect in attachment for these viruses. However, at 0 and 60 min post-adsorption, 30 and 60 percent of the virus particles were internalized, respectively, for all strains tested (Figure III-3C). Therefore, native σ1 length and flexibility are not required for reovirus internalization, but these features of σ1 appear to augment attachment to host cells.

Length and IDR1 of σ1 are required for reovirus attachment- To directly investigate the role of σ1 length and flexibility in reovirus attachment, I adsorbed L929 cells with the L and IDR mutants at 4°C for 30 or 60 min and quantified virus binding by flow cytometry (Figure III-4). Compared with WT virus, I found that cell binding was reduced by 65 to 78% for L1, L2, and ΔIDR1 at both 30 and 60 min post-adsorption. The binding of ΔIDR2 to cells was reduced by about 10 to 17% compared with WT virus, but this difference was not statistically significant. These results show that σ1 length and IDR1 are required for efficient reovirus attachment to L929 cells.

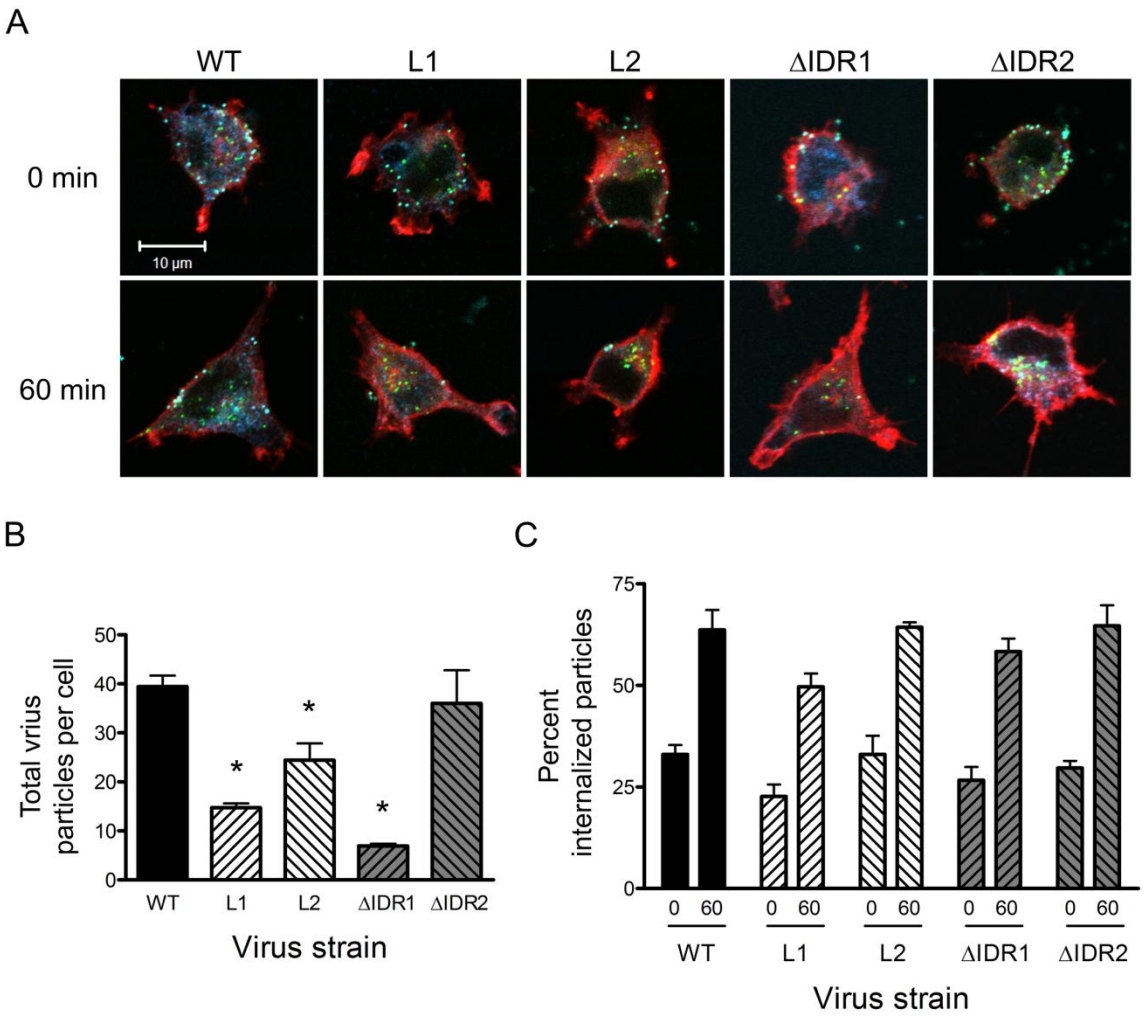

FIGURE III-3. Internalization of L and IDR mutant reoviruses. L929 cells were adsorbed with 50,000 particles/cell of Alexa Fluor 488-labeled WT, L, and IDR reoviruses (green) at RT for 30 min. The inoculum was removed, cells were incubated in fresh medium for the intervals shown, stained without cellular permeabilization for actin (red) and extracellular reovirus (blue), and imaged by confocal microscopy. (A) Representative digital fluorescence images of cells infected with L and IDR viruses at 0 and 60 min post-adsorption. Actin, extracellular reovirus, and intracellular reovirus are depicted in red, aquamarine, and green, respectively. Scale bars, 10 μm. (B) Quantification of the total number of reovirus particles at 60 min post-adsorption in single planes of view for 15-20 cells per virus strain for three independent experiments. Error bars indicate SEM. *, $P < 0.05$ in comparison to WT virus. (C) Quantification of the percent internalized reovirus particles at 0 and 60 min post-adsorption in single planes of view for 15-20 cells per virus strain for three independent experiments. Error bars indicate SEM. *, $P < 0.05$ in comparison to WT virus.

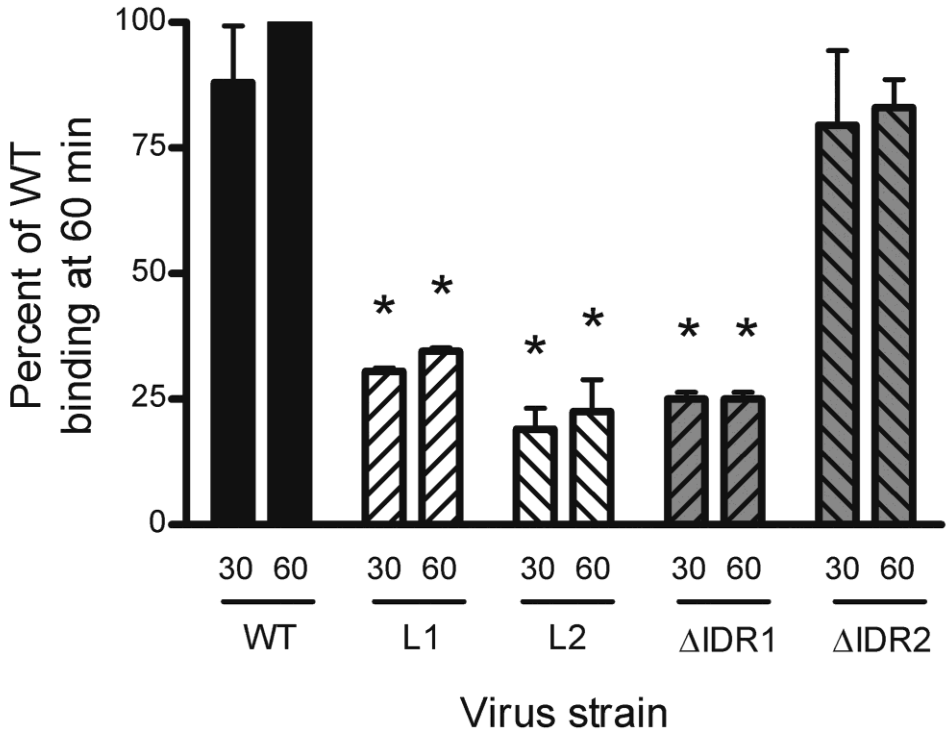

FIGURE III-4. Attachment of L and IDR mutant reoviruses. L929 cells were adsorbed with 50,000 particles/cell of WT, L, and IDR viruses at 4°C for either 30 or 60 min. Following adsorption, cells were incubated with reovirus-specific polyclonal antiserum, and virus attachment was assessed by flow cytometry. Results are presented as the percentage of WT virus (WT) binding after 60 min of incubation for two independent replicates. Error bars represent SD. *, $P < 0.02$ in comparison with WT virus.

Discussion

Optimum length and IDR1 of reovirus σ1 are required for reovirus attachment to the cell surface- It is clear from my results that optimum length and IDR1 of the σ1 molecule are required for efficient reovirus binding to cells. L1, L2, and ΔIDR1 showed delayed replication kinetics (Figure III-1A and B) and infected approximately 75% fewer cells compared with WT virus (Figure III-1C and B). These viruses exhibited delayed bypass of an ammonium chloride replication block (Figure III-2A and B), which is likely entirely

due to inefficient attachment (Figure III-4), as internalization of these mutants is not altered (Figure III-3C). Moreover, the reduction in binding to cells detected for L1, L2, and ΔIDR1 (Figure III-4) corresponds to the decrease in infectivity observed for these viruses (Figure III-1C).

Sigma 1 length could limit steric hindrance from the bulk of the virion to allow for appropriate cell-surface receptor engagement. Thus, diminished σ1 length may reduce the efficiency of the adhesion strengthening required for reovirus to optimally engage the host cell surface. Although the α-helical fragment of L1 σ1 is longer than that of L2 (Figure II-1A, Table II-1), I did not note any obvious phenotypic differences between L1 and L2 in the assays employed in this study. It is possible that mutants with even shorter σ1 proteins would be more severely compromised. However, I did not attempt to generate such viruses. On the other hand, decreased attachment detected for ΔIDR1 could be explained by the diminished amount of σ1 in the ΔIDR1 outer capsid described in Chapter II of this dissertation. Studies of L and IDR mutant attachment kinetics could provide a more detailed understanding of the mechanisms that govern the multi-step binding of reovirus to its receptors.

IDR2 of reovirus σ1 is required for endosomal escape- My findings suggest that flexibility of σ1 at IDR2 is required for a replicative step that takes place after protease-dependent uncoating of reovirus in the endocytic pathway but before initiation of viral protein synthesis. Following an initial delay, ΔIDR2 produced WT-level yields of viral progeny at the end of a single infectious cycle (24 h) (Figure III-1B). In addition, ΔIDR2 infected a significantly lower percentage of cells compared with WT virus (Figure III-

1D), again consistent with a prolonged eclipse phase. However, the interval required by ΔIDR2 to bypass a block to replication imposed by ammonium chloride did not differ from WT (Figure III-2B). Concordantly, ΔIDR2 did not exhibit defects in internalization (Figure III-3C) or attachment (Figure III-4).

The underlying mechanism for the defect in ΔIDR2 replication is not clear from my work. However, σ1 must be shed from the λ2 turrets to allow export of nascent transcripts through unobstructed λ2 channels at the icosahedral vertices of transcribing reovirus cores (24, 43). Since σ1 dissociates from λ2 at some point after endosomal proteolysis of the reovirus outer capsid (24, 25), it is possible that IDR2 of σ1 is required to facilitate this process. Alternatively, IDR2 may be involved in viral RNA transcription or protein synthesis in some way, but this explanation does not seem likely. Little σ1 would be available following disassembly and endosomal escape to serve a function in viral transcription or translation. Reovirus attaches to L929 cells with a high affinity (7, 8). Therefore, σ1 is unlikely to dissociate from the membrane and actively participate in regulating translation of viral proteins. In addition, the hydrophobic λ2-enclosed segment of σ1 (53, 54, 100) would associate with hydrophobic moieties available in the environment following release from virion vertices, which would decrease σ1 availability for mediation of subsequent replicative steps.

CHAPTER IV

VISUALIZATION OF VIRION-ASSOCIATED σ1 BY ELECTRON MICROSCOPY

Introduction

A high-resolution structure of capsid-associated σ1 is not available. The reovirus attachment protein is a trimer with the N-terminus enclosed by pentameric turrets of λ2 at virion vertices (43). This trimer-pentamer mismatch precludes the imaging of virus-bound σ1 using cryo-EM because icosahedral averaging is required for reconstruction of the reovirus capsid. Another reason for difficulty in visualizing σ1 by this technique could be its flexibility at IDR1 and IDR2 (Figure I-2 and Figure I-3) (53). Negative-stain EM images of full-length purified σ1 suggest that this viral attachment protein preferentially assumes several different conformations (Figure I-3): extended or bent at regions that dimensionally correspond to the N-terminus, IDR1, or IDR2 (Figure I-3) (53). While these findings represent preliminary evidence for σ1 flexibility, they deliver no information about the folding of capsid-associated σ1. Negative-stain EM images of T2 reovirus virions and ISVPs showed rare filamentous densities extending from the capsid surface (54). Specimen scarcity caused at least in part by resolution limitations precluded image averaging for reconstruction of the most common conformations of virus-associated σ1. Therefore, only snapshots of virion-bound σ1 are currently available. The purpose of this study was to fill this knowledge gap by producing averaged negative-stain EM images of σ1 fibers extending from the capsid surface.

Results

To begin studies aimed at determining the most common conformations of virion-associated σ1, purified virions of strain T3D reovirus (the WT strain used in Chapters II and III) were adsorbed onto carbon-coated plastic EM grids, stained with 0.75% uranyl formate, and imaged by electron microscopy at 36,000x magnification. Figure IV-1 shows representative images of negatively-stained reovirus virions. Densities representing putative σ1 filaments are indicated with white arrows. Examination of two hundred virions revealed that only approximately 28% of the particles contained on average less than one extended filamentous density per particle. Virions were preferentially oriented around the fivefold (~80%) and threefold (~20%) symmetry axes. Sample background was grainy and included a considerable number of what might be heat-shock proteins, which may have prevented visualization of additional extended σ1 filaments. Specimen scarcity precluded image averaging for reconstruction of the most

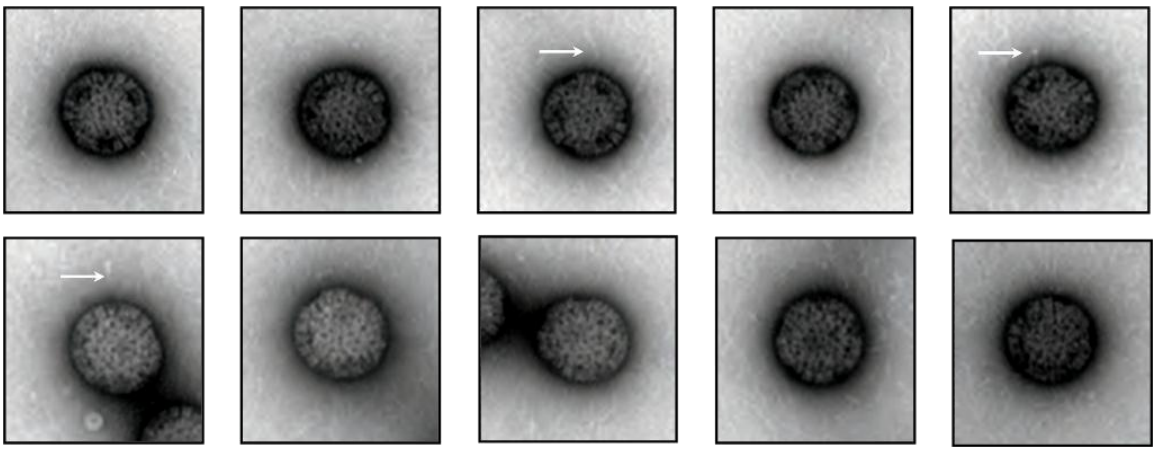

Figure IV-1. Examples of negative-stain electron microscopic images of T3D reovirus virions. Densities representing putative σ1 filaments are indicated with white arrows.

common conformations of capsid-associated σ1 using a higher-power electron microscope at 100,000x magnification due to technical limitations of the instrument. These findings are similar to those made using strain T2J reovirus by Furlong et al. in 1988 (54).

Discussion

In these studies, I have shown that it is possible to visualize virion-associated T3D reovirus σ1 using negative-stain EM. However, the presence of extended capsid-associated filamentous densities was rare (Figure IV-1). Difficulty in visualizing extended σ1 using this technique could be explained by σ1 folding on the virion surface, grainy sample background, or inappropriate staining conditions. Specimen scarcity precluded me from imaging virion-associated σ1 at 100,000x magnification using a higher-power electron microscope.

ISVPs may contain more extended capsid-associated σ1 fibers. Therefore, specimen scarcity could be remedied by imaging these disassembly intermediates instead of virions. Sample background is likely composed of cellular remnants (e.g., actin chains and heat-shock proteins) and could be eliminated by gel filtration or passing purified virions through a sucrose gradient. Finally, staining conditions could be modified to achieve more desirable image clarity. Results of these future studies could be the first source of information about the folding of full-length capsid-associated σ1.

CHAPTER V

SUMMARY AND FUTURE DIRECTIONS

Introduction

The length and flexibility of adenovirus fiber are important determinants of adenovirus tropism (121) and internalization efficiency (139), respectively. During the course of my dissertation research, I found that despite extensive structural similarities between the adenovirus and reovirus attachment proteins (123), the function of σ1 length and flexibility in reovirus replication differs from the role of fiber length and flexibility in the adenovirus life cycle. Length of the reovirus attachment protein is unlikely to significantly contribute to reovirus tropism in the infected host. Despite dramatic serotype-dependent differences in tropism (41, 137), σ1 varies only between 455 and 470 amino acids for strains of each of the three reovirus serotypes (100). However, I found that optimum σ1 length is required for the efficient attachment of reovirus to cells (Chapter III), perhaps because this feature of σ1 reduces steric hindrance from the much larger virion during receptor engagement. On the other hand, flexibility of σ1 at IDR2 is required for a replicative event that follows proteolytic disassembly of reovirus particles in the endocytic pathway and may permit efficient σ1 dissociation from λ2 turrets prior to viral endosomal escape (Chapter III). Finally, flexibility of σ1 at IDR1 is required for stable encapsidation of the σ1 protein during particle assembly (Chapter II) and thus also for reovirus attachment to the cell surface (Chapter III). Determination of capsid-associated σ1 conformations is ongoing (Chapter IV). This work reveals new functions for reovirus σ1 and provides insights into molecular events at the virus-cell interface that

lead to productive infection. In this chapter, I will discuss broader implications of my studies and suggest areas for future research.

Direct evidence for σ1 flexibility

Only circumstantial evidence for σ1 flexibility at IDR1 and IDR2 exists today (Chapter I). However, Chapters II and III of this dissertation report results that strongly suggest that σ1 IDR1 is required for stable σ1 encapsidation and that reovirus depends on σ1 IDR2 for some aspect of endosomal escape. Direct studies of σ1 flexibility at these regions would lend credence to the idea that flexibility is a feature of σ1 that confers functionality and to the notion that σ1 undergoes conformational changes during viral particle disassembly. This knowledge could inform a deeper understanding of how reovirus interacts with host receptors both at the cell surface and within the endosome.

To gather direct evidence for σ1 flexibility, future studies should be directed toward EM imaging of purified WT T3D, ΔIDR1, and ΔIDR2 σ1 proteins. Reovirus attachment molecules could be isolated by briefly heating viral particles, pelleting virions by ultracentrifugation, and concentrating the resulting σ1-containing supernatant (54). Cryo- or negative-stain EM images of purified WT T3D, ΔIDR1, and ΔIDR2 σ1 proteins could then be sorted and averaged to determine their preferred folding. Significantly decreased σ1 bending at IDR1 in ΔIDR1 and at IDR2 in ΔIDR2 would provide convincing evidence for σ1 flexibility at these regions. In addition, high-resolution cryo-EM renditions of the reovirus attachment protein would supply detailed information about the structure of full-length σ1.

Imaging purified σ1 has obvious limitations. These experiments do not directly contribute to the more biologically-significant question about the folding of capsid-associated σ1. In Chapter IV, I present negative-stain EM images of WT T3D virions. These and similar previous studies (54) have shown that virion-associated filamentous densities attributable to σ1 are only rarely visible. Specimen scarcity precludes determination of the most common conformations of capsid-associated σ1. This problem may be circumvented by imaging reovirus ISVPs, which appear to contain more extended fibers by EM (53). Unfortunately, the folded virion-associated form of σ1 could not be imaged using this strategy. Crystallographic approaches to studies of reovirus particle structure may present a solution to this problem.

Interactions of σ1 IDR1 with the outer capsid

Studies presented in Chapter II reveal that σ1 IDR1 is required for stable σ1 encapsidation. While it is known that the N-terminus of the reovirus attachment molecule is enclosed by pentameric turrets of λ2, σ1 has not been shown to directly interact with any other outer-capsid protein (129). It is possible that IDR1 stabilizes σ1 on the virion in its folded conformation by attaching σ1 to the virion surface. Alternatively, σ1 may be incorporated into the outer capsid in its folded form and cannot extend from the virion surface due to physical confinement by other outer-capsid proteins.

To distinguish between these possibilities, future research should focus on determining whether WT T3 σ1 binds other outer-capsid proteins. This question could be answered using several strategies. In coimmunoprecipitation experiments (109), cells could be transfected with σ1- and either σ3- or μ1-containing plasmids. Cell lysates

would be incubated with mAb to σ1 9BG5 (22), precipitated, and analyzed by immunobloting using mAbs against either σ3 (4F2) (132) or μ1 (8H6) (132). If this method fails due to low levels of protein synthesis or antibody incompatibility, affinity chromatography would be a viable alternative (109). In these studies, competent *Escherichia coli* would be transformed with plasmids encoding His-tagged forms of σ3 or μ1. To purify proteins, bacterial lysates would be passed through nickel- or cobalt-containing columns. On the other hand, σ1 could be purified directly from virions as previously described (54), biotinylated, and bound to a streptavidin agarose column. Finally, preparations of His-tagged forms of σ3 or μ1 would be passed through the streptavidin-σ1 agarose column, and bound specimens would be eluted under high-salt conditions. To provide adequate detection sensitivity, fractions would be tested for presence of σ3 or μ1 by liquid chromatography-mass spectrometry (LC-MS). Unfortunately, protein modifications necessary for affinity chromatography may preclude detection of important interactions due to possible misfolding or steric hindrance. In addition, σ1 assembly into trimers may be problematic, which could prevent the formation of appropriate protein-protein interactions and thus also detection of these interactions using coimmunoprecipitation.

A yeast-two-hybrid screen is another strategy that could be employed to identify σ1 interactions with other outer-capsid proteins (109). The first step of these studies would be to construct plasmids encoding arbitrary σ1 fragments fused to the DNA-binding domain of a transcription factor that regulates the expression of a His reporter gene (“bait”) and machinery necessary to synthesize an essential amino acid (e.g., tryptophan). A library of plasmids encoding parts of σ3 or μ1 fused to the activation

domain of a transcription factor that regulates the expression of a His reporter gene ("fish") and machinery necessary to synthesize an essential amino acid (e.g., leucine) would also be generated. Individual pairs of "bait" and "fish" plasmids would then be transformed into yeast cells grown in media lacking tryptophan and leucine. Subsequent plating of the yeast on histidine-deficient agar would select for cells that contain the interacting genes. The binding proteins would then be identified by sequencing plasmids isolated from these cells.

An alternative library-based method is phage display (109). In these studies, σ1 would be purified from virions as previously described (54), biotinylated and immobilized to streptavidin-coated microtiter plates. A library of bacteriophages displaying arbitrary fragments of σ3 or μ1 fused to a coat protein would be generated and added to σ1-coated wells. Attached phages would be amplified in appropriate bacterial hosts and sequenced to identify the interacting protein. If σ1 binds other outer capsid proteins, library-based methods could allow detection of specific protein sequences that mediate this interaction. One disadvantage of library-based strategies is their dependence on fusion proteins. Some interactions may be missed due to misfolding or steric hindrance. In addition, quaternary structure of σ1 may be essential for σ1 interaction with the reovirus outer capsid. If this is the case, library-based methods will not be useful.

Role of σ1 length and flexibility in reovirus pathogenesis

Reovirus σ1 is an important determinant of reovirus dissemination to and tropism for various host tissues (129). Although results presented in Chapters II and III of this thesis suggest that σ1 length but not flexibility both may be important for reovirus

attachment to the cell surface, this conclusion may not be true in the context of an infected animal. For example, σ1 length and flexibility may both be important for reovirus engagement of JAM-A within the TJ. Moreover, reovirus binds a yet unidentified neuronal receptor that is distinct from JAM-A (3). It is not known what features of σ1 mediate this interaction. Studies of reovirus pathogenesis using the L and IDR reovirus mutants (described in Chapter II) may contribute to answering both of these questions.

As animal studies can be cumbersome and expensive, the first step in this series of experiments would be to monitor survival of C57BL/6 mouse pups following peroral (PO) inoculation with WT, L1, L2, ΔIDR1, and ΔIDR2 reoviruses. To determine the role of distinct σ1 regions in reovirus dissemination, L and IDR viruses with significantly attenuated virulence would be inoculated into C57BL/6 mouse pups via PO, intramuscular (IM), and intracranial (IC) routes. There are three barriers to reovirus dissemination from the intestine to the CNS: the intestinal epithelium, blood vessel endothelium, and the blood brain barrier (BBB). Reovirus is a fecal-oral pathogen, which means that PO inoculation represents the most natural route. IM inoculation removes the barriers of intestinal epithelium and blood vessel endothelium, and IC inoculation additionally bypasses the BBB. Titering reovirus in the intestine, blood, and brain over several days following infection could reveal the dissemination barriers that pose particular problems to the σ1 length and flexibility mutants. On the other hand, decreased L/IDR reovirus titers in the brain following IC inoculation could identify particular regions of σ1 responsible for binding the unknown neuronal receptor for reovirus.

Conclusion

Engagement of cell surface receptors is the first step of viral replication. Reovirus depends on its attachment protein σ1 for this purpose. The term "attachment protein" can be misleading as it suggests that the only function of σ1 is cell binding. Length and flexibility are features of σ1 that distinguish it among the proteins used by other nonenveloped viruses to engage cellular receptors. My dissertation research has enhanced an understanding of how these characteristics allow for efficient reovirus attachment and permit successful endosomal escape and stable capsid assembly. This work raises several important questions that will collectively contribute to a more holistic appreciation of σ1 functions and an enhanced understanding of virus-receptor interactions. First, providing direct evidence for σ1 flexibility at IDR1 and IDR2 and identifying outer-capsid proteins that interact with IDR1 will give more credence to the idea that σ1 folds on the virion surface and is extended in the ISVP. Second, defining the most common conformations of virion- and ISVP-associated σ1 will improve an understanding of the conformational changes that σ1 undergoes during viral particle disassembly. Finally, determining whether σ1 length and flexibility influence reovirus pathogenesis may reveal regions of σ1 responsible for efficient reovirus dissemination and tropism for various host tissues. Thus, knowledge gained from this research on mechanisms of reovirus interactions with host cells should broaden a general understanding of how viruses successfully complete initial replicative steps, contribute new insights into the virus-host interactions that lead to viral disease, and move the field towards robust and targeted development of reovirus-based vectors for vaccine and oncolytic applications.

CHAPTER VI

DETAILED METHODS OF PROCEDURE

Cells

Spinner-adapted L929 murine fibroblasts were grown in Joklik's spinner-modified minimum essential medium (SMEM; Lonza; Walkersville, MD) supplemented to contain 5% heat-inactivated fetal bovine serum (HI FBS; Invitrogen; Carlsbad, CA), 2 mM L-glutamine (Invitrogen), 100 U/ml penicillin (Invitrogen), 100 µg/ml streptomycin (Invitrogen), and 25 ng/ml amphotericin B (Sigma-Aldrich; St. Louis, MO). HeLa cells were grown in Dulbecco's modified Eagle medium (DMEM; Invitrogen) supplemented to contain 10% HI FBS, 2 mM L-glutamine, 100 U/ml penicillin, 100 µg/ml streptomycin, and 25 ng/ml amphotericin B. BHK-T7 cells were grown in DMEM supplemented to contain 5% HI FBS, 2 mM L-glutamine, 2% MEM amino acid solution (Invitrogen), and 1 mg/ml geneticin (Invitrogen).

Viruses

Recombinant reoviruses containing mutations in the σ1 protein were generated by plasmid-based reverse genetics using cloned reovirus cDNAs (74, 75). The pT7-T3DS1.T249I template was used to engineer the pT7-T3DS1.T249I.R202W, pT7-T3DS1.T249I.L1, pT7-T3DS1.T249I.L2, pT7-T3DS1.T249I.ΔIDR1, and pT7-T3DS1.T249I.ΔIDR2 plasmids by QuikChange site-directed mutagenesis (Stratagene; La Jolla, CA). Monolayers of approximately 3×10^6 BHK-T7 cells were co-transfected with

3.5 µg each of five plasmid constructs representing the T3D reovirus genome (pT7-T3DL1, pT7-T3DL2-M3, pT7-T3DL3-M1, and pT7-T3DM2-S2-S3-S4 in combination with pT7-T3DS1.T249I or one of the altered pT7-T3DS1.T249I plasmids) using 3 µl TransIT-LT1 transfection reagent (Mirus Bio LLC; Madison, WI) per µg of plasmid DNA. Following 48 h of incubation, recombinant viruses were isolated by plaque purification using L929 cells. Virus stocks were prepared as described (12). Virions were purified by Freon extraction from cell lysates and subsequent CsCl gradient centrifugation (54). Bands corresponding to reovirus particle density (1.36 mg/dL) were collected and dialyzed against virion storage buffer (150 mM NaCl, 15 mM $MgCl_2$, 10 mM Tris-HCl (pH 7.4)). The S1 gene sequences of mutant viruses were verified using PCR products generated from viral RNA subjected to OneStep reverse transcription-PCR (RT-PCR) (Qiagen; Valencia, CA) using S1-specific primers (72). The sequences of S1 gene-specific primers employed for mutagenesis and sequencing were: 5'-CATGAATT CATGGATCC TCGCCTACGTTAAGAAG-3' (forward) and 5'-CAGAAGCTTCTGA TCCTC AC GTGAAACTACGC-3' (reverse). The concentration of pure reovirus virions was determined by spectrophotometry using the following equivalence: 1 absorbance unit (AU) at 260 nm = 2.1×10^{12} particles/ml. Viral titer was determined by plaque assay using L929 cells (131).

Electrophoresis of the reovirus genome

Whole reovirus virions were incubated at 95°C for 10 min in sodium dodecyl sulfate (SDS)-polyacrylamide gel electrophoresis (PAGE) buffer (62.5 mM Tris HCl (pH 6.8), 2% sodium dodecyl sulfate, 10% glycerol, 0.004% bromophenol blue), loaded into

wells of pre-cast 4-20% gradient Tris-tricine polyacrylamide gels (Bio-Rad Laboratories; Hercules, CA) at 5×10^{10} particles/well, and electrophoresed at a constant current of 15 mAmp for 16 h. Following electrophoresis, the gel was stained with ethidium bromide and visualized by UV transillumination.

Hemagglutination assays

Purified virions were distributed into 96-well U-bottom microtiter plates (Costar) at an initial concentration of 10^{11} particles/well and serially diluted 1:2 in 50 µl PBS. Calf erythrocytes (Colorado Serum Company; Denver, CO) were washed twice with PBS, resuspended at 1% vol/vol in PBS, delivered to virus-containing wells at 50 µl/well, and incubated at 4°C for 3.5 h. HA titer is defined as 10^{11} particles divided by the number of particles/HA unit. One HA unit is the particle number sufficient to produce HA (a partial or complete shield of erythrocytes on the well bottom).

Fluorescence-linked immunosorbent assay

Purified virions were adsorbed onto 96-well Immulon® 2HB flat-bottom microtiter plates (Fisher Scientific; Suwanee, GA) at a concentration of 4×10^{10} particles/well in 0.05 M carbonate-bicarbonate buffer (pH 9.6) (Sigma-Aldrich). Following incubation at 4°C overnight, plates were blocked with 2% bovine serum albumin (BSA) in 0.05 M carbonate-bicarbonate buffer (pH 9.6) at 37°C for 2 h. Wells were washed four times with PBS containing 0.05% Tween-20 prior to incubation with either σ1-specific mAb 9BG5 (22) or σ3-specific mouse mAb 4F2 (132) at 52 and 7 µg/ml, respectively, in PBS containing 1% BSA. Plates were incubated at 37°C for 1 h, washed five times with

0.05% Tween-20 in PBS, incubated with IRDye 800 CW goat anti-mouse secondary antibody (LI-COR; Lincoln, NE) at a dilution of 1:1000 in PBS containing 1% BSA, washed four times with 0.05% Tween-20 in PBS, rinsed with PBS, and visualized using an Odyssey Infrared Imaging System (LI-COR). Well fluorescence intensity was determined using Odyssey Application Software Version 3.0 (LI-COR). Integrated well fluorescence signal for σ1 (9BG5) was divided by that obtained for σ3 (4F2) to quantify the results.

Generation of σ1 head-specific antiserum

The C-terminal head domain of T3D σ1 (amino acids 293-455) was expressed and purified as described (116). Rabbit polyclonal serum specific for the T3D σ1 head was generated by Cocalico Biologicals. A single New Zealand white rabbit was immunized with the T3D σ1 C-terminal head domain and boosted at 2, 3, and 7 weeks post-immunization.

Immunoblot of reovirus σ1 and σ3 proteins

Purified reovirus virions were incubated at 95°C for 10 min in SDS-PAGE buffer, placed into wells of pre-cast 4-20% gradient Tris-tricine polyacrylamide gels at 10^{10} particles/well, and electrophoresed at 100 V for 1.5 h. Viral proteins were transferred onto nitrocellulose membranes at 12 V for 45 min and blocked in Odyssey blocking buffer (LI-COR) at RT for 1 h. Membranes were incubated with rabbit polyclonal serum specific for the σ1 head and mouse mAb 4F2 specific for σ3 (132) at a 1:1000 dilution and 7 μg/ml, respectively, in Odyssey blocking buffer supplemented to contain 0.2%

Tween-20 at RT for 1 h. Membranes were incubated with Alexa Fluor 647-labeled goat anti-rabbit (Invitrogen) and IRDye 800CW goat anti-mouse secondary antibodies at 1:5000 and 1:10000 dilutions, respectively, in Odyssey blocking buffer supplemented to contain 0.2% Tween-20 at RT for 1 h and scanned using an Odyssey Infrared Imaging System. Protein band intensity was quantified using Odyssey Application Software Version 3.0. Integrated protein band fluorescence for σ1 was divided by that for σ3 to normalize the results.

Electrophoresis of whole reovirus virions in agarose gels

Purified reovirus virions (5×10^{10} particles) in 5% Ficoll and 0.05% bromophenol blue were loaded onto 0.7% agarose gels prepared in TAE buffer (40 mM Tris-HCl, 5 mM sodium acetate, 1 mM ethylene diamine tetraacetate, pH 7.9) supplemented to contain 0.5 µg/ml ethidium bromide and electrophoresed at 15 mAmp at RT for 17 h. Following electrophoresis, bands were visualized by UV transillumination.

Reovirus replication in L929 cells

Monolayers of L929 cells seeded in 24-well plates (Costar; Corning Incorporated; Corning, NY) at 2×10^5 cells/well were adsorbed with reovirus strains at an MOI of 0.01 PFU/cell at RT for 1 h. Inocula were aspirated. Cells were washed once with PBS and incubated in fresh medium at 37°C for various intervals. Virus titers in cell lysates were determined by plaque assay using L929 cells. Viral yields were determined using the following formula: $\log_{10}\text{yield}_{tx} = \log_{10}(\text{PFU/ml})_{tx} - \log_{10}(\text{PFU/ml})_{t0}$ where t_x is the time post-adsorption.

Assessment of reovirus infectivity by indirect immunofluorescence

Monolayers of L929 cells or HeLa cells seeded in 24-well plates at 2×10^5 cells/well were adsorbed with reovirus strains at an MOI of 2 PFU/cell at RT for 1 h. Inocula were aspirated. Cells were washed once with PBS and incubated in fresh medium at 37°C for various intervals. Cells were washed once with PBS and fixed with ice-cold methanol for at least 30 min. Cells were washed twice with PBS prior to blocking with 5% BSAin PBS at RT for 15 min. Cells were incubated with a polyclonal reovirus-specific serum (138) at a dilution of 1:500 in PBS containing 0.5% TX-100 at 37°C for 1 h. Primary antibody was removed, and cells were washed twice with PBS and incubated with 4',6-diamidino-2-phenylindole (DAPI) (Invitrogen) and Alexa Fluor 488-labeled goat anti-rabbit fluorescent secondary antibody (Invitrogen), both at a dilution of 1:1000 in PBS containing 0.5% TX-100, at 37°C for 1 h. Cells were washed twice with PBS, and infected cells were visualized by fluorescence microscopy. Results are expressed as the percent of infected cells present in a 10X field of view.

The effect of σ1 blockade on reovirus infectivity was tested by incubating reovirus strains with PBS, PBS containing mouse $IgG_{2\alpha}$, or PBS containing σ1-specific monoclonal antibody (mAb) 9BG5 (22) at RT for 1 h prior to adsorption onto L929 cells seeded in 24-well plates at 2×10^5 cells/well at an MOI of 2 PFU/cell at RT for 1 h. The dependence of reovirus infection on sialic acid and JAM-A was tested by treatment of HeLa cells seeded in 24-well plates at 2×10^5 cells/well with PBS, 40 mU *A. ureafaciens* neuraminidase, or 10 µg/ml hJAM-A-specific mAb J10.4 (82) at RT for 1 h prior to adsorption with reovirus strains at an MOI of 500 PFU/cell at RT for 1 h. Cells were

washed and incubated in fresh medium at 37°C for 20 h. Infectivity was assessed by indirect immunofluorescence.

Assay of ammonium chloride bypass kinetics

Monolayers of L929 cells seeded in 24-well plates at 2×10^5 cells/well were adsorbed with reovirus strains at an MOI of 25 PFU/cell at 4°C for 1 h. Following adsorption, virus inocula were removed, cells were washed with cold PBS, and 1 ml of pre-warmed medium was added to each well. Ammonium chloride was delivered to wells at various times post-adsorption to provide a final concentration of 25 mM. At 20 h post-adsorption, cells were washed once with PBS, fixed with ice-cold methanol, and processed for immunofluorescence staining. The percent infected cells was determined in a 10X field of view and normalized to the untreated condition to quantify the results.

Evaluation of reovirus internalization by confocal microscopy

Glass cover slips (1.5 mm) were placed in 24-well plates and treated with 1.6 mg/ml BD Matrigel® (BD Life Sciences; Franklin Lakes, NJ) diluted in incomplete medium at RT for 1 h with continuous rocking. Cover slips were rinsed with incomplete medium, seeded with 6.5×10^4 L929 cells each, and incubated at 37°C overnight. The medium was removed, and cells were adsorbed with WT, L, and IDR reoviruses labeled with Alexa Fluor 488 as described (51) at 5×10^4 virus particles per cell at RT for 30 min with continuous rocking. Virus inocula were aspirated, and cells were either washed twice with PBS and fixed immediately with 10% formalin or incubated in complete medium at 37°C for 1 h, rinsed once with PBS, and fixed. Formalin was quenched with

an equivalent volume of 0.1 M glycine. Cells were washed twice with PBS, blocked with PBS-BG (0.5% BSA, 0.1% glycine) at RT for 10 min, and incubated with polyclonal reovirus-specific serum at a 1:1000 dilution in PBS-BG at RT for 1 h. Cells were rinsed three times with PBS-BG at RT for 15 min with continuous rocking and incubated with an Alexa Fluor 647-labeled goat anti-rabbit secondary antibody (Invitrogen) and Alexa Fluor 546-labeled phalloidin (Invitrogen) at 1:1000 and 1:100 dilutions in PBS-BG, respectively, at RT for 1 h. Cells were rinsed three times with PBS-BG at RT for 15 min with continuous rocking. Cover slips were mounted onto glass slides using Aqua-Poly/Mount (Polysciences; Warrington, PA) and viewed using a Zeiss LSM 510 Meta Inverted Confocal Microscope. Cells were selected for imaging in the phalloidin channel to limit observer bias.

Assessment of reovirus attachment to cells by flow cytometry

L929 cells (10^6) in 1.5-mL tubes were adsorbed with reovirus strains at 5×10^4 particles/cell at 4°C for either 30 or 60 min with continuous rotation. Following adsorption, cells were washed with ice-cold PBS supplemented to contain 5% BSA (PBS-BSA) and incubated with reovirus-specific rabbit polyclonal antiserum at a 1:2500 dilution in PBS-BSA at 4°C for 30 min with continuous rotation. Cells were washed twice with ice-cold PBS-BSA and incubated with Alexa Fluor 647-labeled goat anti-rabbit secondary antibody (Invitrogen) at a 1:1000 dilution in PBS-BSA at 4°C for 30 min with continuous rotation. Following two washes with ice-cold PBS-BSA, cells were fixed in 1% paraformaldehyde in PBS and scored for virus binding by flow cytometry using a 3-Laser BD LSRII flow cytometer (BD Biosciences; Franklin Lakes, NJ). Results

were quantified by normalizing mean fluorescence intensities (MFIs) of cell populations adsorbed with the L and IDR reovirus mutants for either 30 or 60 min to the MFI of the cell population adsorbed with WT virus for 60 min.

Electron microscopy

A drop of approximately 2 µL of purified virions at 1×10^{12} particles/ml was briefly adsorbed onto a glow-discharged carbon-coated plastic grid, stained with freshly prepared 0.75% uranyl formate for 2 min, washed twice in virion storage buffer, and dried. Two hundred particles were imaged at RT using FEI Morgani 100 kV electron microscope at 36,000x magnification.

Statistical analysis

Mean values were compared using two-tailed Student's *t* tests. *P* values < 0.05 were considered to be statistically significant. Standard error of the mean (SEM) was used as a measure of variability for means calculated for three independent experiments containing multiple replicates. Standard deviation (SD) was used as a measure of variability among individual data points.

APPENDIX A

OPTIMUM LENGTH AND FLEXIBILITY OF REOVIRUS ATTACHMENT PROTEIN σ1 ARE REQUIRED FOR EFFICIENT VIRAL INFECTION

Magdalena Bokiej, Kristen M. Ogden, Mine Ikizler, Dirk M. Reiter, Thilo Stehle, and Terence S. Dermody

Journal of Virology: accepted for publication (July 11th 2012)

Optimum Length and Flexibility of Reovirus Attachment Protein σ1 Are Required for Efficient Viral Infection

Magdalena Bokiej,[2,3] Kristen M. Ogden,[2,3†] Mine Ikizler,[1,3] Dirk M. Reiter,[4] Thilo Stehle,[4] and Terence S. Dermody[1,2,3*]

Departments of Pediatrics[1] and Pathology, Microbiology, and Immunology[2] and Elizabeth B. Lamb Center for Pediatric Research,[3] Vanderbilt University School of Medicine, Nashville, Tennessee 37232 and Interfaculty Institute for Biochemistry,[4] University of Tuebingen, D-72076 Tuebingen, Germany.

*Corresponding author. Mailing address: Lamb Center for Pediatric Research, D7235 MCN, Vanderbilt University School of Medicine, Nashville, TN 37232. Phone: (615) 343-9943. Fax: (615) 343-7659. E-mail: terry.dermody@vanderbilt.edu.

† Present address: National Institutes of Health, Bethesda, MD.

Running title: Reovirus σ1 length and flexibility

ABSTRACT

Reovirus attachment protein σ1 is an elongated trimer with head-and-tail morphology that engages cell-surface carbohydrate and junctional adhesion molecule-A (JAM-A). The σ1 protein is comprised of three domains partitioned by two flexible linkers termed inter-domain regions (IDRs). To determine the importance of σ1 length and flexibility at different stages of reovirus infection, we generated viruses with mutant σ1 molecules of altered length and flexibility and tested these viruses for the capacity to bind the cell surface, internalize, uncoat, induce protein synthesis, assemble, and replicate. We reduced the length of the α-helical σ1 tail to engineer mutants L1 and L2 and deleted midpoint and head-proximal σ1 IDRs to generate ΔIDR1 and ΔIDR2, respectively. Decreasing length or flexibility of σ1 resulted in delayed reovirus infection and reduced viral titers. L1, L2, and ΔIDR1 but not ΔIDR2 displayed reduced cell attachment, but altering σ1 length or flexibility did not diminish the efficiency of virion internalization. Replication of ΔIDR2 was hindered at a post-disassembly step. Differences between wild-type and σ1 mutant viruses were not attributable to alterations in σ1 folding, as determined by experiments assessing engagement of cell-surface carbohydrate and JAM-A by the L and IDR viruses. However, ΔIDR1 harbored substantially less σ1 on the outer capsid. Taken together, these data suggest that σ1 length is required for reovirus binding to cells. In contrast, IDR1 is required for stable σ1 encapsidation, and IDR2 is required for a post-uncoating replication step. Thus, the structural architecture of σ1 is required for efficient reovirus infection of host cells.

INTRODUCTION

Attachment to cellular receptors is the first step in viral replication and serves an important role in viral tissue tropism and pathogenesis. This process may involve multistep adhesion accompanied by considerable conformational rearrangements of viral and host molecules (30) and stimulation of intracellular signaling (49). Enveloped viruses engage receptors using glycoproteins that stud the outside of their lipid bilayers, e.g., the glycoprotein complex of HIV (36, 38), gp350 of Epstein-Barr virus (47), and the hemagglutinin of influenza virus (22, 31). Nonenveloped viruses engage receptors by capsid protrusions, e.g., VP4 of rotavirus (40), or indentations, e.g., VP1 of rhinovirus (16, 56). Adenovirus and reovirus are exceptions among nonenveloped animal viruses. These viruses feature elongated attachment spikes that span the equivalent of a capsid radius in length (24, 53). Flexibility of the adenovirus fiber permits simultaneous engagement of multiple receptors (66). In turn, fiber length appears to influence adenovirus tropism (58). It is not understood how the conformation of the reovirus attachment molecule contributes to receptor engagement and subsequent replicative steps.

Mammalian orthoreoviruses (reoviruses) form nonenveloped icosahedral particles composed of two protein shells (19) that enclose ten segments of double-stranded (ds) RNA (28). The outer capsid contains four structural proteins: σ1, σ3, μ1, and λ2. The σ1 protein, which is anchored into pentameric λ2 turrets at the capsid vertices (19), functions as the reovirus attachment molecule (37, 64). This protein recognizes at least two cellular receptors: sialic

acid (14, 55) and junctional adhesion molecule-A (JAM-A) (4). JAM-A serves as a proteinaceous receptor for all reovirus serotypes (4, 9, 54), and sialic acid is a co-receptor for serotype 3 strains (14, 27, 50).

The σ1 protein is an important determinant of reovirus dissemination within the host and tropism for host cells and tissues (4, 5, 17). This long fiber-like molecule is comprised of three discernible structural regions: an N-terminal α-helical coiled-coil, a central β-spiral interrupted by a short stretch of α-helix, and a C-terminal globular head (15, 48, 55). These domains are partitioned by two flexible segments termed inter-domain regions (IDRs) 1 and 2 (15, 24, 55). Sigma 1 engages its receptors using two distinct receptor-binding domains (RBDs) via adhesion strengthening (3). Sequences in the σ1 tail of type 3 reovirus bind sialic acid (14, 55), whereas sequences in the σ1 head engage JAM-A (4, 33).

It is possible that optimal interactions between σ1 and its receptors require that the reovirus attachment protein be long and flexible. Intramolecular mobility of σ1 at IDR1 and IDR2 (15, 24, 55) may allow movement of the spatially-independent RBDs with respect to one another as well as to the rest of the virion and permit efficient, sequential engagement of sialic acid and JAM-A during adhesion strengthening. On the other hand, σ1 length may limit steric hindrance from the bulk of the virion and thus facilitate σ1-receptor interactions that result in productive infection. Considering that the utilization of molecular length and flexibility for receptor engagement is rare among nonenveloped animal viruses, the role of σ1 may extend beyond host cell binding. Some evidence suggests that σ1 is folded on the surface of virions and extends only upon

proteolytic cleavage of the virus particle during viral disassembly (19, 25, 45). Hence, length and flexibility of σ1 might allow the attachment molecule to assume a conformation during viral particle assembly that primes it for subsequent disassembly events. The fate of σ1 upon reovirus entry into the endocytic compartment is not known. However, it is clear that σ1 must be released from the λ2 pentamers to allow exit of nascent mRNAs from transcribing core particles (10). Length and flexibility of σ1 may be required to facilitate this process.

In this study, we used reverse genetics (34, 35) to generate a panel of reovirus mutants with σ1 molecules of varying length and flexibility and evaluated the capacity of these mutants to bind the cell surface, internalize, uncoat, induce protein synthesis, assemble, and replicate. We reduced the length of the α-helical σ1 tail to engineer L1 and L2 reoviruses and deleted midpoint and head-proximal σ1 IDRs to generate ΔIDR1 and ΔIDR2, respectively. We found that σ1 length and flexibility are required for efficient reovirus infectivity and replication. L1, L2, and ΔIDR1 showed reduced capacity to attach to cells. In comparison with wild-type (WT) virus, none of the σ1 mutant viruses exhibited defects in internalization. Although not altered in attachment, ΔIDR2 was impeded at a post-disassembly replication step. None of these differences were attributable to changes in the folding of the mutant σ1 molecules. Surprisingly, ΔIDR1 virions harbored less σ1 on the outer capsid than WT virus. Thus, σ1 length is required for efficient receptor engagement, IDR1 is required for stable σ1 encapsidation, and IDR2 is required for efficient reovirus uncoating. This new information enhances an

understanding of the functions mediated by the filamentous reovirus attachment protein.

MATERIALS AND METHODS

Cells. Spinner-adapted L929 murine fibroblasts were grown in Joklik's spinner-modified minimum essential medium (SMEM; Lonza; Walkersville, MD) supplemented to contain 5% heat-inactivated fetal bovine serum (HI FBS; Invitrogen; Carlsbad, CA), 2 mM L-glutamine (Invitrogen), 100 U/ml penicillin (Invitrogen), 100 µg/ml streptomycin (Invitrogen), and 25 ng/ml amphotericin B (Sigma-Aldrich; St. Louis, MO). HeLa cells were grown in Dulbecco's modified Eagle medium (DMEM; Invitrogen) supplemented to contain 10% HI FBS, 2 mM L-glutamine, 100 U/ml penicillin, 100 µg/ml streptomycin, and 25 ng/ml amphotericin B. BHK-T7 cells were grown in DMEM supplemented to contain 5% HI FBS, 2 mM L-glutamine, 2% MEM amino acid solution (Invitrogen), and 1 mg/ml geneticin (Invitrogen).

Viruses. Recombinant reoviruses containing mutations in the σ1 protein were generated by plasmid-based reverse genetics using cloned type 3 Dearing (T3D) reovirus cDNAs (34, 35). The pT7-T3DS1.T249I template was used to engineer the pT7-T3DS1.T249I.R202W, pT7-T3DS1.T249I.L1, pT7-T3DS1.T249I.L2, pT7-T3DS1.T249I.ΔIDR1, and pT7-T3DS1.T249I.ΔIDR2 plasmids by QuikChange site-directed mutagenesis (Stratagene; La Jolla, CA). Monolayers of approximately 3×10^6 BHK-T7 cells were co-transfected with 3.5 µg each of five plasmid constructs representing the T3D reovirus genome (pT7-T3DL1, pT7-T3DL2-M3, pT7-T3DL3-M1, and pT7-T3DM2-S2-S3-S4 in combination with pT7-T3DS1.T249I or one of the altered pT7-T3DS1.T249I plasmids) using 3 µl TransIT-LT1 transfection reagent (Mirus Bio LLC; Madison,

WI) per µg of plasmid DNA. Following 48 h of incubation, recombinant viruses were isolated by plaque purification using L929 cells. Virus stocks were prepared as described (6). Virions were purified by Freon extraction from cell lysates and subsequent CsCl gradient centrifugation (25). Bands corresponding to reovirus particle density (1.36 mg/dL) were collected and dialyzed against virion storage buffer (150 mM NaCl, 15 mM $MgCl_2$, 10 mM Tris-HCl [pH 7.4]). The S1 gene sequences of mutant viruses were verified using PCR products generated from viral RNA subjected to OneStep reverse transcription-PCR (RT-PCR) (Qiagen; Valencia, CA) using S1-specific primers (32). Sequences of the S1 gene-specific primers employed for mutagenesis and sequencing are available from the corresponding author upon request. The concentration of pure reovirus virions was determined by spectrophotometry using the following equivalence: 1 AU at 260 nm = 2.1×10^{12} particles/ml. Viral titer was determined by plaque assay using L929 cells (62).

Electrophoresis of the reovirus genome. Whole reovirus virions were incubated at 95°C for 10 min in sodium dodecyl sulfate (SDS)-polyacrylamide gel electrophoresis (PAGE) buffer (62.5 mM Tris HCl [pH 6.8], 2% sodium dodecyl sulfate, 10% glycerol, 0.004% bromophenol blue), loaded into wells of pre-cast 4-20% gradient Tris-tricine polyacrylamide gels (Bio-Rad Laboratories; Hercules, CA) at 5×10^{10} particles/well, and electrophoresed at a constant current of 15 mAmp for 16 h. Following electrophoresis, the gel was stained with ethidium bromide and visualized by UV transillumination.

Virus replication in L929 cells. Monolayers of L929 cells seeded in 24-well plates (Costar; Corning Incorporated; Corning, NY) at 2×10^5 cells/well were adsorbed with reovirus strains at a multiplicity of infection (MOI) of 0.01 plaque forming units (PFU)/cell at room temperature (RT) for 1 h. Inocula were aspirated. Cells were washed once with phosphate buffered saline (PBS) and incubated in fresh medium at 37°C for various intervals. Virus titers in cell lysates were determined by plaque assay using L929 cells. Viral yields were determined using the following formula: $\log_{10}\text{yield}_{tx} = \log_{10}(\text{PFU/ml})_{tx} - \log_{10}(\text{PFU/ml})_{t0}$ where t_x is the time post-adsorption.

Assessment of reovirus infectivity by indirect immunofluorescence. Monolayers of L929 cells or HeLa cells seeded in 24-well plates at 2×10^5 cells/well were adsorbed with reovirus strains at an MOI of 2 PFU/cell at RT for 1 h. Inocula were aspirated. Cells were washed once with PBS and incubated in fresh medium at 37°C for various intervals. Cells were washed once with PBS and fixed with ice-cold methanol for at least 30 min. Cells were washed twice with PBS prior to blocking with 5% bovine serum albumin (BSA) in PBS at RT for 15 min. Cells were incubated with a polyclonal reovirus-specific serum (65) at a dilution of 1:500 in PBS containing 0.5% TX-100 at 37°C for 1 h. Primary antibody was removed, and cells were washed twice with PBS and incubated with 4',6-diamidino-2-phenylindole (DAPI) (Invitrogen) and Alexa Fluor 488-labeled goat anti-rabbit fluorescent secondary antibody (Invitrogen), both at a dilution of 1:1000 in PBS containing 0.5% TX-100, at 37°C for 1 h. Cells were washed twice with PBS, and infected cells were visualized by fluorescence

microscopy. Results are expressed as the percent of infected cells present in a 10X field of view.

The effect of σ1 blockade on reovirus infectivity was tested by incubating reovirus strains with PBS, PBS containing mouse $IgG_{2\alpha}$, or PBS containing σ1-specific monoclonal antibody (mAb) 9BG5 (8) at RT for 1 h prior to adsorption onto L929 cells seeded in 24-well plates at 2×10^5 cells/well at an MOI of 2 PFU/cell at RT for 1 h. The dependence of reovirus infection on sialic acid and JAM-A was tested by treatment of HeLa cells seeded in 24-well plates at 2×10^5 cells/well with PBS, 40 mU *Arthrobacter ureafaciens* neuraminidase, or 10 µg/ml hJAM-A-specific mAb J10.4 (39) at RT for 1 h prior to adsorption with reovirus strains at an MOI of 500 PFU/cell at RT for 1 h. Cells were washed and incubated in fresh medium at 37°C for 20 h. Infectivity was assessed by indirect immunofluorescence.

Hemagglutination (HA) assays. Purified virions were distributed into 96-well U-bottom microtiter plates (Costar) at an initial concentration of 10^{11} particles/well and serially diluted 1:2 in 50 µl PBS. Calf erythrocytes (Colorado Serum Company; Denver, CO) were washed twice with PBS, resuspended at 1% vol/vol in PBS, delivered to virus-containing wells at 50 µl/well, and incubated at 4°C for 3.5 h. HA titer is defined as 10^{11} particles divided by the number of particles/HA unit. One HA unit is the particle number sufficient to produce HA (a partial or complete shield of erythrocytes on the well bottom).

Fluorescent-linked immunosorbent assay (FLISA). Purified virions were adsorbed onto 96-well Immulon® 2HB flat-bottom microtiter plates (Fisher

Scientific; Suwanee, GA) at a concentration of 4×10^{10} particles/well in 0.05 M carbonate-bicarbonate buffer (pH 9.6) (Sigma-Aldrich). Following incubation at 4°C overnight, plates were blocked with 2% BSA in 0.05 M carbonate-bicarbonate buffer (pH 9.6) at 37°C for 2 h. Wells were washed four times with PBS containing 0.05% Tween-20 prior to incubation with either σ1-specific mAb 9BG5 (8) or σ3-specific mouse mAb 4F2 (63) at 52 and 7 μg/ml, respectively, in PBS containing 1% BSA. Plates were incubated at 37°C for 1 h, washed five times with 0.05% Tween-20 in PBS, incubated with IRDye 800 CW goat anti-mouse secondary antibody (LI-COR; Lincoln, NE) at a dilution of 1:1000 in PBS containing 1% BSA, washed four times with 0.05% Tween-20 in PBS, rinsed with PBS, and visualized using an Odyssey Infrared Imaging System (LI-COR). Well fluorescence intensity was determined using Odyssey Application Software Version 3.0 (LI-COR). Integrated well fluorescence signal for σ1 (9BG5) was divided by that obtained for σ3 (4F2) to quantify the results.

Generation of σ1 head-specific antiserum. The C-terminal head domain of T3D σ1 (amino acids 293-455) was expressed and purified as described (57). Rabbit polyclonal serum specific for the T3D σ1 head was generated by Cocalico Biologicals. A single New Zealand white rabbit was immunized with the T3D σ1 C-terminal head domain and boosted at 2, 3, and 7 weeks post-immunization.

Immunoblot of reovirus σ1 and σ3 proteins. Purified reovirus virions were incubated at 95°C for 10 min in SDS-PAGE buffer, placed into wells of pre-cast 4-20% gradient Tris-tricine polyacrylamide gels at 10^{10} particles/well, and electrophoresed at 100 V for 1.5 h. Viral proteins were transferred onto

nitrocellulose membranes at 12 V for 45 min and blocked in Odyssey blocking buffer (LI-COR) at RT for 1 h. Membranes were incubated with rabbit polyclonal serum specific for the σ1 head and mouse mAb 4F2 specific for σ3 (63) at a 1:1000 dilution and 7 μg/ml, respectively, in Odyssey blocking buffer supplemented to contain 0.2% Tween-20 at RT for 1 h. Membranes were incubated with Alexa Fluor 647-labeled goat anti-rabbit (Invitrogen) and IRDye 800CW goat anti-mouse secondary antibodies at 1:5000 and 1:10000 dilutions, respectively, in Odyssey blocking buffer supplemented to contain 0.2% Tween-20 at RT for 1 h and scanned using an Odyssey Infrared Imaging System. Protein band intensity was quantified using Odyssey Application Software Version 3.0. Integrated protein band fluorescence for σ1 was divided by that for σ3 to normalize the results.

Assay of ammonium chloride bypass kinetics. Monolayers of L929 cells seeded in 24-well plates at 2×10^5 cells/well were adsorbed with reovirus strains at an MOI of 25 PFU/cell at 4°C for 1 h. Following adsorption, virus inocula were removed, cells were washed with cold PBS, and 1 ml of pre-warmed medium was added to each well. Ammonium chloride was delivered to wells at various times post-adsorption to provide a final concentration of 25 mM. At 20 h post-adsorption, cells were washed once with PBS, fixed with ice-cold methanol, and processed for immunofluorescence staining. The percent infected cells was determined in a 10X field of view and normalized to the untreated condition to quantify the results.

Evaluation of reovirus internalization by confocal microscopy. Glass cover slips (1.5 mm) were placed in 24-well plates and treated with 1.6 mg/ml BD Matrigel® (BD Life Sciences; Franklin Lakes, NJ) diluted in incomplete medium at RT for 1 h with continuous rocking. Cover slips were rinsed with incomplete medium, seeded with 6.5×10^4 L929 cells each, and incubated at 37°C overnight. The medium was removed, and cells were adsorbed with WT, L, and IDR reoviruses labeled with Alexa Fluor 488 as described (23) at 5×10^4 virus particles per cell at RT for 30 min with continuous rocking. Virus inocula were aspirated, and cells were either washed twice with PBS and fixed immediately with 10% formalin or incubated in complete medium at 37°C for 1 h, rinsed once with PBS, and fixed. Formalin was quenched with an equivalent volume of 0.1 M glycine. Cells were washed twice with PBS, blocked with PBS-BG (0.5% BSA, 0.1% glycine) at RT for 10 min, and incubated with polyclonal reovirus-specific serum at a 1:1000 dilution in PBS-BG at RT for 1 h. Cells were rinsed three times with PBS-BG at RT for 15 min with continuous rocking and incubated with an Alexa Fluor 647-labeled goat anti-rabbit secondary antibody (Invitrogen) and Alexa Fluor 546-labeled phalloidin (Invitrogen) at 1:1000 and 1:100 dilutions in PBS-BG, respectively, at RT for 1 h. Cells were rinsed three times with PBS-BG at RT for 15 min with continuous rocking. Cover slips were mounted onto glass slides using Aqua-Poly/Mount (Polysciences; Warrington, PA) and viewed using a Zeiss LSM 510 Meta Inverted Confocal Microscope. Cells were selected for imaging in the phalloidin channel to limit observer bias.

Assessment of reovirus attachment to cells by flow cytometry. L929

cells (10^6) in 1.5-mL tubes were adsorbed with reovirus strains at 5×10^4 particles/cell at 4°C for either 30 or 60 min with continuous rotation. Following adsorption, cells were washed with ice-cold PBS supplemented to contain 5% BSA (PBS-BSA) and incubated with reovirus-specific rabbit polyclonal antiserum at a 1:2500 dilution in PBS-BSA at 4°C for 30 min with continuous rotation. Cells were washed twice with ice-cold PBS-BSA and incubated with Alexa Fluor 647-labeled goat anti-rabbit secondary antibody (Invitrogen) at a 1:1000 dilution in PBS-BSA at 4°C for 30 min with continuous rotation. Following two washes with ice-cold PBS-BSA, cells were fixed in 1% paraformaldehyde in PBS and scored for virus binding by flow cytometry using a 3-Laser BD LSRII flow cytometer (BD Biosciences; Franklin Lakes, NJ). Results were quantified by normalizing mean fluorescence intensities (MFIs) of cell populations adsorbed with the L and IDR reovirus mutants for either 30 or 60 min to the MFI of the cell population adsorbed with WT virus for 60 min.

Statistical analysis. Mean values were compared using two-tailed Student's *t* tests. *P* values < 0.05 were considered to be statistically significant. Standard error of the mean (SEM) was used as a measure of variability for means calculated for independent experiments containing multiple replicates. Standard deviation (SD) was used as a measure of variability among individual data points.

RESULTS

Construction and characterization of reovirus σ1 length and flexibility mutants. To investigate the function of σ1 length and flexibility in the reovirus life cycle, we engineered a panel of recombinant reoviruses bearing σ1 molecules of varied length and flexibility using reverse genetics (34, 35) (Fig. 1A). Mutations altering the length and flexibility of σ1 were introduced into the S1 gene-containing plasmid pT7-T3DS1.T249I by site-directed mutagenesis. We used a parental plasmid encoding a T249I substitution in the short α-helical region of the T3D σ1 body domain (Fig. 1A) to prevent proteolytic degradation of σ1 (13). As the sialic acid-binding pocket in σ1 resides in the second and third β-spiral repeats of the σ1 body domain (55), we truncated sequences in the α-helical region of the σ1 tail (20, 48) to alter σ1 length. Amino acid residues 51-100 were removed from mutant L1, and residues 83-155 were removed from mutant L2 (Table 1, Fig. 1A). IDR1 (residues 155-164) and IDR2 (residues 291-294) were deleted from σ1 to engineer ΔIDR1 and ΔIDR2 reoviruses, respectively (Table 1, Fig. 1A). Despite three attempts, a reovirus mutant lacking both IDR1 and IDR2 (ΔIDR12) could not be recovered (Table 1). L and IDR mutant reovirus S1 gene sequences were verified using cDNA obtained by RT-PCR from purified viral dsRNA. Electrophoresis of the dsRNA gene segments of mutant reoviruses revealed the anticipated genotypes (Fig. 1B). Thus, reovirus mutants with alterations in σ1 length and truncations of each of the IDRs can be recovered by reverse genetics.

As a first step to determine whether any properties attributable to σ1 are altered in the L and IDR mutants, we tested the infectivity of the L and IDR reoviruses by calculating particle-to-PFU ratios for several independent purifications of each virus (Table 1). The majority of virus stocks had particle:PFU ratios between 150 and 650, which is consistent with previously reported values for reovirus (18, 29). Despite some sample-to-sample variation, only ΔIDR1 had a significantly higher particle/PFU ratio compared with WT virus (Student's *t* test, $P < 0.01$). This result suggests that removal of IDR1 from the σ1 molecule diminishes the efficiency of reovirus infection.

Sigma 1 length and flexibility are required for reovirus replication in cell culture. To directly test whether σ1 length and flexibility influence reovirus replication, we quantified viral yields following infection of L929 cells over a 24-h time course. Cells were infected with WT, L, or IDR reoviruses at an MOI of 0.01 PFU/cell, and viral titers were determined by plaque assay at various intervals post-adsorption (Fig. 2A and B). The L and IDR mutants exhibited longer eclipse periods compared with WT virus. L2 and ΔIDR2 produced yields similar to WT following completion of the first replicative cycle (24 h) (6), but the replication kinetics of these viruses were significantly delayed (Student's *t* test, $P < 0.05$). On the other hand, L1 and ΔIDR1 replicated more slowly than WT virus throughout the course of the first replicative cycle (Student's *t* test, $P < 0.05$). These data suggest that length and flexibility of σ1 are required for reovirus replication in cultured cells.

Sigma 1 length and flexibility are required for reovirus infection in cell culture. Given the key role of σ1 in reovirus attachment (3, 4, 14, 33, 55), we next quantified L and IDR mutant infectivity in a viral protein production assay to evaluate the efficiency of the initial stages of infection. Monolayers of L929 cells were adsorbed with WT, L, and IDR reoviruses at an MOI of 2 PFU/cell, and viral infectivity was scored at various times post-adsorption by indirect immunofluorescence (Fig. 2C and D). The L and IDR reoviruses showed delayed kinetics of viral protein synthesis indicative of decreased infection compared with WT virus (Student's *t* test, $P < 0.05$). The percentage of cells infected by L1, L2, and ΔIDR1 was only 25% of that produced by WT virus at 24 h post-adsorption. In comparison with the other mutant viruses, ΔIDR2 appeared less disabled. The percentage of cells infected by this virus was 60% of that observed for WT virus at 24 h post-adsorption. These findings suggest that an impediment to L and IDR reovirus mutant replication occurs at a step in the viral life cycle prior to or during translation of viral proteins.

IDR1 is required for maintenance of σ1 within the outer capsid. We next evaluated the conformation and functional profile of mutant L and IDR σ1 molecules. To assess whether the mutant σ1 proteins are folded properly, we determined whether pre-treatment of L and IDR mutant virions with mAb 9BG5, which binds to a conformational epitope in the σ1 head (52), inhibits infection (Fig. 3). Cells were adsorbed with either vehicle- or antibody-treated virus stocks at an MOI of 2 PFU/cell, incubated in fresh medium at 37°C for 22 h, and stained with a polyclonal reovirus-specific serum. Following adsorption with a control

$IgG_{2\alpha}$ antibody, each of the viruses tested retained full capacity to infect L929 cells. In contrast, the infectivity of WT, L, and IDR reoviruses was substantially diminished by incubation with mAb 9BG5. These results suggest that the L and IDR mutant reoviruses harbor σ1 molecules with head regions that are properly folded.

To assess the capacity of σ1 to engage sialic acid, we performed HA assays using bovine erythrocytes. The capacity of reovirus to produce HA is determined by binding to sialylated glycans on erythrocytes (26, 51). Serial dilutions of virus were incubated with red blood cells at 4°C, and HA titer was determined after 3.5 h incubation (Fig. 4A and B). The HA capacity of L1, L2, and ΔIDR2 was comparable to that of WT virus. The T3D σ1-R202W mutant cannot bind sialic acid (55) and, consequently, produced no HA in this assay. In contrast, the HA titer of ΔIDR1 was approximately 80% less than that of WT. From these data, we concluded that the reduced capacity of ΔIDR1 to cross-link erythrocytes is attributable to either altered folding of the σ1 sialic-acid-binding region or decreased encapsidation of σ1 onto the ΔIDR1 virion.

To distinguish between these two possibilities, we quantified relative amounts of capsid-associated σ1 and σ3 in WT, L, and IDR virions using σ1-specific mAb 9BG5 (8) and σ3-specific mAb 4F2 (63) by FLISA (Fig. 5A and B). After normalizing the σ1 signal intensity to the σ3 signal intensity to control for viral particle number, the σ1 signal for ΔIDR1, but not the other mutants, was decreased compared with WT virus. To confirm these results, we quantified relative amounts of σ1 on L and IDR capsids by immunoblotting virion proteins

using a polyclonal serum specific for the σ1 head and σ3-specific mAb 4F2 (63) as a loading control (Fig. 6A-D). Concordant with the FLISA results, the relative amount of encapsidated σ1 was diminished exclusively for ΔIDR1. Taken together, these results suggest that the σ1 molecules of the L and IDR reoviruses are folded properly, but the amount of σ1 expressed on the ΔIDR1 capsid is diminished. It is possible that the lower amount of σ1 displayed by ΔIDR1 occurs as a consequence of either reduced stability of σ1 at capsid vertices or decreased encapsidation of σ1 during viral assembly.

L and IDR reovirus infection is dependent on sialic acid and JAM-A. To test whether the L and IDR reovirus mutants engage the known reovirus receptors, we tested the infectivity of WT and mutant reoviruses using HeLa cells after treatment with vehicle, *A. ureafaciens* neuraminidase, or JAM-A-specific mAb J10.4 (39). Pre-treated cells were adsorbed with reovirus strains at an MOI of 500 PFU/cell (calculated based on titers determined using L929 cells), incubated in fresh medium at 37°C for 22 h, and stained with a polyclonal reovirus-specific antiserum (Fig. 7). Following treatment with neuraminidase, the infectivity of the L and IDR viruses was decreased by 50-70% in comparison to the vehicle-treated condition. Similarly, incubation of cells with mAb J10.4 diminished infectivity of the L and IDR viruses by 90% in comparison to cells treated with vehicle. These data suggest that the L and IDR reoviruses engage sialic acid and JAM-A in a mechanism that leads to infection.

The L and IDR replication defect occurs prior to endosomal escape. Following attachment to host cells, reovirus is internalized into the endocytic

pathway where the viral particle undergoes acid-dependent proteolytic disassembly (2, 7, 12, 21, 59, 61), which allows the virus to gain access to the cytoplasm (1, 11). To determine whether σ1 length and flexibility are required for steps in the reovirus life cycle preceding endosomal escape, monolayers of L929 cells were adsorbed with reovirus strains at an MOI of 25 PFU/cell at 4°C to synchronize attachment, incubated at 37°C in fresh medium, and exposed to ammonium chloride to prevent endosomal acidification at defined intervals post-adsorption. After an overnight incubation, cells were scored for infection by indirect immunofluorescence (Fig. 8A and B). L1, L2, and ΔIDR1 mutant viruses bypassed the ammonium chloride blockade more slowly than WT reovirus (Student's *t* test, $P < 0.05$). These findings indicate that σ1 length and IDR1 are required for steps in reovirus replication that precede endosomal escape. The ΔIDR2 mutant bypassed the pH blockade with kinetics similar to those observed for WT virus (Student's *t* test, $P > 0.05$), suggesting that IDR2 is required for efficient completion of replication steps that temporally fall between endosomal escape and viral protein synthesis.

Internalization of L and IDR mutants is not altered. To directly assess the role of σ1 length and flexibility in reovirus internalization, we adsorbed L929 cells with Alexa Fluor 488-labeled L and IDR mutant reoviruses at 50,000 particles/cell and fixed cells at 0 and 60 min post-adsorption. We then stained cells without prior permeabilization with phalloidin to visualize actin and polyclonal reovirus-specific serum (65) to visualize extracellular reovirus particles. We quantified internalization of reovirus virions by confocal microscopy.

The inoculum dose used in this experiment allowed us to detect signal for the most disabled L and IDR mutant viruses and has been used previously for evaluation of reovirus internalization (41-44). Representative confocal micrographs of reovirus-infected L929 cells are shown in Fig. 9A. Cell surface-associated and intracellular particles are depicted in aquamarine and green, respectively. The average number of total particles per cell (extracellular and intracellular) was significantly diminished for L1, L2, and ΔIDR1 at 0 (Fig 9A, data not shown) and 60 min (Fig. 9A and B) post-adsorption, suggesting a defect in attachment for these viruses. However, at 0 and 60 min post-adsorption, 30 and 60 percent of the virus particles were internalized, respectively, for all strains tested (Fig. 9C). Therefore, native σ1 length and flexibility are not required for reovirus internalization, but these features of σ1 appear to augment attachment to host cells.

Length and IDR1 of σ1 are required for reovirus attachment. To directly investigate the role of σ1 length and flexibility in reovirus attachment, we adsorbed L929 cells with the L and IDR mutants at 4°C for 30 or 60 min and quantified virus binding by flow cytometry (Fig. 10). Compared with WT virus, we found that cell binding was reduced by 65 to 78% for L1, L2, and ΔIDR1 at both 30 and 60 min post-adsorption. The binding of ΔIDR2 to cells was reduced by about 10 to 17% compared with WT virus, but this difference was not statistically significant. These results show that σ1 length and IDR1 are required for efficient reovirus attachment to L929 cells.

DISCUSSION

Adenovirus and reovirus display elongated filamentous attachment spikes that extend from their capsids (24, 53). This architectural feature distinguishes these viruses from other nonenveloped animal viruses that engage receptors via capsid protrusions (40) or indentations (56). Thus, the structure of adenovirus fiber and reovirus σ1 raises the possibility that these molecules serve functions in viral replication in addition to cell attachment. In fact, flexibility of the adenovirus fiber is required for efficient internalization of the virus (66). It is not known how the conformation of the reovirus attachment molecule contributes to receptor engagement and subsequent replicative steps. In this study, we used plasmid-based reverse genetics (34, 35) to engineer mutant viruses bearing σ1 molecules of varying length and flexibility (Fig. 1A and B, Table 1) and defined the capacity of these mutants to bind to cells, internalize, uncoat, induce viral protein synthesis, replicate, and assemble. We found that σ1 length and flexibility are required for efficient reovirus attachment, uncoating, and stable σ1 encapsidation during viral particle assembly.

We shortened the reovirus attachment protein by deleting parts of the α-helical tail domain (48) to avoid altering the sialic acid RBD located in the β-spiral body domain of the molecule (14, 55). Seven and 10 α-helical turns were removed from σ1 to generate the L1 and L2 reoviruses, respectively (Fig. 1A, Table 1). We also deleted the midpoint and head-proximal IDRs of σ1 to engineer ΔIDR1 and ΔIDR2, respectively (Fig. 1A, Table 1). We were unable to recover a virus lacking both IDR1 and IDR2 (Table 1). Since our results indicate

that both of these sequences are required for efficient reovirus replication, we think that a double IDR deletion virus is not viable.

The mutations altering length and flexibility of σ1 characterized in this study do not appear to affect σ1 folding. L and IDR virus infection of L929 cells was neutralized by mAb 9BG5, which recognizes a conformational epitope in the σ1 head domain (8, 52) (Fig. 3). This finding suggests that there are no gross alterations in the σ1 head. Moreover, following adsorption of HeLa cells with JAM-A-specific mAb J10.4 (39), infection by the L and IDR mutants was abolished (Fig. 7), suggesting that the JAM-A RBD of these reoviruses is not misfolded. Surprisingly, FLISAs using 9BG5 revealed that the relative amount of encapsidated σ1 is reduced in ΔIDR1 but not in L1, L2, or ΔIDR2 (Fig. 5A and B). Immunoblot analysis of L and IDR capsid proteins using a polyclonal antiserum specific for the σ1 head also showed that only ΔIDR1 of the mutants tested harbors less σ1 compared with WT virus (Fig. 6A-D). Finally, the particle:PFU ratio for ΔIDR1 was increased (Table 1), suggesting that a higher proportion of ΔIDR1 than WT virions is functionally impaired. Hence, the decreased attachment to L929 cells observed for ΔIDR1 (Fig. 10) is most likely attributable to stoichiometrically less σ1 on the ΔIDR1 capsid.

Since a mAb specific for the σ1 sialic acid RBD is not available, we tested the capacity of the L and IDR mutants to engage sialic acid using HA assays (Fig. 4A and B). The HA capacities of L1, L2, and ΔIDR2 were comparable to WT virus, suggesting that the sialic acid RBD of these viruses is properly folded. However, the HA titer of ΔIDR1 was decreased by approximately 80%. This

reduction is not likely caused by misfolding of the ΔIDR1 sialic acid RBD. Following treatment of HeLa cells with neuraminidase to remove cell-surface sialic acid, infection of WT, L, and IDR reoviruses was reduced to the same extent (Fig. 7), suggesting that all of the viruses tested rely in part on sialic acid binding for infection and, therefore, that their σ1 sialic acid RBD is properly folded. These results provide further evidence that the conformations of the L and IDR mutant σ1 molecules are not grossly altered and that the amount of σ1 on the ΔIDR1 capsid is reduced.

The hydrophobic N-terminus of σ1 directly interacts with pentameric turrets formed by λ2 at the capsid vertices and thus tethers the reovirus attachment molecule to the virion surface (19). Other outer-capsid proteins have not been reported to directly interact with σ1 but such contacts cannot be excluded based on the available evidence. However, the reovirus attachment molecule is likely collapsed in some way on the surface of virions and extends outward only upon proteolytic removal of σ3 during the formation of infectious subvirion particles (ISVPs) during viral disassembly (19, 25, 45). Interestingly, ISVPs display decreased infectivity following exposure to heat (46), which might be attributable to decreased stability of the extended conformer of σ1 at the capsid vertices. Therefore, IDR1 may stabilize σ1 by allowing it to adopt a folded conformation on the virion surface. IDR1 also could permit σ1 to assume a conformation amenable to capsid assembly. Alternatively, IDR1 may interact with other outer-capsid proteins (λ2, μ1, or σ3) to allow for stable σ1 encapsidation in the virion.

Our findings suggest that flexibility of σ1 at IDR2 is required for a replicative step that takes place after protease-dependent uncoating of reovirus in the endocytic pathway but before initiation of viral protein synthesis. Following an initial delay, ΔIDR2 produced WT-level yields of viral progeny at the end of a single infectious cycle (24 h) (Fig. 2B). In addition, ΔIDR2 infected a significantly lower percentage of cells compared with WT virus (Fig. 2D), again consistent with a prolonged eclipse phase. However, the interval required by ΔIDR2 to bypass a block to replication imposed by ammonium chloride did not differ from WT (Fig. 8B). Concordantly, ΔIDR2 did not exhibit defects in attachment (Fig. 10) or internalization (Fig. 9).

The underlying mechanism for the defect in ΔIDR2 replication is not clear from our study. However, σ1 must be shed from the λ2 turrets to allow export of nascent transcripts through unobstructed λ2 channels at the icosahedral vertices of transcribing reovirus cores (10, 19). Since σ1 dissociates from λ2 at some point after endosomal proteolysis of the reovirus outer capsid (10, 11), we think that IDR2 of σ1 is required to facilitate this process. An alternative possibility is that IDR2 is involved in viral RNA transcription or protein synthesis in some way, but this explanation does not seem likely. Little σ1 would be available following disassembly and endosomal escape to serve a function in viral transcription or translation.

It is clear from our results that optimum length of the σ1 molecule is required for efficient reovirus binding to cells. L1 and L2 both showed delayed replication kinetics (Fig. 2A) and infected approximately 75% fewer cells

compared with WT virus (Fig. 2C). Both mutants exhibited delayed bypass of an ammonium chloride replication block (Fig. 8), which we think is entirely due to inefficient attachment (Fig. 10), as internalization of these mutants is not altered (Fig. 9). Moreover, the reduction in binding to cells detected for L1 and L2 (Fig. 10) corresponds to the decrease in infectivity observed for these mutants (Fig. 2C). Therefore, σ1 length could limit steric hindrance from the bulk of the virion to allow for appropriate cell-surface receptor engagement. Although the α-helical fragment of L1 σ1 is longer than that of L2 (Fig. 1A, Table 1), we did not note any obvious phenotypic differences between L1 and L2 in the assays employed in this study. It is possible that mutants with even shorter σ1 proteins would be more severely compromised. However, we did not attempt to generate such viruses in our study.

The length and flexibility of adenovirus fiber are important determinants of adenovirus tropism (58) and internalization efficiency (66), respectively. In this study, we found that despite extensive structural similarities between the adenovirus and reovirus attachment proteins (60), the function of σ1 length and flexibility in reovirus replication differs from the role of fiber length and flexibility in the adenovirus life cycle. We do not think that length of the reovirus attachment protein contributes significantly to reovirus tropism in the infected host. Despite dramatic serotype-dependent differences in tropism (17, 64), σ1 varies only between 455 and 470 amino acids for strains of each of the three reovirus serotypes (48). However, we found that σ1 length is required for the efficient binding of reovirus to cells, perhaps because this feature of σ1 reduces steric

hindrance from the respectively much larger virion during receptor engagement. On the other hand, flexibility of σ1 at IDR2 is required for a replicative event that follows proteolytic disassembly of reovirus particles in the endocytic pathway and may permit efficient σ1 dissociation from λ2 turrets prior to viral endosomal escape. Finally, flexibility of σ1 at IDR1 is required for stable encapsidation of the σ1 protein during particle assembly. This work reveals new functions for reovirus σ1 and provides insights into molecular events at the virus-cell interface that lead to productive infection.

ACKNOWLEDGEMENTS

We thank Karl Boehme and Denise Wetzel for critical reviews of the manuscript. We thank Kerstin Reiss at the University of Tuebingen and Seva Gurevich, Jens Meiler, Earl Ruley, Ben Spiller, and John Williams at Vanderbilt University for critical advice. We thank Regan Cox and Bernardo Mainou for technical assistance with the confocal microscopy experiments. We are grateful to members of the Dermody laboratory for useful suggestions during the course of this study. The confocal microscopy experiments were conducted in the Vanderbilt Cell Imaging Shared Resource.

This work was supported by Public Health Service awards T32 GM07347 for the Medical Scientist Training Program and R01 AI76983 and the Elizabeth B. Lamb Center for Pediatric Research. Additional support was provided by Public Health Service awards P30 CA68485 for the Vanderbilt-Ingram Cancer Center and P60 DK20593 for the Vanderbilt Diabetes Research and Training Center.

REFERENCES

1. **Agosto MA, Ivanovic T, Nibert ML.** 2006. Mammalian reovirus, a nonfusogenic nonenveloped virus, forms size-selective pores in a model membrane. Proc. Natl. Acad. Sci. U. S. A. **103:**16496-16501.
2. **Baer GS, Dermody TS.** 1997. Mutations in reovirus outer-capsid protein σ3 selected during persistent infections of L cells confer resistance to protease inhibitor E64. J. Virol. **71:**4921-4928.
3. **Barton ES, Connolly JL, Forrest JC, Chappell JD, Dermody TS.** 2001. Utilization of sialic acid as a coreceptor enhances reovirus attachment by multistep adhesion strengthening. J. Biol. Chem. **276:**2200-2211.
4. **Barton ES, Forrest JC, Connolly JL, Chappell JD, Liu Y, Schnell F, Nusrat A, Parkos CA, Dermody TS.** 2001. Junction adhesion molecule is a receptor for reovirus. Cell **104:**441-451.
5. **Barton ES, Youree BE, Ebert DH, Forrest JC, Connolly JL, Valyi-Nagy T, Washington K, Wetzel JD, Dermody TS.** 2003. Utilization of sialic acid as a coreceptor is required for reovirus-induced biliary disease. J. Clin. Invest. **111:**1823-1833.
6. **Berard A, Coombs KM.** 2009. Mammalian reoviruses: propagation, quantification, and storage. Curr. Protoc. Microbiol. **Chapter 15:**Unit15C 1.
7. **Borsa J, Sargent MD, Lievaart PA, Copps TP.** 1981. Reovirus: evidence for a second step in the intracellular uncoating and transcriptase activation process. Virology **111:**191-200.

8. **Burstin SJ, Spriggs DR, Fields BN.** 1982. Evidence for functional domains on the reovirus type 3 hemagglutinin. Virology **117:**146-155.

9. **Campbell JA, Shelling P, Wetzel JD, Johnson EM, Wilson GAR, Forrest JC, Aurrand-Lions M, Imhof B, Stehle T, Dermody TS.** 2005. Junctional adhesion molecule-A serves as a receptor for prototype and field-isolate strains of mammalian reovirus. J. Virol. **79:**7967-7978.

10. **Chandran K, Farsetta DL, Nibert ML.** 2002. Strategy for nonenveloped virus entry: a hydrophobic conformer of the reovirus membrane penetration protein μ1 mediates membrane disruption. J. Virol. **76:**9920-9933.

11. **Chandran K, Parker JS, Ehrlich M, Kirchhausen T, Nibert ML.** 2003. The delta region of outer-capsid protein μ1 undergoes conformational change and release from reovirus particles during cell entry. J. Virol. **77:**13361-13375.

12. **Chang CT, Zweerink HJ.** 1971. Fate of parental reovirus in infected cell. Virology **46:**544-555.

13. **Chappell JD, Barton ES, Smith TH, Baer GS, Duong DT, Nibert ML, Dermody TS.** 1998. Cleavage susceptibility of reovirus attachment protein σ1 during proteolytic disassembly of virions is determined by a sequence polymorphism in the σ1 neck. J. Virol. **72:**8205-8213.

14. **Chappell JD, Duong JL, Wright BW, Dermody TS.** 2000. Identification of carbohydrate-binding domains in the attachment proteins of type 1 and type 3 reoviruses. J. Virol. **74:**8472-8479.

15. **Chappell JD, Prota A, Dermody TS, Stehle T.** 2002. Crystal structure of reovirus attachment protein σ1 reveals evolutionary relationship to adenovirus fiber. EMBO J. **21:**1-11.

16. **Colonno RJ, Condra JH, Mizutani S, Callahan PL, Davies ME, Murcko MA.** 1988. Evidence for the direct involvement of the rhinovirus canyon in receptor-binding. Proceedings of the National Academy of Sciences of the United States of America **85:**5449-5453.

17. **Dichter MA, Weiner HL.** 1984. Infection of neuronal cell cultures with reovirus mimics in vitro patterns of neurotropism. Ann. Neurol. **16:**603-610.

18. **Doyle JD, Danthi P, Kendall EA, Ooms LS, Wetzel JD, Dermody TS.** 2012. Molecular determinants of proteolytic disassembly of the reovirus outer capsid. J. Biol. Chem. **287:**8029-38.

19. **Dryden KA, Wang G, Yeager M, Nibert ML, Coombs KM, Furlong DB, Fields BN, Baker TS.** 1993. Early steps in reovirus infection are associated with dramatic changes in supramolecular structure and protein conformation: analysis of virions and subviral particles by cryoelectron microscopy and image reconstruction. J. Cell Biol. **122:**1023-1041.

20. **Duncan R, Horne D, Cashdollar LW, Joklik WK, Lee PWK.** 1990. Identification of conserved domains in the cell attachment proteins of the three serotypes of reovirus. Virology **174:**399-409.

21. **Ebert DH, Deussing J, Peters C, Dermody TS.** 2002. Cathepsin L and cathepsin B mediate reovirus disassembly in murine fibroblast cells. J. Biol. Chem. **277:**24609-24617.

22. **Eisen MB, Sabesan S, Skehel JJ, Wiley DC.** 1997. Binding of the influenza A virus to cell-surface receptors: structures of five hemagglutinin-sialyloligosaccharide complexes determined by X-ray crystallography. Virology **232:**19-31.

23. **Fecek RJ, Busch R, Lin H, Pal K, Cunningham CA, Cuff CF.** 2006. Production of Alexa Fluor 488-labeled reovirus and characterization of target cell binding, competence, and immunogenicity of labeled virions. J. Immunol. Methods **314:**30-7.

24. **Fraser RDB, Furlong DB, Trus BL, Nibert ML, Fields BN, Steven AC.** 1990. Molecular structure of the cell-attachment protein of reovirus: correlation of computer-processed electron micrographs with sequence-based predictions. J. Virol. **64:**2990-3000.

25. **Furlong DB, Nibert ML, Fields BN.** 1988. Sigma 1 protein of mammalian reoviruses extends from the surfaces of viral particles. J. Virol. **62:**246-256.

26. **Gentsch JR, Pacitti AF.** 1987. Differential interaction of reovirus type 3 with sialylated receptor components on animal cells. Virology **161:**245-248.

27. **Gentsch JR, Pacitti AF.** 1985. Effect of neuraminidase treatment of cells and effect of soluble glycoproteins on type 3 reovirus attachment to murine L cells. J. Virol. **56:**356-364.

28. **Gomatos PJ, Tamm I.** 1963. The secondary structure of reovirus RNA. Proc. Natl. Acad. Sci. U. S. A. **49:**707-714.

29. **Hand R, Tamm I.** 1973. Initiation of DNA synthesis in mammalian cells and its inhibition by reovirus infection. J. Mol. Biol. **82:**175-183.

30. **Hewat EA, Neumann E, Blaas D.** 2002. The concerted conformational changes during human rhinovirus 2 uncoating. Mol. Cell **10:**317-26.

31. **Kida H, Webster RG, Yanagawa R.** 1983. Inhibition of virus-induced hemolysis with monoclonal antibodies to different antigenic areas on the hemagglutinin molecule of A/seal/Massachusetts/1/80 (H7N7) influenza virus. Arch. Virol. **76:**91-9.

32. **Kim M, Garant KA, zur Nieden NI, Alain T, Loken SD, Urbanski SJ, Forsyth PA, Rancourt DE, Lee PW, Johnston RN.** 2011. Attenuated reovirus displays oncolysis with reduced host toxicity. Br. J. Cancer **104:**290-9.

33. **Kirchner E, Guglielmi KM, Strauss HM, Dermody TS, Stehle T.** 2008. Structure of reovirus σ1 in complex with its receptor junctional adhesion molecule-A. PLoS Pathog. **4:**e1000235.

34. **Kobayashi T, Antar AAR, Boehme KW, Danthi P, Eby EA, Guglielmi KM, Holm GH, Johnson EM, Maginnis MS, Naik S, Skelton WB, Wetzel JD, Wilson GJ, Chappell JD, Dermody TS.** 2007. A plasmid-

based reverse genetics system for animal double-stranded RNA viruses. Cell Host Microbe **1:**147-157.

35. **Kobayashi T, Ooms LS, Ikizler M, Chappell JD, Dermody TS.** 2010. An improved reverse genetics system for mammalian orthoreoviruses. Virology **2:**194-200.

36. **Kwong PD, Wyatt R, Robinson J, Sweet RW, Sodroski J, Hendrickson WA.** 1998. Structure of an HIV gp120 envelope glycoprotein in complex with the CD4 receptor and a neutralizing antibody. Nature **393:**648-659.

37. **Lee PWK, Hayes EC, Joklik WK.** 1981. Protein σ1 is the reovirus cell attachment protein. Virology **108:**156-163.

38. **Lifson JD, Feinberg MB, Reyes GR, Rabin L, Banapour B, Chakrabarti S, Moss B, Wong-Staal F, Steimer KS, Engleman EG.** 1986. Induction of CD4-dependent cell fusion by the HTLV-III/LAV envelope glycoprotein. Nature **323:**725-8.

39. **Liu Y, Nusrat A, Schnell FJ, Reaves TA, Walsh S, Ponchet M, Parkos CA.** 2000. Human junction adhesion molecule regulates tight junction resealing in epithelia. J. Cell Sci. **113:**2363-2374.

40. **Ludert JE, Feng N, Yu JH, Broome RL, Hoshino Y, Greenberg HB.** 1996. Genetic mapping indicates that VP4 is the rotavirus cell attachment protein in vitro and in vivo. J. Virol. **70:**487-493.

41. **Maginnis MS, Forrest JC, Kopecky-Bromberg SA, Dickeson SK, Santoro SA, Zutter MM, Nemerow GR, Bergelson JM, Dermody TS.**

2006. β1 integrin mediates internalization of mammalian reovirus. J. Virol. **80:**2760-2770.

42. **Maginnis MS, Mainou BA, Derdowski AM, Johnson EM, Zent R, Dermody TS.** 2008. NPXY motifs in the β1 integrin cytoplasmic tail are required for functional reovirus entry. J. Virol. **82:**3181-3191.

43. **Mainou BA, Dermody TS.** 2011. Src kinase mediates productive endocytic sorting of reovirus during cell entry. J. Virol. **85:**3203-13.

44. **Mainou BAD, T. S.** 2012. Transport to late endosomes is required for efficient reovirus infection. J. Virol. Published electronically ahead of print.

45. **Metcalf P, Cyrklaff M, Adrian M.** 1991. The 3-dimensional structure of reovirus obtained by cryoelectron microscopy. EMBO J. **10:**3129-3136.

46. **Middleton JK, Agosto MA, Severson TF, Yin J, Nibert ML.** 2007. Thermostabilizing mutations in reovirus outer-capsid protein μ1 selected by heat inactivation of infectious subvirion particles. Virology **361:**412-425.

47. **Nemerow GR, Mold C, Schwend VK, Tollefson V, Cooper NR.** 1987. Identification of Gp350 as the viral glycoprotein mediating attachment of Epstein-Barr virus (Ebv) to the Ebv/C3d Receptor of B-Cells - sequence homology of Gp350 and C3-complement fragment C3d. J. Virol. **61:**1416-1420.

48. **Nibert ML, Dermody TS, Fields BN.** 1990. Structure of the reovirus cell-attachment protein: a model for the domain organization of σ1. J. Virol. **64:**2976-2989.

49. **Norkin LC, Anderson HA, Wolfrom SA, Oppenheim A.** 2002. Caveolar endocytosis of simian virus 40 is followed by brefeldin A-sensitive transport to the endoplasmic reticulum, where the virus disassembles. J. Virol. **76:**5156-66.

50. **Paul RW, Choi AH, Lee PWK.** 1989. The α-anomeric form of sialic acid is the minimal receptor determinant recognized by reovirus. Virology **172:**382-385.

51. **Paul RW, Lee PWK.** 1987. Glycophorin is the reovirus receptor on human erythrocytes. Virology **159:**94-101.

52. **Pelletier J, Nicholson R, Bassel-Duby R, Fields BN, Sonenberg N.** 1987. Expression of reovirus type 3 Dearing σ1 and σs polypeptides in Escherichia coli. J. Gen. Virol. **68:**135-145.

53. **Pettersson U, Philipson L, Hoglund S.** 1968. Structural proteins of adenoviruses. II. Purification and characterization of the adenovirus type 2 fiber antigen. Virology **35:**204-15.

54. **Prota AE, Campbell JA, Schelling P, Forrest JC, Peters TR, Watson MJ, Aurrand-Lions M, Imhof B, Dermody TS, Stehle T.** 2003. Crystal structure of human junctional adhesion molecule 1: implications for reovirus binding. Proc. Natl. Acad. Sci. U. S. A. **100:**5366-5371.

55. **Reiter DM, Frierson JM, Halvorson EE, Kobayashi T, Dermody TS, Stehle T.** 2011. Crystal structure of reovirus attachment protein σ1 in complex with sialylated oligosaccharides. PLoS Pathog. **7:**e1002166.

56. **Rossmann MG, He Y, Kuhn RJ.** 2002. Picornavirus-receptor interactions. Trends Microbiol. **10:**324-331.

57. **Schelling P, Guglielmi KM, Kirchner E, Paetzold B, Dermody TS, Stehle T.** 2007. The reovirus σ1 aspartic acid sandwich: a trimerization motif poised for conformational change. J. Biol. Chem. **282:**11582-11589.

58. **Shayakhmetov DM, Papayannopoulou T, Stamatoyannopoulos G, Lieber A.** 2000. Efficient gene transfer into human CD34(+) cells by a retargeted adenovirus vector. J. Virol. **74:**2567-83.

59. **Silverstein SC, Astell C, Levin DH, Schonberg M, Acs G.** 1972. The mechanism of reovirus uncoating and gene activation in vivo. Virology **47:**797-806.

60. **Stehle T, Dermody TS.** 2003. Structural evidence for common functions and ancestry of the reovirus and adenovirus attachment proteins. Rev. Med. Virol. **13:**123-132.

61. **Sturzenbecker LJ, Nibert ML, Furlong DB, Fields BN.** 1987. Intracellular digestion of reovirus particles requires a low pH and is an essential step in the viral infectious cycle. J. Virol. **61:**2351-2361.

62. **Virgin HW, IV, Bassel-Duby R, Fields BN, Tyler KL.** 1988. Antibody protects against lethal infection with the neurally spreading reovirus type 3 (Dearing). J. Virol. **62:**4594-4604.

63. **Virgin HW, IV, Mann MA, Fields BN, Tyler KL.** 1991. Monoclonal antibodies to reovirus reveal structure/function relationships between

capsid proteins and genetics of susceptibility to antibody action. J. Virol. **65:**6772-6781.

64. **Weiner HL, Powers ML, Fields BN.** 1980. Absolute linkage of virulence and central nervous system tropism of reoviruses to viral hemagglutinin. J. Infect. Dis. **141:**609-616.

65. **Wetzel JD, Wilson GJ, Baer GS, Dunnigan LR, Wright JP, Tang DSH, Dermody TS.** 1997. Reovirus variants selected during persistent infections of L cells contain mutations in the viral S1 and S4 genes and are altered in viral disassembly. J. Virol. **71:**1362-1369.

66. **Wu E, Pache L, Von Seggern DJ, Mullen TM, Mikyas Y, Stewart PL, Nemerow GR.** 2003. Flexibility of the adenovirus fiber is required for efficient receptor interaction. J. Virol. **77:**7225-35.

FIGURE LEGENDS

FIG 1 Sigma 1 length (L) and interdomain region (IDR) reovirus mutants. (A) Schematic of wild-type (WT), L1, L2, ΔIDR1, and ΔIDR2 reovirus σ1 proteins. The α-helices, β-spiral repeats, and β-barrel are shown in blue, yellow, and red, respectively. Receptor-binding domains are indicated by underlines. The position of the T249I mutation is shown with black dots. Deletions of σ1 sequence are indicated with inverted triangles. SA, sialic acid; JAM-A, junctional adhesion molecule-A; IDR1, interdomain region 1; IDR2, interdomain region 2. (B) Segmented dsRNA genomes of L and IDR mutant viruses. Viral gene segments from virions of WT, R202W, L1, L2, ΔIDR1, and ΔIDR2 reovirus strains were resolved by SDS-PAGE, stained with ethidium bromide, and visualized by UV transillumination. Large (L), medium (M), and small (S) class gene segments are designated. S1 gene segments are indicated by white arrows.

FIG 2 Mutant reovirus replication and infectivity in L929 cells. (A, B) Cells were adsorbed with WT, L (A), and IDR (B) mutant reoviruses at an MOI of 0.01 PFU/cell. The inoculum was removed, fresh medium was added, and cells were incubated at 37°C for the times shown. Titers of virus in cell lysates were determined by plaque assay using L929 cells. Results are expressed as mean viral yield, which is defined as $\log_{10}(\text{titer})_{tx} - \log_{10}(\text{titer})_{t0}$ where *tx* is time post-adsorption, for three independent experiments. Error bars represent SEM. (C, D) Cells were adsorbed with WT, L (C), and IDR (D) mutant reoviruses at an MOI of 2 PFU/cell and processed for indirect immunofluorescence at the times shown

post-adsorption. Results are expressed as mean percent of infected cells in a 10X field of view for three independent experiments. Error bars represent SEM.

FIG 3 Infection by L and IDR mutant reoviruses is dependent on σ1. WT, L, and IDR reoviruses were incubated in PBS, PBS containing mouse $IgG_{2\alpha}$, or PBS containing σ1-specific mAb 9BG5 at RT for 1 h prior to adsorption at an MOI of 2 PFU/cell onto L929 cells at RT for 1 h. Cells were washed and incubated in fresh medium at 37°C for 20 h. Infectivity was assessed by indirect immunofluorescence. Results are expressed as mean percent of infected cells in a 10X field of view for three independent experiments. Error bars represent SEM. *, $P < 0.01$ in comparison to the mock-treated condition (PBS).

FIG 4 Hemagglutination (HA) assay of L and IDR mutant reoviruses. (A) Purified virions were serially diluted in PBS and incubated with bovine erythrocytes (1% vol/vol in PBS) at 4°C for 3.5 h. Erythrocyte shields indicate HA, and erythrocyte buttons indicate absence of erythrocyte cross-linking. (B) Results are expressed as mean $\log_2$ (HA titer) for four independent experiments. HA titer is defined as 10^{11} particles divided by the number of particles/HA unit. One HA unit equals the particle number sufficient to produce HA. Error bars represent SEM. *, $P < 0.001$ in comparison to WT virus.

FIG 5 Fluorescence linked immunosorbent assay (FLISA) of L and IDR mutant virus particles using σ1-specific mAb 9BG5 and σ3-specific mAb 4F2. (A) Purified virions (4×10^{10}) were adsorbed onto 96-well high-binding ELISA plates, incubated with primary antibodies, exposed to fluorescent secondary antibodies,

and visualized using an infrared imaging system. This panel shows representative signals obtained for σ1 and σ3. (B) Quantification of the σ1:σ3 FLISA signal intensity ratio for L and IDR mutant reoviruses. Results are expressed as mean well fluorescence intensity ratio for two independent experiments. Error bars represent SEM. *, $P < 0.05$ in comparison to WT virus.

FIG 6 Immunoblot analyses of (A) L and (B) IDR mutant reovirus σ1 and σ3 proteins. WT, L1, L2, ΔIDR1, and ΔIDR2 virion proteins were resolved by SDS-PAGE and transferred onto nitrocellulose membranes. Membranes were probed with a polyclonal σ1 head-specific serum and σ3-specific mAb 4F2. After incubation with fluorescent secondary antibodies, protein bands were visualized using an infrared imaging system. The σ3 band serves as an internal loading control. Quantification of the σ1:σ3 immunoblot band intensity ratio for L (C) and IDR (D) mutant reoviruses. Results are expressed as mean protein band fluorescence intensity ratio for three independent experiments. Error bars represent SEM. *, $P < 0.05$ in comparison to WT virus.

FIG 7 Infectivity of L and IDR mutant reoviruses is dependent on sialic acid and JAM-A. HeLa cells were treated with PBS (-), 40 mU/ml *A. ureafaciens* neuraminidase (N), or 10 μg/ml hJAM-specific mAb J10.4 (J) prior to adsorption with WT, L, and IDR mutant reoviruses at an MOI of 500 PFU/cell at RT for 1 h. Cells were washed and incubated in fresh medium at 37°C for 20 h. Infectivity was assessed by indirect immunofluorescence. Results are expressed as mean percent of infected cells in a 10X field of view for three independent experiments.

Error bars represent SEM. *, $P < 0.01$ in comparison to the untreated condition (PBS).

FIG 8 Kinetics of ammonium chloride blockade bypass by (A) L and (B) IDR mutant reoviruses in L929 cells. Cells were adsorbed with the reovirus strains shown at an MOI of 25 PFU/cell at 4°C for 1 h. Following adsorption, cells were washed with cold PBS and incubated in fresh medium at 37°C for 20 h. Ammonium chloride was added to the medium at the indicated times post-adsorption to achieve a final concentration of 25 mM. Infectivity was assessed by indirect immunofluorescence. Results are expressed as mean percent of infected cells in a 10X field of view normalized to the untreated condition (No AC) for three independent experiments. Error bars represent SEM.

FIG 9 Internalization of L and IDR mutant reoviruses. L929 cells were adsorbed with 50,000 particles/cell of Alexa Fluor 488-labeled WT, L, and IDR reoviruses (green) at RT for 30 min. The inoculum was removed, cells were incubated in fresh medium for the intervals shown, stained without cellular permeabilization for actin (red) and extracellular reovirus (blue), and imaged by confocal microscopy. (A) Representative digital fluorescence images of cells infected with L and IDR viruses at 0 and 60 min post-adsorption. Actin, extracellular reovirus, and intracellular reovirus are depicted in red, aquamarine, and green, respectively. Scale bars, 10 μm. (B) Quantification of the total number of reovirus particles at 60 min post-adsorption in single planes of view for 15-20 cells per virus strain for three independent experiments. Error bars indicate SEM. *, $P < 0.05$ in comparison to WT virus. (C) Quantification of the percent internalized

reovirus particles at 0 and 60 min post-adsorption in single planes of view for 15-20 cells per virus strain for three independent experiments. Error bars indicate SEM. *, $P < 0.05$ in comparison to WT virus.

FIG 10 Attachment of L and IDR mutant reoviruses. L929 cells were adsorbed with 50,000 particles/cell of WT, L, and IDR viruses at 4°C for either 30 or 60 min. Following adsorption, cells were incubated with reovirus-specific polyclonal antiserum, and virus attachment was assessed by flow cytometry. Results are presented as the percentage of WT virus (WT) binding after 60 min of incubation for two independent replicates. Error bars represent SD. *, $P < 0.02$ in comparison with WT virus.

TABLE 1. Characterization of L and IDR mutant reoviruses.

Virus strain	Mutation in σ1	Particle:PFU ratio[a]
WT[b]	-	149.1 (8)
R202W[c]	R202W	162.1 (3)
L1	Δ 51Q-100S	245.3 (3)
L2	Δ 83R-155Q	213.4 (6)
ΔIDR1	Δ 155Q-164T	543.0 (5)[d]
ΔIDR2	Δ 291S-294P	285.3 (3)
ΔIDR1/2	Δ 55Q-164T/Δ291S-294P	NR[e]

[a] Virus particle concentration was determined by spectrophotometry using the equivalence of 1 AU at 260 nm = 2.1×10^{12} particles/ml. Titers (in PFU/ml) were determined by plaque assay. The number of independent viral purification stocks tested is shown in parentheses.

[b] rsT3D.σ1.T249I (WT)

[c] rsT3D.σ1.R202W/T249I (R202W)

[d] $P < 0.05$ in comparison with WT virus

[e] Not recoverable

FIGURE 1

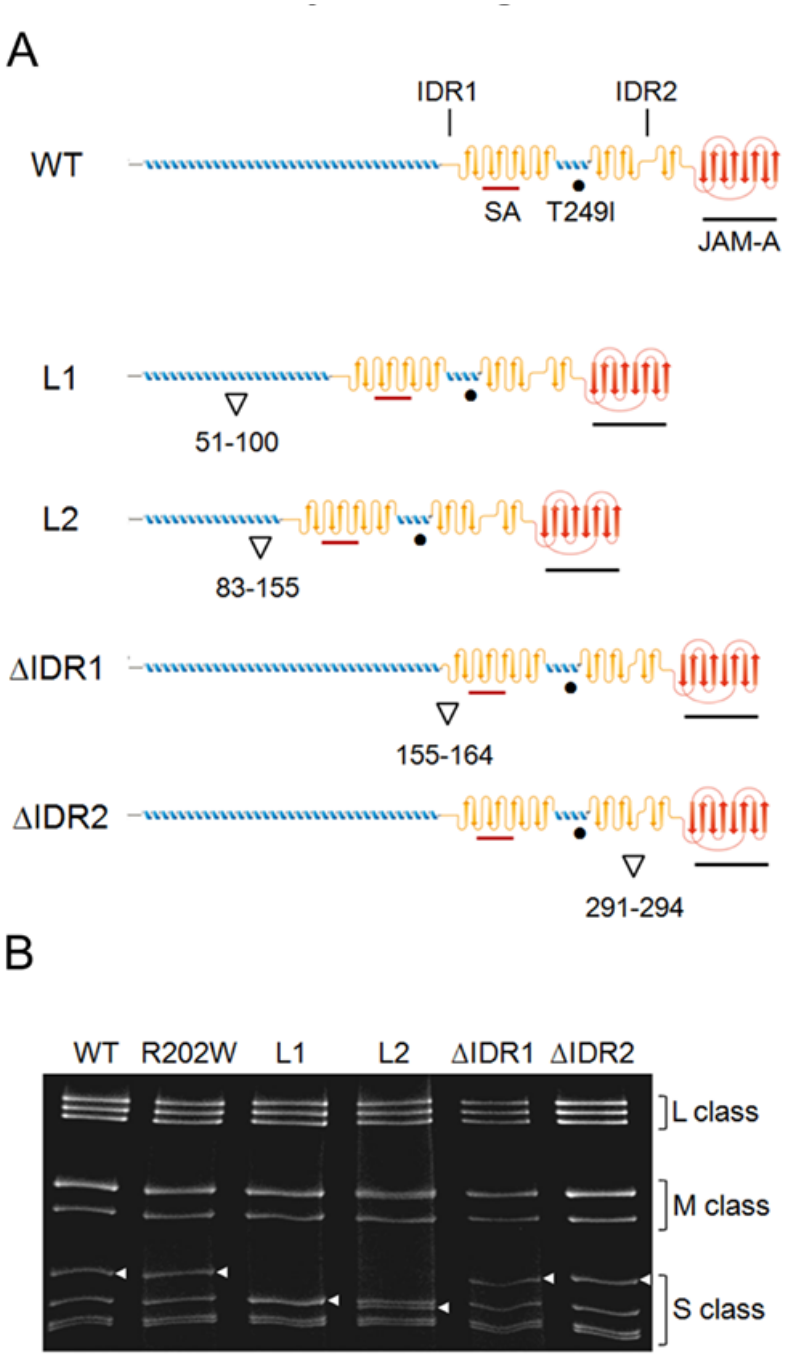
A
IDR1
IDR2
WT
SA
T249I
JAM-A
L1
51-100
L2
83-155
ΔIDR1
155-164
ΔIDR2
291-294
B
WT
R202W
L1
L2
ΔIDR1
ΔIDR2
L class
M class
S class

FIGURE 2

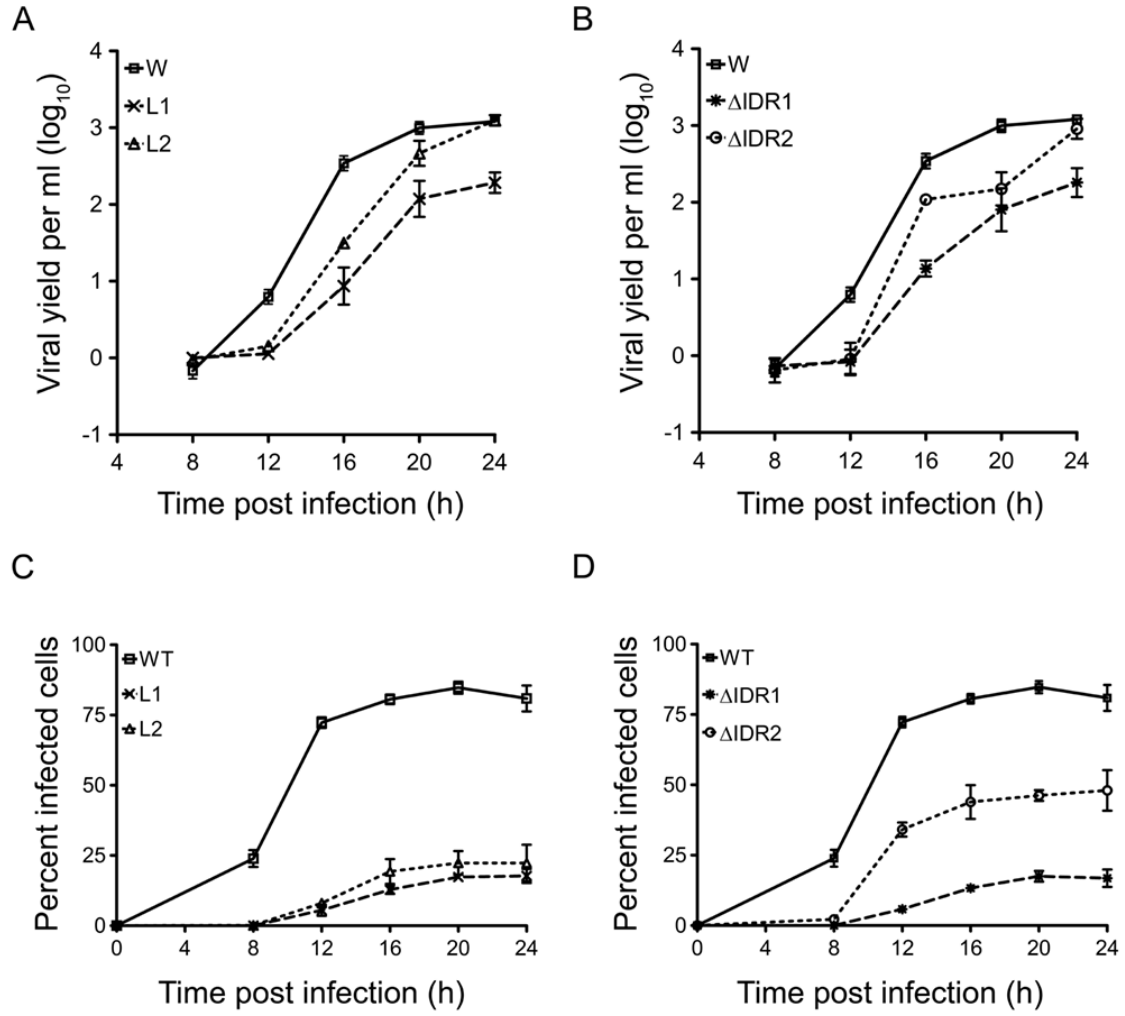
A
B
C
D
Viral yield per ml (log10)
Time post infection (h)
W
L1
L2
ΔIDR1
ΔIDR2
Percent infected cells
WT

FIGURE 3

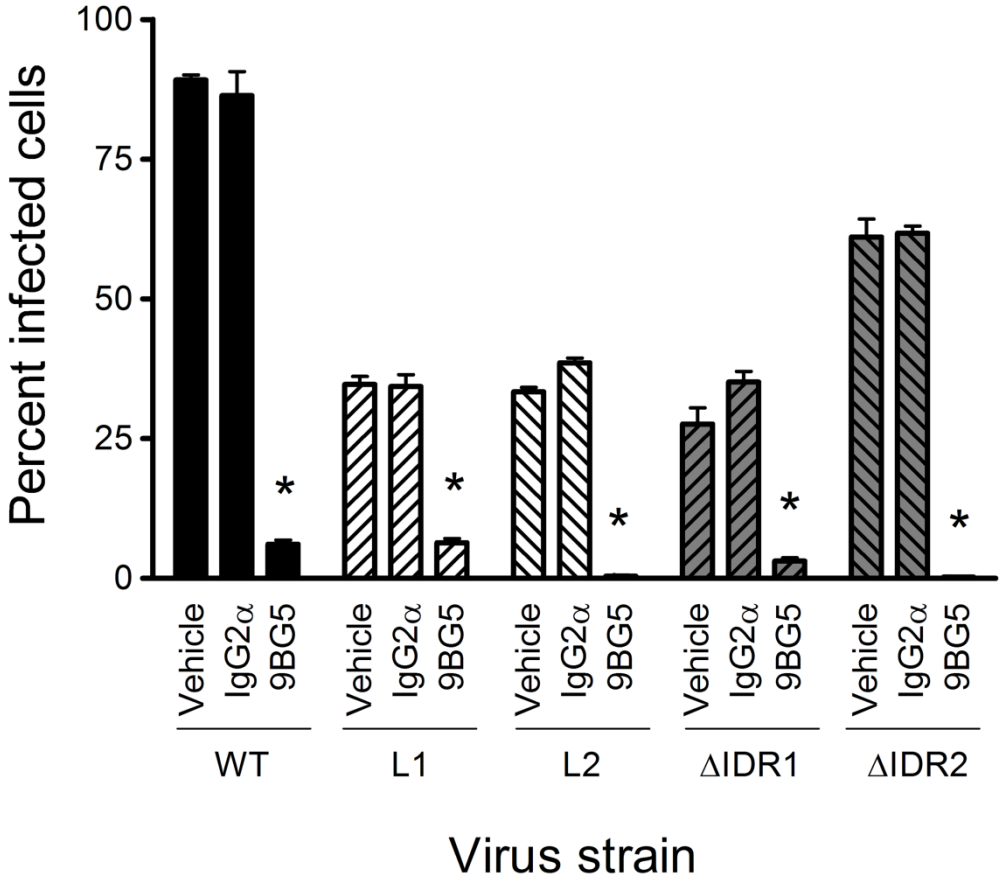

FIGURE 4

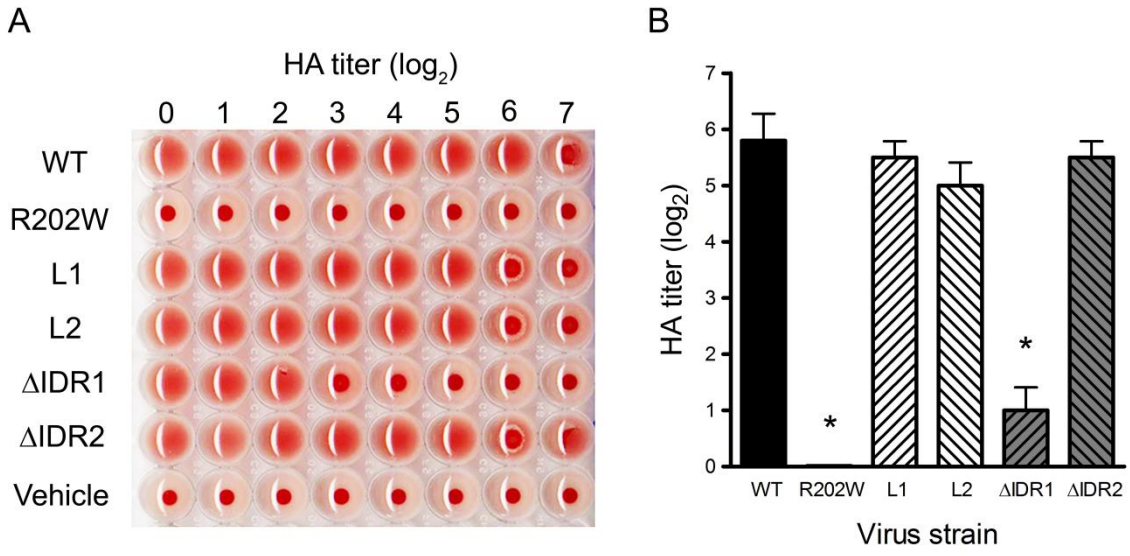

FIGURE 5

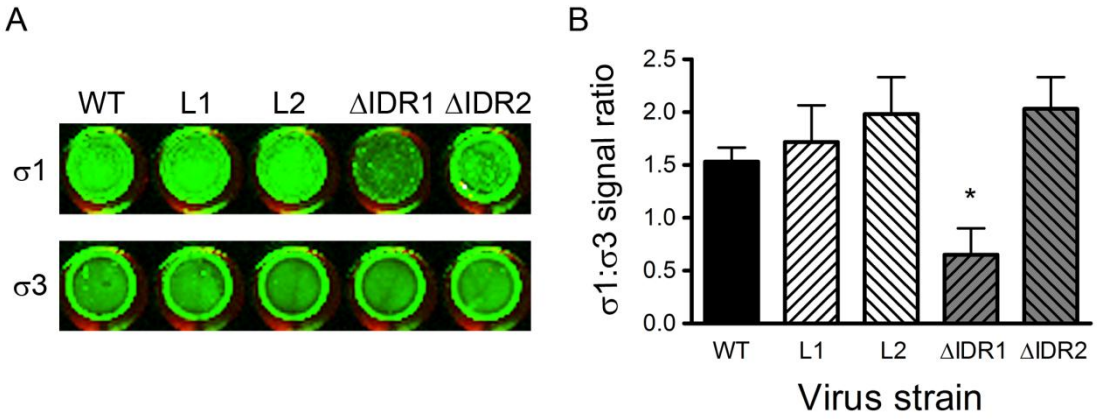

FIGURE 6

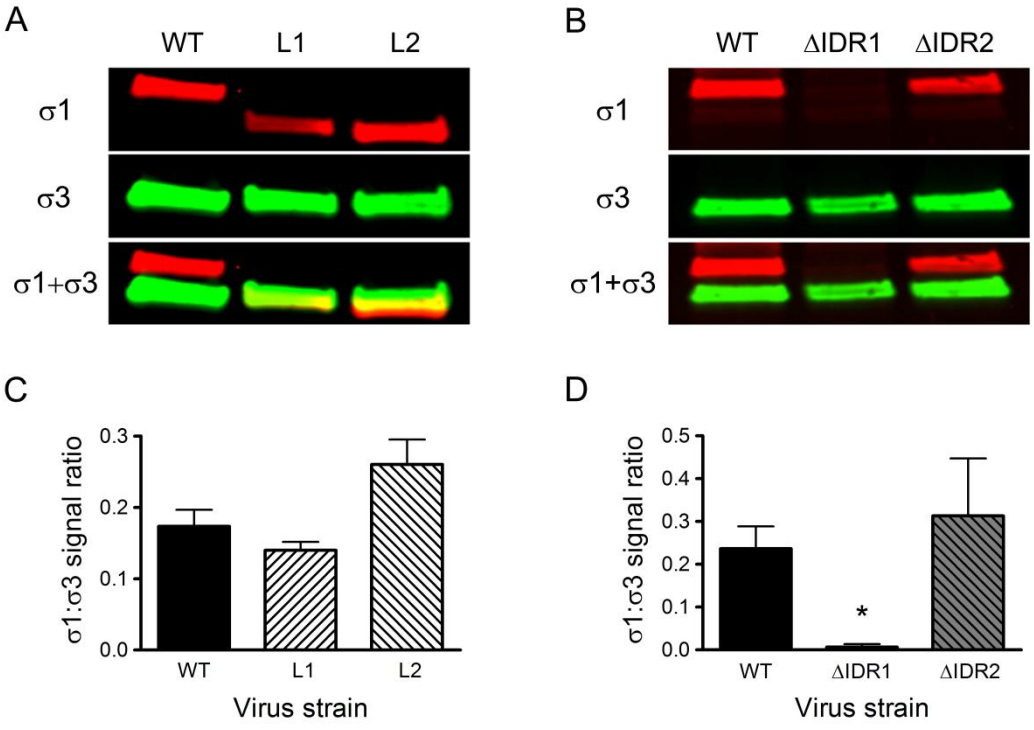

FIGURE 7

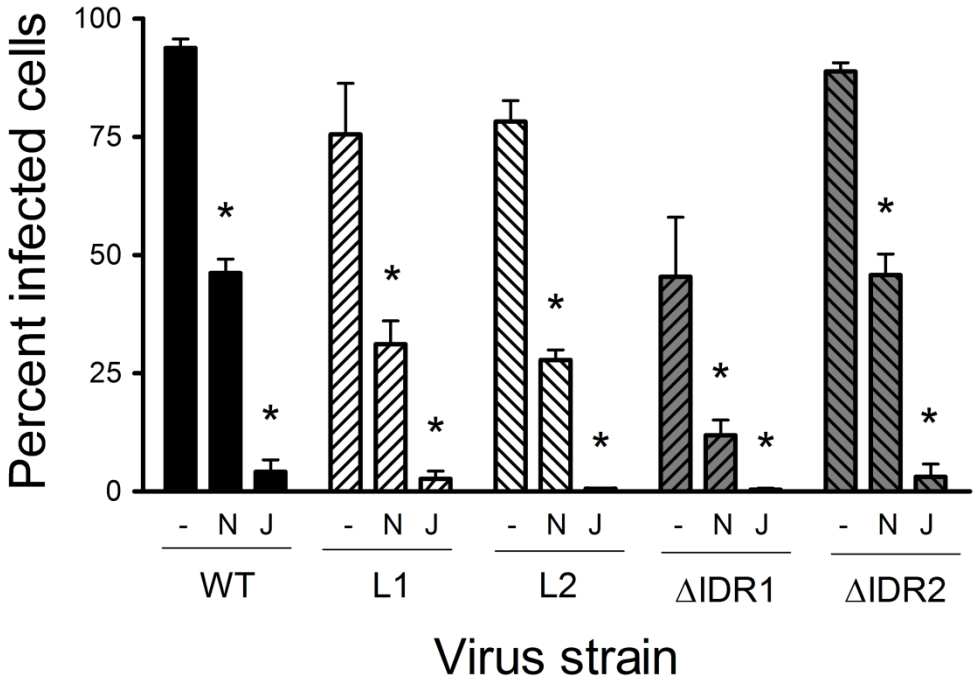
Percent infected cells
100
75
50
25
0
*
- N J
WT
L1
L2
ΔIDR1
ΔIDR2
Virus strain

FIGURE 8

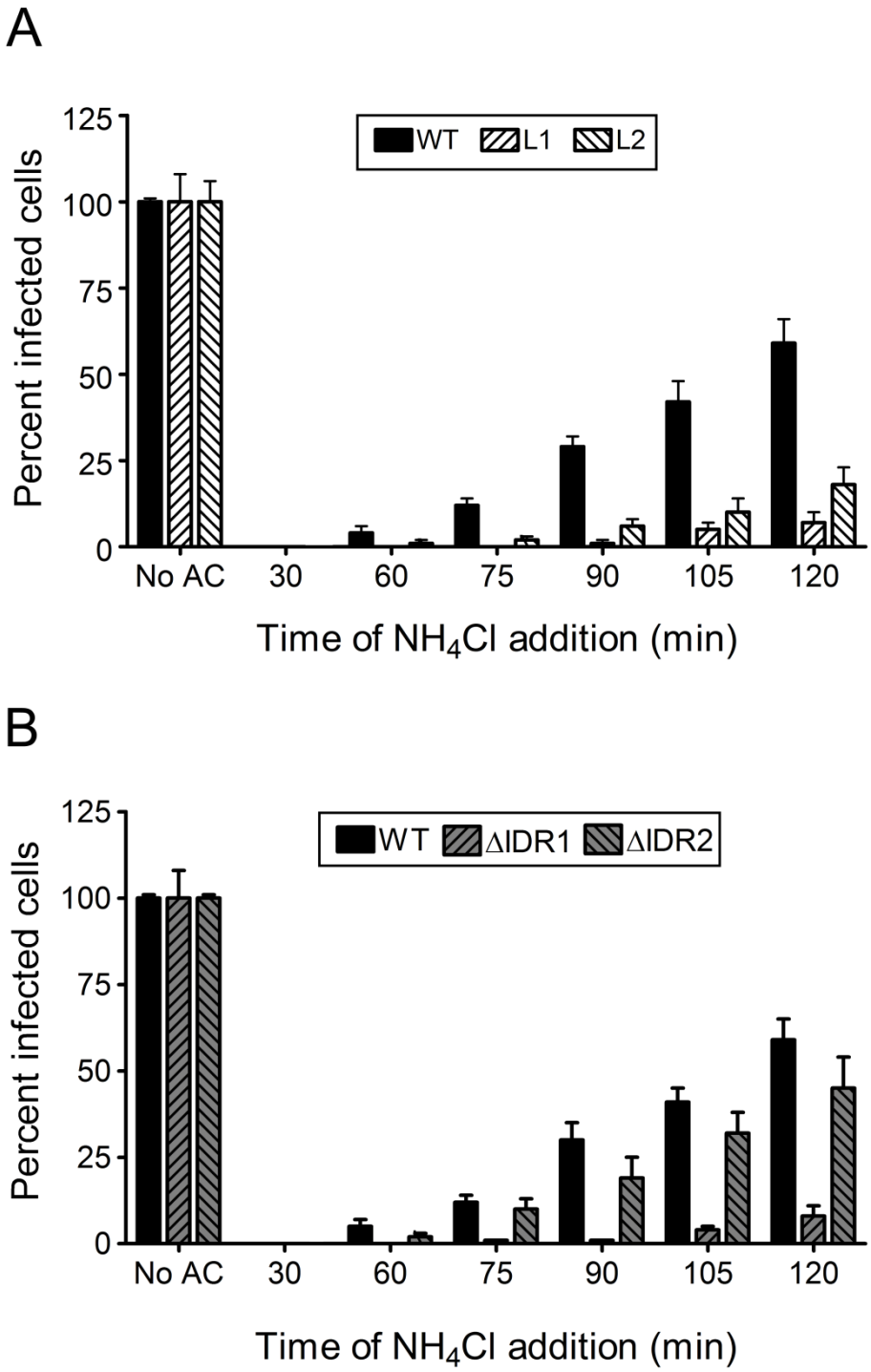
A
125
100
75
50
25
0
Percent infected cells
WT
L1
L2
No AC
30
60
75
90
105
120
Time of NH4Cl addition (min)
B
125
100
75
50
25
0
Percent infected cells
WT
ΔIDR1
ΔIDR2
No AC
30
60
75
90
105
120
Time of NH4Cl addition (min)

FIGURE 9

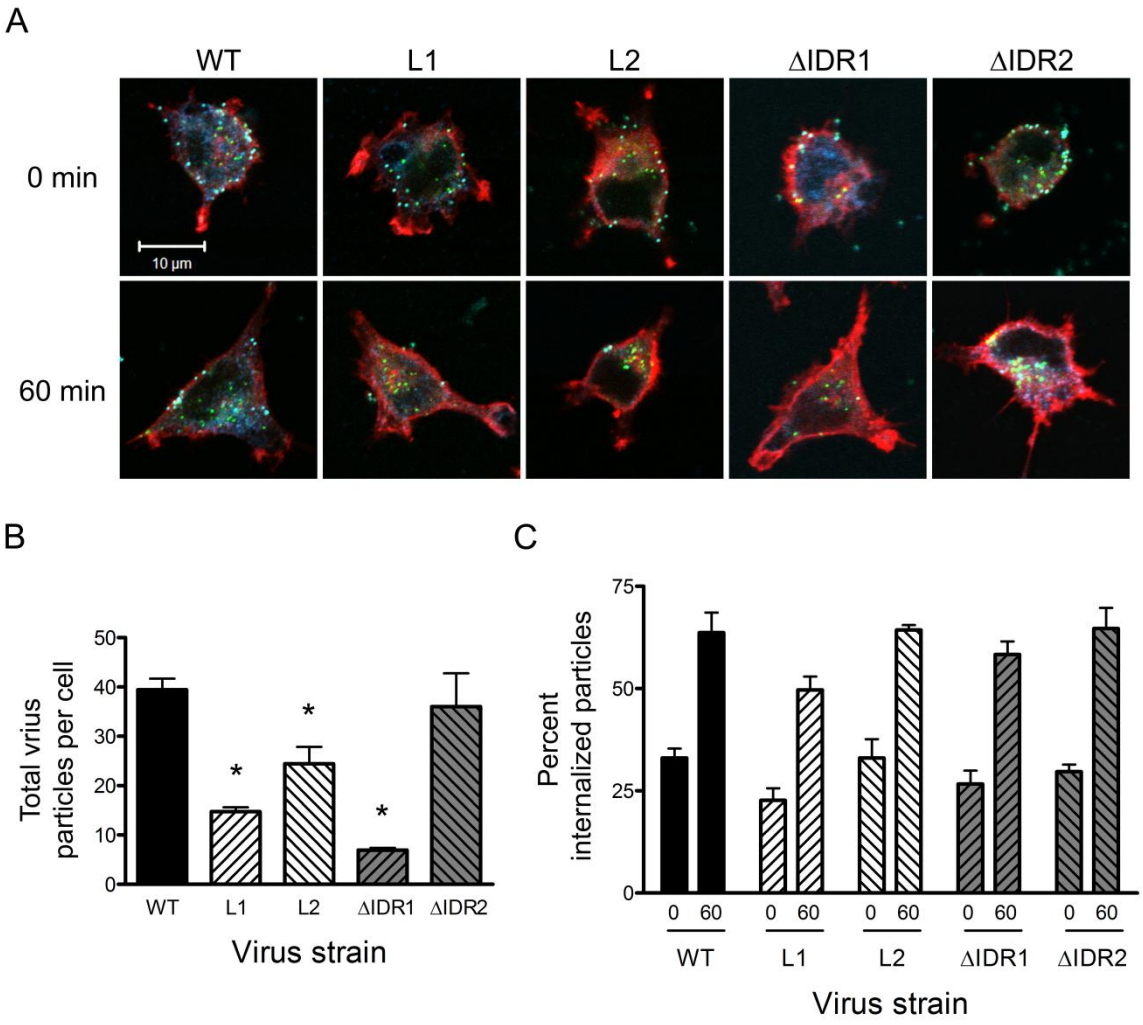
A
WT
L1
L2
ΔIDR1
ΔIDR2
0 min
60 min
10 μm
B
Total vrius particles per cell
50
40
30
20
10
0
*
*
*
WT
L1
L2
ΔIDR1
ΔIDR2
Virus strain
C
Percent internalized particles
75
50
25
0
0 60
0 60
0 60
0 60
0 60
WT
L1
L2
ΔIDR1
ΔIDR2
Virus strain

FIGURE 10

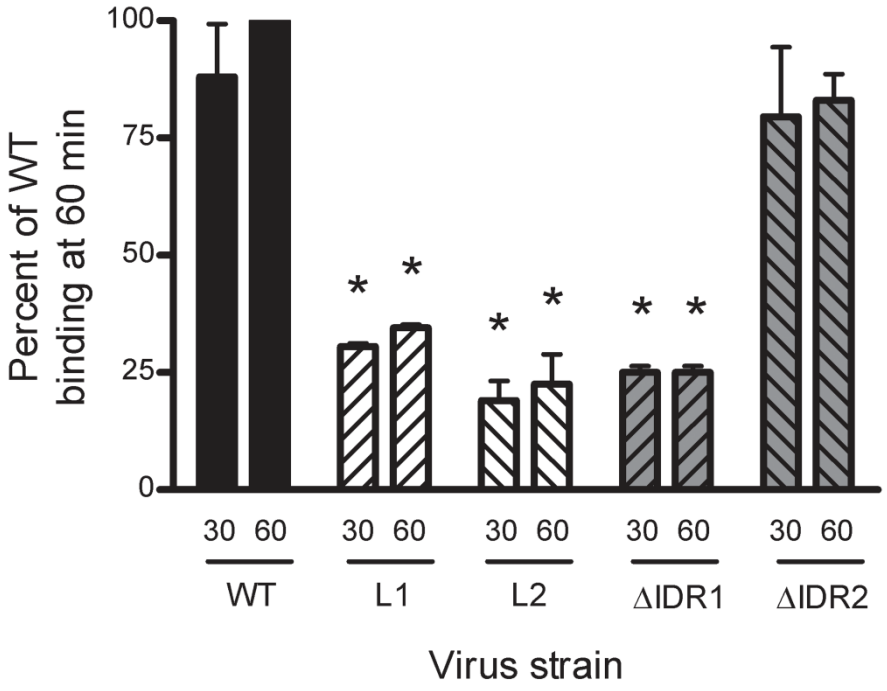
100
75
50
25
0
Percent of WT
binding at 60 min
*
*
*
*
*
*
30 60
30 60
30 60
30 60
30 60
WT
L1
L2
ΔIDR1
ΔIDR2
Virus strain

REFERENCES

1. **Abrahams JP, Leslie AG, Lutter R, Walker JE.** 1994. Structure at 2.8 Å resolution of F1-ATPase from bovine heart mitochondria. Nature **370:**621-8.

2. **Agosto MA, Ivanovic T, Nibert ML.** 2006. Mammalian reovirus, a nonfusogenic nonenveloped virus, forms size-selective pores in a model membrane. Proceedings of the National Academy of Sciences USA **103:**16496-16501.

3. **Antar AAR, Konopka JL, Campbell JA, Henry RA, Perdigoto AL, Carter BD, Pozzi A, Abel TW, Dermody TS.** 2009. Junctional adhesion molecule-A is required for hematogenous dissemination of reovirus. Cell Host & Microbe **5:**59-71.

4. **Antczak JB, Joklik WK.** 1992. Reovirus genome segment assortment into progeny genomes studied by the use of monoclonal antibodies directed against reovirus proteins. Virology **187:**760-776.

5. **Baer GS, Dermody TS.** 1997. Mutations in reovirus outer-capsid protein σ3 selected during persistent infections of L cells confer resistance to protease inhibitor E64. Journal of Virology **71:**4921-4928.

6. **Baer GS, Ebert DH, Chung CJ, Erickson AH, Dermody TS.** 1999. Mutant cells selected during persistent reovirus infection do not express mature cathepsin L and do not support reovirus disassembly. Journal of Virology **73:**9532-9543.

7. **Barton ES, Connolly JL, Forrest JC, Chappell JD, Dermody TS.** 2001. Utilization of sialic acid as a coreceptor enhances reovirus attachment by multistep adhesion strengthening. Journal of Biological Chemistry **276:**2200-2211.

8. **Barton ES, Forrest JC, Connolly JL, Chappell JD, Liu Y, Schnell F, Nusrat A, Parkos CA, Dermody TS.** 2001. Junction adhesion molecule is a receptor for reovirus. Cell **104:**441-451.

9. **Barton ES, Youree BE, Ebert DH, Forrest JC, Connolly JL, Valyi-Nagy T, Washington K, Wetzel JD, Dermody TS.** 2003. Utilization of sialic acid as a coreceptor is required for reovirus-induced biliary disease. Journal of Clinical Investigation **111:**1823-1833.

10. **Bass DM, Bodkin D, Dambrauskas R, Trier JS, Fields BN, Wolf JL.** 1990. Intraluminal proteolytic activation plays an important role in replication of type 1 reovirus in the intestines of neonatal mice. Journal of Virology **64:**1830-1833.

11. **Bazzoni G, Martinez-Estrada OM, Mueller F, Nelboeck P, Schmid G, Bartfai T, Dejana E, Brockhaus M.** 2000. Homophilic interaction of junctional adhesion molecule. Journal of Biological Chemistry **275:**30970-30976.

12. **Berard A, Coombs KM.** 2009. Mammalian reoviruses: propagation, quantification, and storage. Current Protocols in Microbiology **Chapter 15:**Unit15C 1.

13. **Bergelson JM, Cunningham JA, Droguett G, Kurt-Jones EA, Krithivas A, Hong JS, Horwitz MS, Crowell RL, Finberg RW.** 1997. Isolation of a common receptor for Coxsackie B viruses and adenoviruses 2 and 5. Science **275:**1320-1323.

14. **Bodkin DK, Nibert ML, Fields BN.** 1989. Proteolytic digestion of reovirus in the intestinal lumens of neonatal mice. Journal of Virology **63:**4676-4681.

15. **Boehme KW, Frierson JM, Konopka JL, Kobayashi T, Dermody TS.** 2011. The reovirus σ1s protein is a determinant of hematogenous but not neural virus dissemination in mice. Journal of Virology **85:**11781-90.

16. **Boehme KW, Guglielmi KM, Dermody TS.** 2009. Reovirus nonstructural protein σ1s is required for establishment of viremia and systemic dissemination. Proceedings of the National Academy of Sciences USA **106:**19986-19991.

17. **Borsa J, Morash BD, Sargent MD, Copps TP, Lievaart PA, Szekely JG.** 1979. Two modes of entry of reovirus particles into L cells. Journal of General Virology **45:**161-170.

18. **Borsa J, Sargent MD, Lievaart PA, Copps TP.** 1981. Reovirus: evidence for a second step in the intracellular uncoating and transcriptase activation process. Virology **111:**191-200.

19. **Boudin ML, Boulanger P.** 1982. Assembly of adenovirus penton base and fiber. Virology **116:**589-604.

20. **Breun LA, Broering TJ, McCutcheon AM, Harrison SJ, Luongo CL, Nibert ML.** 2001. Mammalian reovirus L2 gene and λ2 core spike protein sequences and whole-genome comparisons of reoviruses type 1 Lang, type 2 Jones, and type 3 Dearing. Virology **287:**333-348.

21. **Bullough PA, Hughson FM, Skehel JJ, Wiley DC.** 1994. Structure of influenza haemagglutinin at the pH of membrane fusion. Nature **371:**37-43.

22. **Burstin SJ, Spriggs DR, Fields BN.** 1982. Evidence for functional domains on the reovirus type 3 hemagglutinin. Virology **117:**146-155.

23. **Campadelli-Fiume G, Cocchi F, Menotti L, Lopez M.** 2000. The novel receptors that mediate the entry of herpes simplex viruses and animal alphaherpesviruses into cells. Reviews in Medical Virology **10:**305-19.

24. **Chandran K, Farsetta DL, Nibert ML.** 2002. Strategy for nonenveloped virus entry: a hydrophobic conformer of the reovirus membrane penetration protein μ1 mediates membrane disruption. Journal of Virology **76:**9920-9933.

25. **Chandran K, Parker JS, Ehrlich M, Kirchhausen T, Nibert ML.** 2003. The delta region of outer-capsid protein μ1 undergoes conformational change and release from reovirus particles during cell entry. Journal of Virology **77:**13361-13375.

26. **Chandran K, Sullivan NJ, Felbor U, Whelan SP, Cunningham JM.** 2005. Endosomal proteolysis of the Ebola virus glycoprotein is necessary for infection. Science **308:**1643-1645.

27. **Chandran K, Zhang X, Olson NH, Walker SB, Chappell JD, Dermody TS, Baker TS, Nibert ML.** 2001. Complete in vitro assembly of the reovirus outer capsid produces highly infectious particles suitable for genetic studies of the receptor-binding protein. Journal of Virology **75:**5335-5342.

28. **Chang CT, Zweerink HJ.** 1971. Fate of parental reovirus in infected cell. Virology **46:**544-555.

29. **Chappell JD, Barton ES, Smith TH, Baer GS, Duong DT, Nibert ML, Dermody TS.** 1998. Cleavage susceptibility of reovirus attachment protein σ1 during proteolytic disassembly of virions is determined by a sequence polymorphism in the σ1 neck. Journal of Virology **72:**8205-8213.

30. **Chappell JD, Duong JL, Wright BW, Dermody TS.** 2000. Identification of carbohydrate-binding domains in the attachment proteins of type 1 and type 3 reoviruses. Journal of Virology **74:**8472-8479.

31. **Chappell JD, Gunn VL, Wetzel JD, Baer GS, Dermody TS.** 1997. Mutations in type 3 reovirus that determine binding to sialic acid are contained in the fibrous tail domain of viral attachment protein σ1. Journal of Virology **71:**1834-1841.

32. **Chappell JD, Prota A, Dermody TS, Stehle T.** 2002. Crystal structure of reovirus attachment protein σ1 reveals evolutionary relationship to adenovirus fiber. EMBO Journal **21:**1-11.

33. **Chen XC, Stehle T, Harrison SC.** 1998. Interaction of polyomavirus internal protein VP2 with the major capsid protein VP1 and implications for participation of VP2 in viral entry. EMBO Journal **12:**3233-3240.

34. **Chroboczek J, Ruigrok RW, Cusack S.** 1995. Adenovirus fiber. Current Topics in Microbiology and Immunology **199 (Pt 1):**163-200.

35. **Colonno RJ, Condra JH, Mizutani S, Callahan PL, Davies ME, Murcko MA.** 1988. Evidence for the direct involvement of the rhinovirus canyon in receptor-binding. Proceedings of the National Academy of Sciences USA **85:**5449-5453.

36. **Coombs KM.** 1998. Stoichiometry of reovirus structural proteins in virus, ISVP, and core particles. Virology **243:**218-228.

37. **Cross RK, Fields BN.** 1972. Temperature-sensitive mutants of reovirus type 3: studies on the synthesis of viral RNA. Journal of Virology **50:**799-809.

38. **Danthi P, Guglielmi KM, Kirchner E, Mainou B, Stehle T, Dermody TS.** 2010. From touchdown to transcription: the reovirus cell entry pathway. Current Topics in Microbiology and Immunology **343:**91-119.

39. **Dermody TS, Nibert ML, Bassel-Duby R, Fields BN.** 1990. A σ1 region important for hemagglutination by serotype 3 reovirus strains. Journal of Virology **64:**5173-5176.

40. **Dermody TS, Nibert ML, Wetzel JD, Tong X, Fields BN.** 1993. Cells and viruses with mutations affecting viral entry are selected during persistent infections of L cells with mammalian reoviruses. Journal of Virology **67:**2055-2063.

41. **Dichter MA, Weiner HL.** 1984. Infection of neuronal cell cultures with reovirus mimics in vitro patterns of neurotropism. Annals of Neurology **16:**603-610.

42. **Doyle JD, Danthi P, Kendall EA, Ooms LS, Wetzel JD, Dermody TS.** 2012. Molecular determinants of proteolytic disassembly of the reovirus outer capsid. Journal of Biological Chemistry **287:**8029-38.

43. **Dryden KA, Wang G, Yeager M, Nibert ML, Coombs KM, Furlong DB, Fields BN, Baker TS.** 1993. Early steps in reovirus infection are associated with dramatic changes in supramolecular structure and protein conformation: analysis of virions and subviral particles by cryoelectron microscopy and image reconstruction. Journal of Cell Biology **122:**1023-1041.

44. **Duncan MR, Stanish SM, Cox DC.** 1978. Differential sensitivity of normal and transformed human cells to reovirus infection. Journal of Virology **28:**444-449.

45. **Duncan R, Horne D, Cashdollar LW, Joklik WK, Lee PWK.** 1990. Identification of conserved domains in the cell attachment proteins of the three serotypes of reovirus. Virology **174:**399-409.

46. **Ebert DH, Deussing J, Peters C, Dermody TS.** 2002. Cathepsin L and cathepsin B mediate reovirus disassembly in murine fibroblast cells. Journal of Biological Chemistry **277:**24609-24617.

47. **Ebnet K, Schulz CU, Meyer Zu Brickwedde MK, Pendl GG, Vestweber D.** 2000. Junctional adhesion molecule interacts with the PDZ domain-containing proteins AF-6 and ZO-1. Journal of Biological Chemistry **275:**27979-27988.

48. **Ehrlich M, Boll W, Van Oijen A, Hariharan R, Chandran K, Nibert ML, Kirchhausen T.** 2004. Endocytosis by random initiation and stabilization of clathrin-coated pits. Cell **118:**591-605.

49. **Eisen MB, Sabesan S, Skehel JJ, Wiley DC.** 1997. Binding of the influenza A virus to cell-surface receptors: structures of five hemagglutinin-sialyloligosaccharide complexes determined by X-ray crystallography. Virology **232:**19-31.

50. **Fan E, Merritt EA, Verlinde CL, Hol WG.** 2000. AB(5) toxins: structures and inhibitor design. Current Opinion in Structural Biology **10:**680-6.

51. **Fecek RJ, Busch R, Lin H, Pal K, Cunningham CA, Cuff CF.** 2006. Production of Alexa Fluor 488-labeled reovirus and characterization of target cell binding, competence, and immunogenicity of labeled virions. Journal of Immunological Methods **314:**30-7.

52. **Forrest JC, Campbell JA, Schelling P, Stehle T, Dermody TS.** 2003. Structure-function analysis of reovirus binding to junctional adhesion molecule 1: implications for the mechanism of reovirus attachment. Journal of Biological Chemistry **278:**48434-48444.

53. **Fraser RDB, Furlong DB, Trus BL, Nibert ML, Fields BN, Steven AC.** 1990. Molecular structure of the cell-attachment protein of reovirus: correlation of computer-processed electron micrographs with sequence-based predictions. Journal of Virology **64:**2990-3000.

54. **Furlong DB, Nibert ML, Fields BN.** 1988. Sigma 1 protein of mammalian reoviruses extends from the surfaces of viral particles. Journal of Virology **62:**246-256.

55. **Gentsch JR, Pacitti AF.** 1987. Differential interaction of reovirus type 3 with sialylated receptor components on animal cells. Virology **161:**245-248.

56. **Gillies S, Bullivant S, Bellamy AR.** 1971. Viral RNA polymerases: electron microscopy of reovirus reaction cores. Science **174:**694-696.

57. **Golden JW, Bahe JA, Lucas WT, Nibert ML, Schiff LA.** 2004. Cathepsin S supports acid-independent infection by some reoviruses. Journal of Biological Chemistry **279:**8547-8557.

58. **Golden JW, Schiff LA.** 2005. Neutrophil elastase, an acid-independent serine protease, facilitates reovirus uncoating and infection in U937 promonocyte cells. Virology Journal **2:**48.

59. **Gomatos PJ, Stoeckenius W.** 1964. Electron microscope studies on reovirus RNA. Proceedings of the National Academy of Sciences USA **52:**1449-1455.

60. **Gomatos PJ, Tamm I.** 1963. The secondary structure of reovirus RNA. Proceedings of the National Academy of Sciences USA **49:**707-714.

61. **Guglielmi KM, Kirchner E, Holm GH, Stehle T, Dermody TS.** 2007. Reovirus binding determinants in junctional adhesion molecule-A. Journal of Biological Chemistry **282:**17930-40.

62. **Hand R, Tamm I.** 1973. Initiation of DNA synthesis in mammalian cells and its inhibition by reovirus infection. Journal of Molecular Biology **82:**175-183.

63. **Hashiro G, Loh PC, Yau JT.** 1977. The preferential cytotoxicity of reovirus for certain transformed cell lines. Archives of Virology **54:**307-315.

64. **Haywood AM.** 1994. Virus receptors: Binding, adhesion strengthening, and changes in viral structure. Journal of Virology **68:**1-5.

65. **Helander A, Silvey KJ, Mantis NJ, Hutchings AB, Chandran K, Lucas WT, Nibert ML, Neutra MR.** 2003. The viral σ1 protein and glycoconjugates containing α2-3-linked sialic acid are involved in type 1 reovirus adherence to M cell apical surfaces. Journal of Virology **77:**7964-7977.

66. **Hewat EA, Neumann E, Blaas D.** 2002. The concerted conformational changes during human rhinovirus 2 uncoating. Molecular Cell **10:**317-26.

67. **Huang I-C, Bosch BJ, Li F, Li W, Lee KH, Ghiran S, Vasilieva N, Dermody TS, Harrison SC, Dormitzer PR, Farzan M, Rottier PJ, Choe H.** 2006. SARS coronavirus, but not human coronavirus NL63, utilizes cathepsin L to infect ACE2-expressing cells. Journal of Biological Chemistry **281:**3198-3203.

68. **Ito Y, Joklik WK.** 1972. Temperature-sensitive mutants of reovirus. II. Anomalous electrophoretic migration of certain hybrid RNA molecules composed of mutant plus strands and wild-type minus strands. Virology **50:**202-208.

69. **Itoh M, Sasaki H, Furuse M, Ozaki H, Kita T, Tsukita S.** 2001. Junctional adhesion molecule (JAM) binds to PAR-3: a possible mechanism for the

recruitment of PAR-3 to tight junctions. Journal of Cell Biology **154:**491-497.

70. **Kida H, Webster RG, Yanagawa R.** 1983. Inhibition of virus-induced hemolysis with monoclonal antibodies to different antigenic areas on the hemagglutinin molecule of A/seal/Massachusetts/1/80 (H7N7) influenza virus. Archives of Virology **76:**91-9.

71. **Kim J, Parker JS, Murray KE, Nibert ML.** 2004. Nucleoside and RNA triphosphatase activities of orthoreovirus transcriptase cofactor μ2. Journal of Biological Chemistry **279:**4394-403.

72. **Kim M, Garant KA, zur Nieden NI, Alain T, Loken SD, Urbanski SJ, Forsyth PA, Rancourt DE, Lee PW, Johnston RN.** 2011. Attenuated reovirus displays oncolysis with reduced host toxicity. British Journal of Cancer **104:**290-9.

73. **Kirchner E, Guglielmi KM, Strauss HM, Dermody TS, Stehle T.** 2008. Structure of reovirus σ1 in complex with its receptor junctional adhesion molecule-A. PLoS Pathogens **4:**e1000235.

74. **Kobayashi T, Antar AAR, Boehme KW, Danthi P, Eby EA, Guglielmi KM, Holm GH, Johnson EM, Maginnis MS, Naik S, Skelton WB, Wetzel JD, Wilson GJ, Chappell JD, Dermody TS.** 2007. A plasmid-based reverse genetics system for animal double-stranded RNA viruses. Cell Host & Microbe **1:**147-157.

75. **Kobayashi T, Ooms LS, Ikizler M, Chappell JD, Dermody TS.** 2010. An improved reverse genetics system for mammalian orthoreoviruses. Virology **2:**194-200.

76. **Kostrewa D, Brockhaus M, D'Arcy A, Dale GE, Nelboeck P, Schmid G, Mueller F, Bazzoni G, Dejana E, Bartfai T, Winkler FK, Hennig M.** 2001. X-ray structure of junctional adhesion molecule: structural basis for homophilic adhesion via a novel dimerization motif. EMBO Journal **20:**4391-4398.

77. **Kwong PD, Wyatt R, Robinson J, Sweet RW, Sodroski J, Hendrickson WA.** 1998. Structure of an HIV gp120 envelope glycoprotein in complex with the CD4 receptor and a neutralizing antibody. Nature **393:**648-659.

78. **Larson SM, Antczak JB, Joklik WK.** 1994. Reovirus exists in the form of 13 particle species that differ in their content of protein sigma 1. Virology **201:**303-11.

79. **Lee PWK, Hayes EC, Joklik WK.** 1981. Protein σ1 is the reovirus cell attachment protein. Virology **108:**156-163.

80. **Lerner AM, Cherry JD, Finland M.** 1963. Haemagglutination with reoviruses. Virology **19:**58-65.

81. **Lifson JD, Feinberg MB, Reyes GR, Rabin L, Banapour B, Chakrabarti S, Moss B, Wong-Staal F, Steimer KS, Engleman EG.** 1986. Induction of CD4-dependent cell fusion by the HTLV-III/LAV envelope glycoprotein. Nature **323:**725-8.

82. **Liu Y, Nusrat A, Schnell FJ, Reaves TA, Walsh S, Ponchet M, Parkos CA.** 2000. Human junction adhesion molecule regulates tight junction resealing in epithelia. Journal of Cell Science **113:**2363-2374.

83. **Ludert JE, Feng NG, Yu JH, Broome RL, Hoshino Y, Greenberg HB.** 1996. Genetic mapping indicates that VP4 is the rotavirus cell attachment protein in vitro and in vivo. Journal of Virology **70:**487-493.

84. **Maginnis MS, Forrest JC, Kopecky-Bromberg SA, Dickeson SK, Santoro SA, Zutter MM, Nemerow GR, Bergelson JM, Dermody TS.** 2006. β1 integrin mediates internalization of mammalian reovirus. Journal of Virology **80:**2760-2770.

85. **Maginnis MS, Mainou BA, Derdowski AM, Johnson EM, Zent R, Dermody TS.** 2008. NPXY motifs in the β1 integrin cytoplasmic tail are required for functional reovirus entry. Journal of Virology **82:**3181-3191.

86. **Mainou BA, Dermody TS.** 2011. Src kinase mediates productive endocytic sorting of reovirus during cell entry. Journal of Virology **85:**3203-13.

87. **Mainou BA, Dermody TS.** 2012. Transport to late endosomes is required for efficient reovirus infection. Journal of Virology (published electronically ahead of print).

88. **Mann MA, Tyler KL, Knipe DM, Fields BN.** 2002. Type 3 reovirus neuroinvasion after intramuscular inoculation: viral genetic determinants of lethality and spinal cord infection. Virology **303:**213-221.

89. **Marcato P, Shmulevitz M, Pan D, Stoltz D, Lee PW.** 2007. Ras transformation mediates reovirus oncolysis by enhancing virus uncoating, particle infectivity, and apoptosis-dependent release. Molecular Therapy **15:**1522-30.

90. **Martin-Padura I, Lostaglio S, Schneemann M, Williams L, Romano M, Fruscella P, Panzeri C, Stoppacciaro A, Ruco L, Villa A, Simmons D, Dejana E.** 1998. Junctional adhesion molecule, a novel member of the immunoglobulin superfamily that distributes at intercellular junctions and modulates monocyte transmigration. Journal of Cell Biology **142:**117-127.

91. **Merckel MC, Huiskonen JT, Bamford DH, Goldman A, Tuma R.** 2005. The structure of the bacteriophage PRD1 spike sheds light on the evolution of viral capsid architecture. Molecular Cell **18:**161-170.

92. **Metcalf P, Cyrklaff M, Adrian M.** 1991. The 3-dimensional structure of reovirus obtained by cryoelectron microscopy. EMBO Journal **10:**3129-3136.

93. **Middleton JK, Agosto MA, Severson TF, Yin J, Nibert ML.** 2007. Thermostabilizing mutations in reovirus outer-capsid protein m1 selected by heat inactivation of infectious subvirion particles. Virology **361:**412-425.

94. **Millward S, Graham AF.** 1970. Structural studies on reovirus: discontinuities in the genome. Proceedings of the National Academy of Sciences USA **65:**422-426.

95. **Morris SM, Cooper JA.** 2001. Disabled-2 colocalizes with the LDLR in clathrin-coated pits and interacts with AP-2. Traffic **2:**111-123.

96. **Morrison LA, Sidman RL, Fields BN.** 1991. Direct spread of reovirus from the intestinal lumen to the central nervous system through vagal autonomic nerve fibers. Proceedings of the National Academy of Sciences USA **88:**3852-3856.

97. **Nason EL, Wetzel JD, Mukherjee SK, Barton ES, Prasad BVV, Dermody TS.** 2001. A monoclonal antibody specific for reovirus outer-capsid protein σ3 inhibits σ1-mediated hemagglutination by steric hindrance. Journal of Virology **75:**6625-6634.

98. **Nemerow GR, Mold C, Schwend VK, Tollefson V, Cooper NR.** 1987. Identification of Gp350 as the viral glycoprotein mediating attachment of Epstein-Barr virus (Ebv) to the Ebv/C3d Receptor of B-Cells - sequence homology of Gp350 and C3-complement fragment C3d. Journal of Virology **61:**1416-1420.

99. **Nibert ML, Chappell JD, Dermody TS.** 1995. Infectious subvirion particles of reovirus type 3 Dearing exhibit a loss in infectivity and contain a cleaved σ1 protein. Journal of Virology **69:**5057-5067.

100. **Nibert ML, Dermody TS, Fields BN.** 1990. Structure of the reovirus cell-attachment protein: a model for the domain organization of σ1. Journal of Virology **64:**2976-2989.

101. **Norkin LC, Anderson HA, Wolfrom SA, Oppenheim A.** 2002. Caveolar endocytosis of simian virus 40 is followed by brefeldin A-sensitive transport to the endoplasmic reticulum, where the virus disassembles. Journal of Virology **76:**5156-66.

102. **Oleinikov AV, Zhao J, Makker SP.** 2000. Cytosolic adaptor protein Dab2 is an intracellular ligand of endocytic receptor gp600/megalin. Biochemical Journal **347:**613-621.

103. **Ozaki H, Ishii K, Horiuchi H, Arai H, Kawamoto T, Okawa K, Iwamatsu A, Kita T.** 1999. Cutting edge: combined treatment of TNF-alpha and IFN-gamma causes redistribution of junctional adhesion molecule in human endothelial cells. Journal of Immunology **163:**553-557.

104. **Pager CT, Dutch RE.** 2005. Cathepsin L is involved in proteolytic processing of the Hendra virus fusion protein. Journal of Virology **79:**12714-12720.

105. **Paul RW, Choi AH, Lee PWK.** 1989. The α-anomeric form of sialic acid is the minimal receptor determinant recognized by reovirus. Virology **172:**382-385.

106. **Paul RW, Lee PWK.** 1987. Glycophorin is the reovirus receptor on human erythrocytes. Virology **159:**94-101.

107. **Pelletier J, Nicholson R, Bassel-Duby R, Fields BN, Sonenberg N.** 1987. Expression of reovirus type 3 Dearing σ1 and σs polypeptides in Escherichia coli. Journal of General Virology **68:**135-145.

108. **Pettersson U, Philipson L, Hoglund S.** 1968. Structural proteins of adenoviruses. II. Purification and characterization of the adenovirus type 2 fiber antigen. Virology **35:**204-15.

109. **Phizicky EM, Fields S.** 1995. Protein-protein interactions: methods for detection and analysis. Microbiological Reviews **59:**94-123.

110. **Prota AE, Campbell JA, Schelling P, Forrest JC, Peters TR, Watson MJ, Aurrand-Lions M, Imhof B, Dermody TS, Stehle T.** 2003. Crystal structure of human junctional adhesion molecule 1: implications for reovirus binding. Proceedings of the National Academy of Sciences USA **100:**5366-5371.

111. **Raaij MJv, Mitraki A, Lavigne G, Cusack S.** 1999. A triple β-spiral in the adenovirus fibre shaft reveals a new structural motif for a fibrous protein. Nature **401:**935-938.

112. **Reinisch KM, Nibert ML, Harrison SC.** 2000. Structure of the reovirus core at 3.6 Å resolution. Nature **404:**960-967.

113. **Reiter DM, Frierson JM, Halvorson EE, Kobayashi T, Dermody TS, Stehle T.** 2011. Crystal structure of reovirus attachment protein σ1 in complex with sialylated oligosaccharides. PLoS Pathogens **7:**e1002166.

114. **Rossmann MG, He Y, Kuhn RJ.** 2002. Picornavirus-receptor interactions. Trends in Microbiology **10:**324-331.

115. **Rubin DH, Wetzel JD, Williams WV, Cohen JA, Dworkin C, Dermody TS.** 1992. Binding of type 3 reovirus by a domain of the σ1 protein important for hemagglutination leads to infection of murine erythroleukemia cells. Journal of Clinical Investigation **90:**2536-2542.

116. **Schelling P, Guglielmi KM, Kirchner E, Paetzold B, Dermody TS, Stehle T.** 2007. The reovirus σ1 aspartic acid sandwich: a trimerization motif poised for conformational change. Journal of Biological Chemistry **282:**11582-11589.

117. **Seliger LS, Zheng K, Shatkin AJ.** 1987. Complete nucleotide sequence of reovirus L2 gene and deduced amino acid sequence of viral mRNA guanylyltransferase. Journal of Biological Chemistry **262:**16289-16293.

118. **Severson EA, Jiang L, Ivanov AI, Mandell KJ, Nusrat A, Parkos CA.** 2008. Cis-dimerization mediates function of junctional adhesion molecule A. Molecular Biology of the Cell **19:**1862-1872.

119. **Shatkin AJ, Sipe JD, Loh PC.** 1968. Separation of 10 reovirus genome segments by polyacrylamide gel electrophoresis. Journal of Virology **12:**986-991.

120. **Shayakhmetov DM, Lieber A.** 2000. Dependence of adenovirus infectivity on length of the fiber shaft domain. Journal of Virology **74:**10274-86.

121. **Shayakhmetov DM, Papayannopoulou T, Stamatoyannopoulos G, Lieber A.** 2000. Efficient gene transfer into human CD34(+) cells by a retargeted adenovirus vector. Journal of Virology **74:**2567-83.

122. **Silverstein SC, Astell C, Levin DH, Schonberg M, Acs G.** 1972. The mechanism of reovirus uncoating and gene activation in vivo. Virology **47:**797-806.

123. **Stehle T, Dermody TS.** 2003. Structural evidence for common functions and ancestry of the reovirus and adenovirus attachment proteins. Reviews in Medical Virology **13:**123-132.

124. **Stiasny K, Allison SL, Marchler-Bauer A, Kunz C, Heinz FX.** 1996. Structural requirements for low-pH-induced rearrangements in the envelope glycoprotein of tick-borne encephalitis virus. Journal of Virology **70:**8142-8147.

125. **Strong JE, Leone G, Duncan R, Sharma RK, Lee PW.** 1991. Biochemical and biophysical characterization of the reovirus cell attachment protein sigma 1: evidence that it is a homotrimer. Virology **184:**23-32.

126. **Sturzenbecker LJ, Nibert ML, Furlong DB, Fields BN.** 1987. Intracellular digestion of reovirus particles requires a low pH and is an essential step in the viral infectious cycle. Journal of Virology **61:**2351-2361.

127. **Tardieu M, Powers ML, Weiner HL.** 1983. Age-dependent susceptibility to reovirus type 3 encephalitis: role of viral and host factors. Annals of Neurology **13:**602-607.

128. **Tomko RP, Xu R, Philipson L.** 1997. HCAR and MCAR: the human and mouse cellular receptors for subgroup C adenoviruses and group B coxsackieviruses. Proceedings of the National Academy of Sciences USA **94:**3352-6.

129. **Tyler KL.** 2001. Mammalian reoviruses, p. 1729-1745. *In* D. M. Knipe and P. M. Howley (ed.), Fields Virology, Fourth ed. Lippincott Williams & Wilkins, Philadelphia.

130. **Tyler KL, McPhee DA, Fields BN.** 1986. Distinct pathways of viral spread in the host determined by reovirus S1 gene segment. Science **233:**770-774.

131. **Virgin HW, IV, Bassel-Duby R, Fields BN, Tyler KL.** 1988. Antibody protects against lethal infection with the neurally spreading reovirus type 3 (Dearing). Journal of Virology **62:**4594-4604.

132. **Virgin HW, IV, Mann MA, Fields BN, Tyler KL.** 1991. Monoclonal antibodies to reovirus reveal structure/function relationships between capsid proteins and genetics of susceptibility to antibody action. Journal of Virology **65:**6772-6781.

133. **Virgin HW, Tyler KL, Dermody TS.** 1997. Reovirus, p. 669-699. *In* N. Nathanson (ed.), Viral Pathogenesis. Lippincott-Raven, New York.

134. **Watanabe Y, Prevec L, Graham AF.** 1967. Specificity in transcription of the reovirus genome. Proceedings of the National Academy of Sciences USA **58:**1040-1047.

135. **Weiner HL, Ault KA, Fields BN.** 1980. Interaction of reovirus with cell surface receptors. I. Murine and human lymphocytes have a receptor for the hemagglutinin of reovirus type 3. Journal of Immunology **124:**2143-2148.

136. **Weiner HL, Drayna D, Averill DR, Jr, Fields BN.** 1977. Molecular basis of reovirus virulence: role of the S1 gene. Proceedings of the National Academy of Sciences USA **74:**5744-5748.

137. **Weiner HL, Powers ML, Fields BN.** 1980. Absolute linkage of virulence and central nervous system tropism of reoviruses to viral hemagglutinin. Journal of Infectious Diseases **141:**609-616.

138. **Wetzel JD, Wilson GJ, Baer GS, Dunnigan LR, Wright JP, Tang DSH, Dermody TS.** 1997. Reovirus variants selected during persistent infections of L cells contain mutations in the viral S1 and S4 genes and are altered in viral disassembly. Journal of Virology **71:**1362-1369.

139. **Wu E, Pache L, Von Seggern DJ, Mullen TM, Mikyas Y, Stewart PL, Nemerow GR.** 2003. Flexibility of the adenovirus fiber is required for efficient receptor interaction. Journal of Virology **77:**7225-35.

140. **Zarbl H, Hastings KEM, Millward S.** 1980. Reovirus core particles synthesize capped oligonucleotides as a result of abortive transcription. Archives of Biochemical Biophysics **202:**348-360.